

***TECHNOLOGY DEVELOPMENT FOR
EXOPLANET MISSIONS***

Technology Milestone Report

*MEMS Deformable Mirror Technology Development for
Space-Based Exoplanet Detection,*

*Paul Bierden
Boston Micromachines Corporation*

Released By:

Dr. Paul Bierden
Principal Investigator
Boston Micromachines Corporation

Date

Approved By:

Dr. Brendan Crill
Deputy Program Chief Technologist
Exoplanet Exploration Program
NASA/Jet Propulsion Laboratory
California Institute of Technology

Date

Dr. Nicholas Siegler
Program Chief Technologist
Exoplanet Exploration Program
NASA/Jet Propulsion Laboratory
California Institute of Technology

Date

Dr. Douglas Hudgins
Program Scientist
Exoplanet Exploration Program
Science Mission Directorate
NASA Headquarters

Date

Table of Contents

1. Executive Summary	3
1.1. Major Accomplishment:	3
1.2. Secondary Accomplishments:	4
2. Introduction	4
2.1. Milestone 1 definition:	4
2.2. Relevance for a Future Exoplanet Mission	4
3. Deformable Mirror Component Fabrication and Test	6
3.1. Fabrication	6
3.2. BMC Opto-electro-mechanical Characterization of Components	10
3.3. Coronagraph Test Bed Component Insertion and Baseline Null Testing	13
3.4. Dynamic Mechanical Testing at ETIF	19
3.5. Post-Exposure Coronagraph Test Bed Component Insertion and Null Testing	25
4. Conclusion	32
4.1. Lessons Learned	32
4.2. Future Work	33
5. Abbreviations, acronyms, and symbols	34
6. References	35
7. Appendix	36
7.1. Appendix A: Pre-Vibe JPL Testing	36
7.2. Appendix B: Initial Princeton Testing	36
7.3. Appendix C: Random-Vibe Test Plan	36
7.4. Appendix D: Post-Vibe JPL Testing in VSG	36
7.5. Appendix E: Post-Vibe JPL Testing in HCIT	36
7.6. Appendix F: 50 x 50 Testing	36

Acknowledgements

I would like to acknowledge to work of the following people in this project for without them it would not have been completed:

Charlie Lam and Steven Cornelissen of Boston Micromachines Corporation for their work in the fabrication and testing of the MEMS DMs.

He Sun and N. Jeremy Kasdin of Princeton University for their characterization of the devices and feedback on the performance.

Tyler Groff of Goddard Space Flight Center for all the work he did in getting the environmental testing completed.

John Trauger, Pin Chen, Frank Greer, Frank Greer, Cory Hill, Brian Gordon, Garreth Ruane, Camilo Mejia Prada, and Eduardo Bendek at JPL for the thorough testing of the devices in the VSG and HCIT. Their results helped validate the project and their valuable advice on testing and failure areas was important for the progress of DMs in future mission.

Nick Siegler and Brendan Crill at JPL for the support of this project and guidance through the TDEM process.

TDEM Milestone Report: MEMS Deformable Mirror Technology

1. Executive Summary

This report discusses the work done in support of NASA's Exoplanet Exploration Program and the ROSES Technology Development for Exoplanet Missions (TDEM), on the first TDEM Milestone for **MEMS Deformable Mirror Technology Development for Space-Based Exoplanet Detection**. The objective of this project was to achieve a technology development milestone that demonstrates the capacity of the MEMS DMs to survive dynamic mechanical environmental stresses associated with launch and deployment in space. Without such technology development, a coronagraph mission using MEMS DMs would not be possible

1.1. Major Accomplishment:

The Milestone for this project was to demonstrate the survivability of MEMS DMs after being exposed to a launch like environment. This milestone was met. Twelve MEMS DMs with 952 actuators were fabricated specifically for this project. These devices were characterized and demonstrated all the optical and electromechanical properties proposed. A sampling of these devices was tested at JPL and Princeton's HCIL. The devices were shown to have $\sim 1\text{nm}$ stability and repeatability at JPL and a contrast of 2×10^{-7} over 6 to $11\lambda/D$ and 9×10^{-7} over 5 to $14 \lambda/D$ at the HCIL. The DMs underwent random-vibration testing at levels relevant to the Roman Space Telescope: the most relevant space telescope with a coronagraph. The devices were then re-tested at BMC, JPL, and Princeton. At BMC the devices had the same optical and electromechanical properties as pre-vibration to within the limits of the instrumentation. At JPL, the DMs demonstrated the same performance as pre-vibe regarding actuator gains, cyclic repeatability, and long-term stability. A second and unplanned test was performed where the DMs were characterized in an interferometer and inserted in a coronagraph in the HCIT. The contrast demonstrated was consistent with surface precision on the order of 0.1 nm. This performance is comparable to the contrast achieved with a BMC DM that did not undergo environmental testing. This test demonstrated that a BMC DM can achieve high contrast after flight-relevant environmental testing. At Princeton, the stable contrast results from pre-vibe were not achieved. A drifting in the DM was indirectly observed through a varying intensity in the subsequent images with the same voltage pattern applied. The exact amount of instability and number of actuators effected could not be determined but was calculated to be on the nm scale. Also, the cause of this instability could not be determined as all actuators were functional. Contamination from the handling of the devices in all the transportation is a suspected cause but it is still uncertain.

1.2. Secondary Accomplishments:

This project dealt with major manufacturing issues in the MEMS foundry process with both micro-contamination affecting surface quality of the mirror and unexpected chemical precipitate leading to electrical shorts in the device. These issues resulted in the foundry re-running the process multiple times and lead to delays in the program. From these issues, though, much was learned about the manufacturing process that was previously unknown and by addressing these issues, a more robust and reliable MEMS manufacturing process was developed. This process has been used by BMC for both its commercial MEMS products and other DMs delivered to NASA for high contrast imaging applications.

2. Introduction

TDEM Technology Milestones are intended to document progress in the development of key technologies for a space-based mission that would detect and characterize exoplanets, thereby gauging the mission concept's readiness to proceed from pre-Phase A to Phase A.

This milestone addresses MEMS deformable mirrors used in high precision wavefront control in high contrast imaging instruments. The objective of this TDEM milestone is the validation of a MEMS deformable mirrors for use in these instruments after being exposed to the environmental conditions that would be experienced during launch and operation.

This milestone reads as follows:

2.1. Milestone 1 definition:

Demonstrate survivability of the BMC 952-actuator MEMS CDM after exposure to dynamic mechanical environments close to those expected in coronagraph launch.

- Validate absence of degradation in CDM optical and electromechanical performance through functional test and interferometric surface mapping.
- Validate CDM performance in an existing coronagraph test bed (HCIL), as measured by the achievable null depth and its stability.

2.2. Relevance for a Future Exoplanet Mission

In the ROSES-NRA the Strategic Astrophysics Technology program calls directly for efforts of this type: "In order to achieve the requisite degree of starlight rejection, the light paths within both coronagraphic and interferometric systems must be controlled to sub-nanometer precision. Advances in control algorithms, sensing technology, and *deformable mirror technology* are central to implementing such instruments on a space-based platform (emphasis added)."

The strategic goal of the work proposed here is to advance MEMS DMs as an enabling technology in NASA's rapidly emerging program for extrasolar planet exploration. That goal is supported by an Astro2010 white paper on *Technologies for Direct Optical Imaging of Exoplanets*, which concluded that DMs are a critical component for all proposed internal coronagraph instrument concepts [1]. That white paper pointed to great strides made by DM developers in the past decade, and acknowledged the components made by Boston Micromachines Corporation to be the most notable MEMS-based technology option.

Conventional DMs (e.g., the 48x48 actuator Northrop Xinetics DMs that are used as baseline technology in the HCIT at JPL) are currently at a higher level of technology maturity than their MEMS-based counterparts. However MEMS components are likely to be of increasing importance in space-based mission concepts because of mass and cost considerations [1].

The Decadal Survey on Astronomy and Astrophysics 2020, *Pathways to Discovery in Astronomy and Astrophysics for the 2020s*, [2] expresses the importance of a Flagship exoplanet direct imaging mission like LUVOIR and HabEx, which both include a coronagraph. The report states in the section on Technology Development Needs for these missions, "There is significant overlap in the advancement of coronagraph-based technologies between LUVOIR and HabEx, and high-priority technologies to mature includevacuum-compatible deformable mirrors"

In this project, a critical milestone was reached for CDM components based on MEMS technology. The benefit to NASA is both timely and important.

3. Deformable Mirror Component Fabrication and Test

3.1. Fabrication

A main component of this project was to perform a MEMS fabrication run to produce twelve DMs for testing. The specifications of those DMS can be seen in Table 1.

Table 1. MEMS DM Specifications

Mirror architecture	952 actuators
Active Aperture Diameter	9.9 mm Circular
# Actuators across active diameter	34
Actuator Pitch	300 μ m
Actuation architecture	Electrostatic
Actuator Stroke	1.5 μ m
Operating Voltage	0-200V
Mirror Surface Figure	<8nm RMS (300 μ m > λ)
Fill Factor	>99.6%
Mirror segment material	Silicon, 1000 Å gold coating

The fabrication process used to manufacture the DM is illustrated in Figure 1. In this fabrication process, batches of 25 wafers were processed together. The process began with depositing insulating layers, then lithographically patterning and reactive ion etching (RIE) the first polysilicon layer to create the wire routing traces of the actuator array. Following device layer patterning, two electrically-isolating thin films were deposited, consisting of low-temperature oxide (LTO) and low-stress silicon nitride. The LTO and silicon nitride layers were then lithographically patterned and etched to provide a path for electrical connectivity between the wire traces and the actuator electrodes, which were produced in a subsequent polysilicon thin film deposition and patterning process (referred to as Poly 0b).

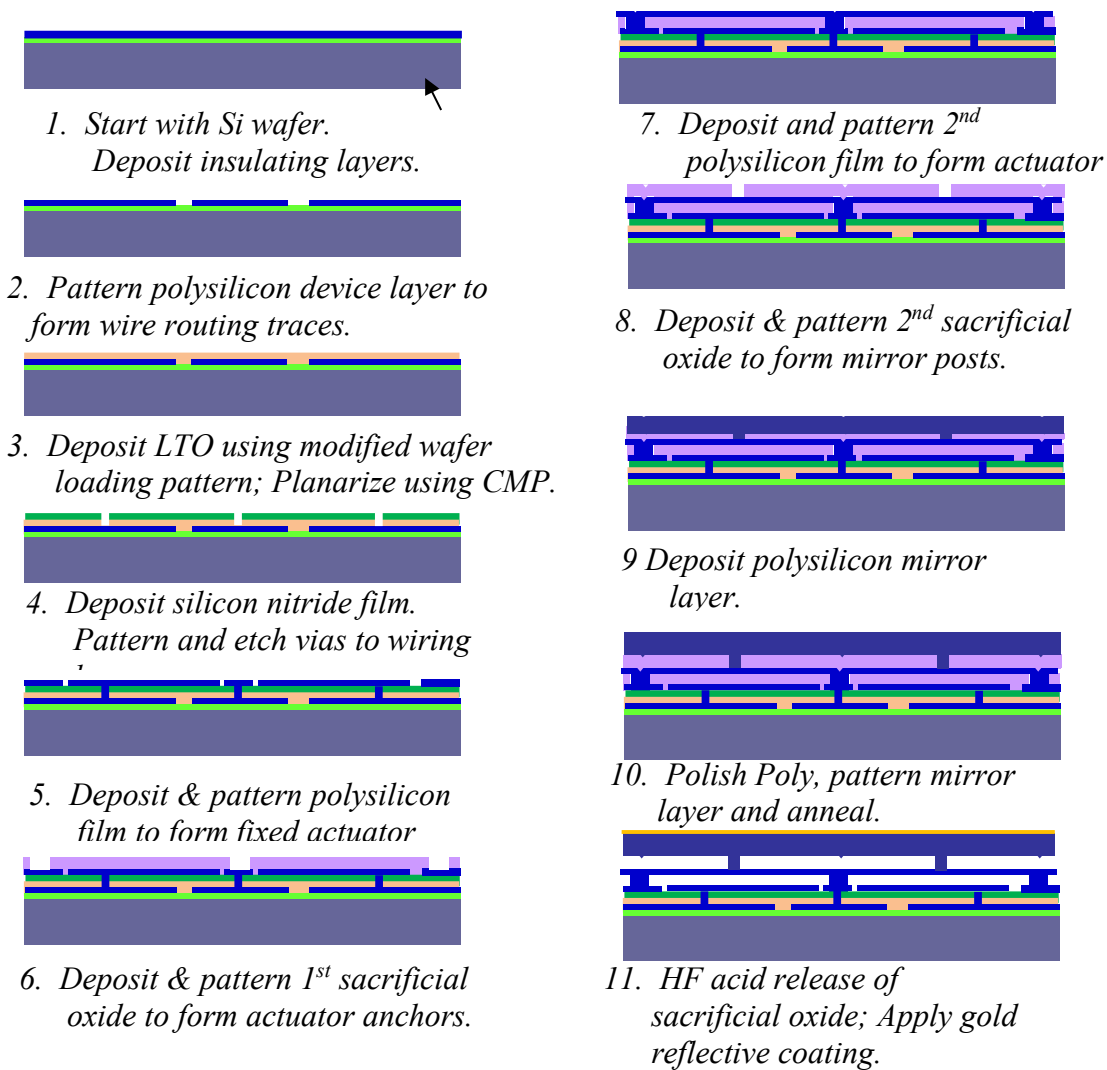


Figure 1. MEMS DM device fabrication process (cross-section of single segment)

After fabricating the array of actuator electrodes, a 5 μ m thick sacrificial layer (referred to as Oxide 1) was deposited on the Poly 0 layer, patterned, and etched. This layer was used to create the actuator gap, the thickness of which determines the stroke of the electrostatic actuators. Following Oxide 1, a second layer of polysilicon, Poly 1, was deposited, patterned, and etched to create actuator anchors and compliant actuator flexures. A second, 5 μ m thick sacrificial layer, Oxide 2, was then deposited, annealed and chemomechanically polished to remove undesired topography resulting from features etched in the underlying layers. Oxide 2 was then patterned and etched to create mirror post attachment points. It also provides space between the actuator flexures and the mirror segments over their full range of motion. Polysilicon was then deposited again to create the mirror layer (Poly 2), and a reactive ion etch (RIE) of this layer was used to define the mirror surface and add etch access holes. Wire bond pad metal was then patterned and deposited through a liftoff process to facilitate wire bond adhesion. Each wafer was then diced into 17mm square chips, and the sacrificial layers were removed

(Oxide 1 and Oxide 2) using a hydrofluoric acid etch, which released the structural polysilicon layers of the DM. The surface flatness of the mirror segments on each chip was then measured using an interferometric surface mapping profilometer (a Zygo Verifire). Finally, a reflective gold film was deposited using electron beam evaporation.

For each of the fabrication layers described above, a lithographic layout was designed. The fabrication process uses 150mm wafers, so on each wafer a number of devices could be designed and positioned, including the 952-actuator DMs used in this project and a number of smaller test devices used to determine electromechanical and surface properties of the DMs. The layout can be seen in Figure 2.

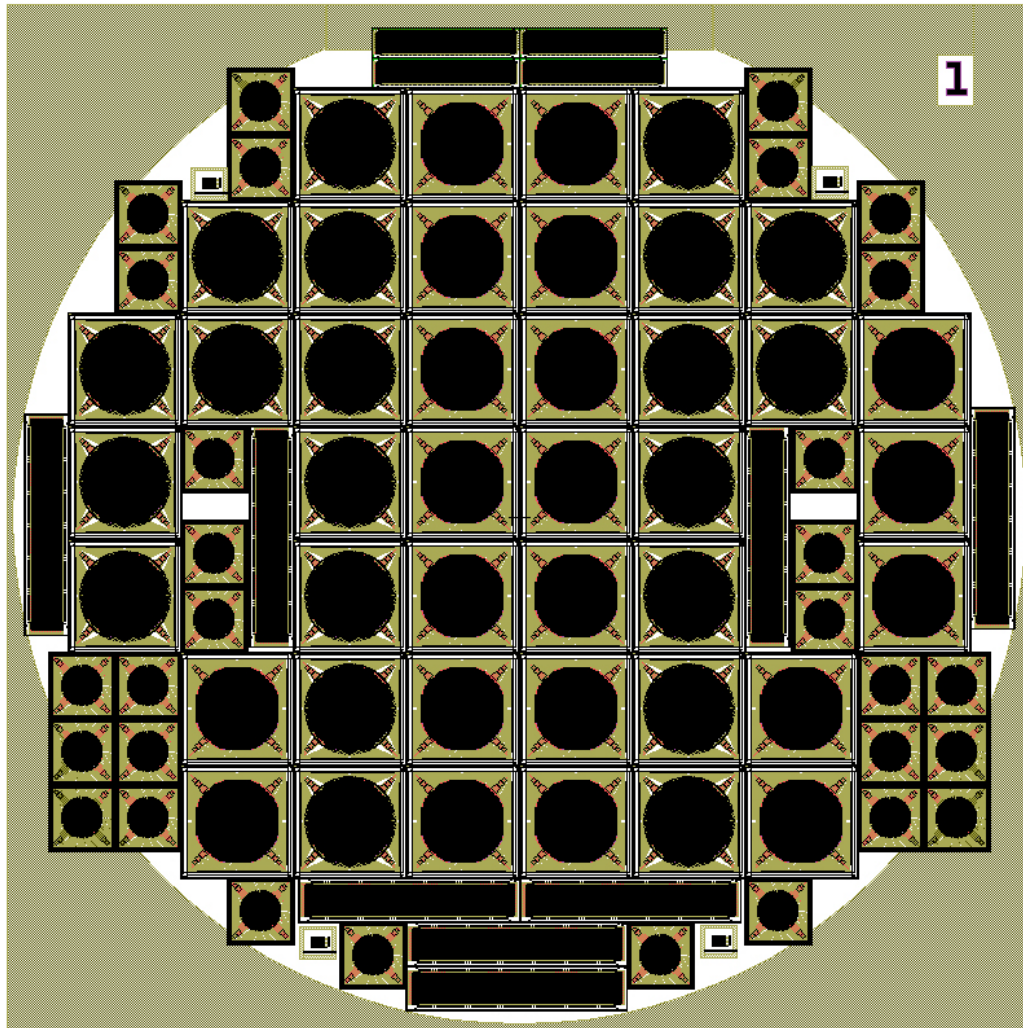


Figure 2: Design layout of MEMS fabrication structures on 150mm wafer.

The fabrication of the DMs was impacted by two major issues which caused delays in the manufacturing process: mask defects and electrical shorts. First, it was discovered during the fabrication process that there was a series of defects in multiple layers of the lithographic masks, resulting in defects in the polysilicon layers. Defects like these cause

mechanical failures in devices and have an impact of the surface quality of the mirrors. Examples of the defects can be seen in Figure 3.

These defects were not discovered until near the end of the fabrication process, after the last polysilicon deposition was completed. Boston Micromachines and the foundry worked together to identify the cause of these defects and put in place procedures to rectify them. The remedies included making new lithographic masks that were protected by a pellicle to prevent contamination. A second batch of wafers was started with these new masks, but the need to restart fabrication caused a delay in the project schedule.

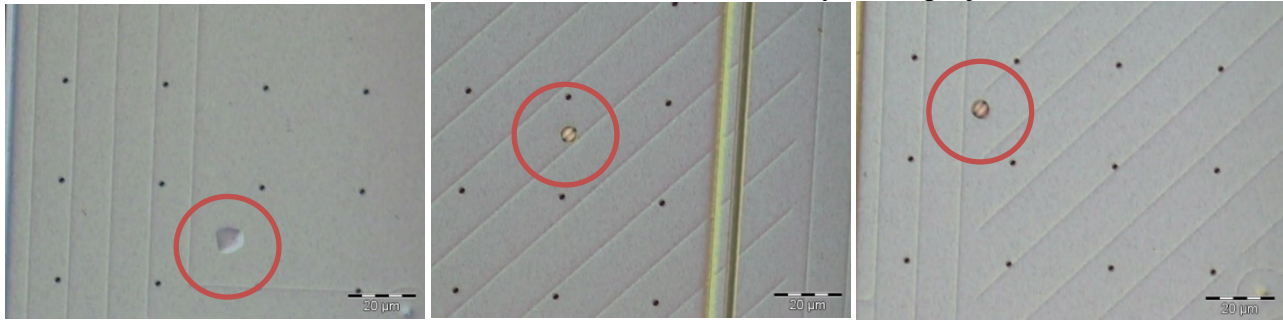


Figure 3a: Defects seen in the Poly1 send ahead wafer. The defects are on the order of 5-10 μm in size.

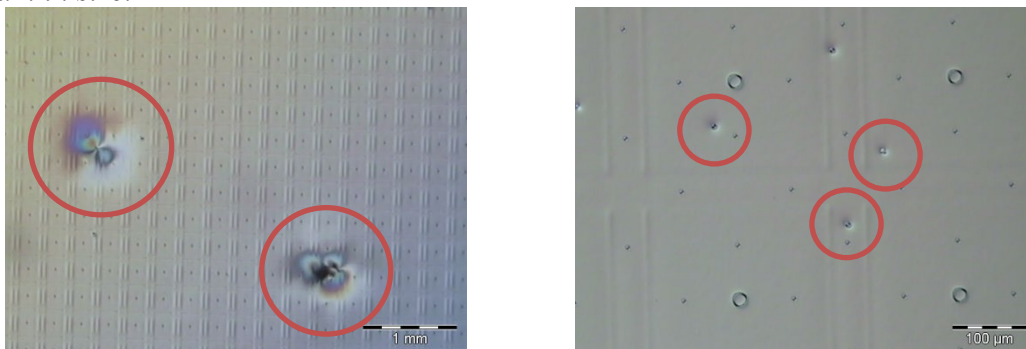


Figure 3b: Defects seen in the Poly2 layer of completed devices. Some of the defects were large (750 μm) and affected the optical quality of the device.

A second manufacturing delay was caused by the discovery of electrical shorts in devices received from the second run of wafers. Again, these shorts were not discovered until late in the fabrication process. Through SEM analysis (Figure 4), it was found that the shorts were caused by a phenomenon called *phosphorus segregation* in which a conductive phosphorus film leaks out and across the cuts in the Poly0 layer, electrically shorting the two sides of the cut. This phosphorus segregation occurred as a result of the high thermal budget for the entire foundry process but could not be seen until wafers experienced the entire thermal budget through the final anneals of Poly2. To remedy the shorting problem, it was necessary to again restart the fabrication process. This third run of wafers implemented a new process where the overall thermal budget was modified, resulting in a reduced or eliminated phosphorous segregation and subsequent reduction of electrical shorts.

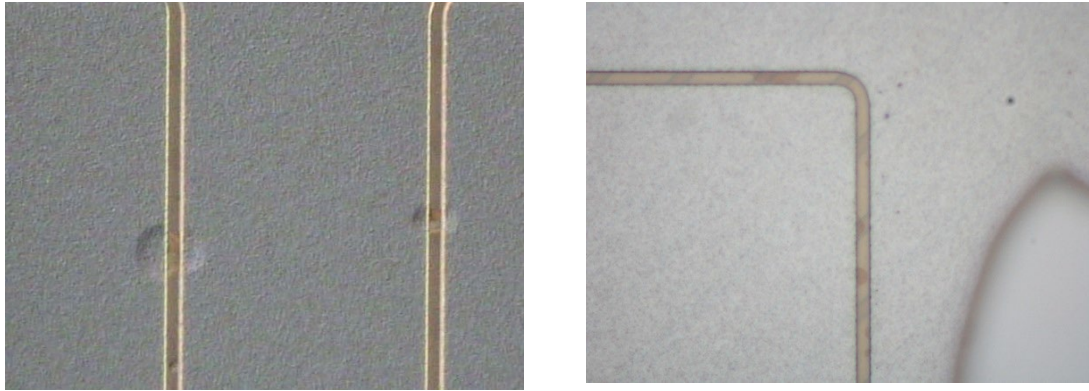


Figure 4a: Optical microscope images of Poly0B showing a discoloration where phosphorous segregation occurred.

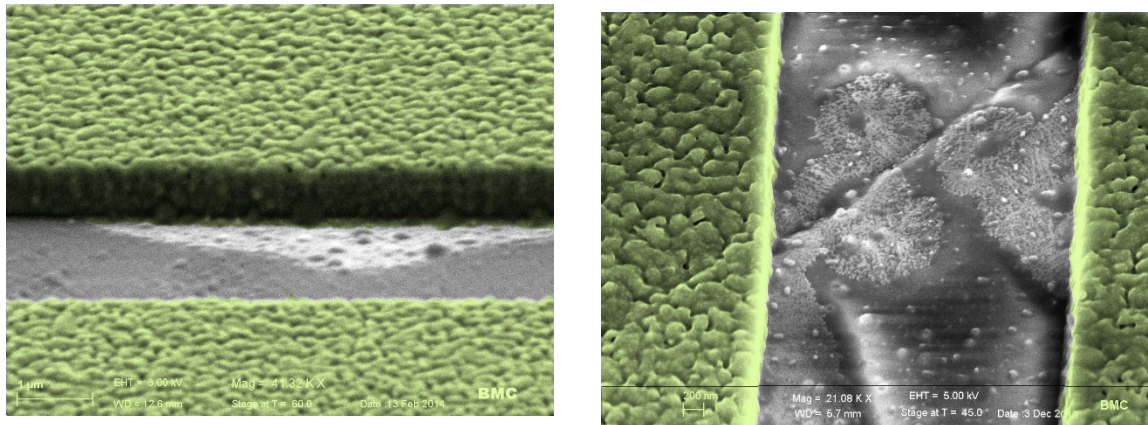


Figure 4b: SEM images showing the phosphorous segregation in a cut in the Poly0B layer (false color green). The phosphorous is the light discoloration seen in the cuts.

This third fabrication run was successful and produced the MEMS DMs for this project. However, the necessity of repeating the fabrication process twice caused an overall delay of approximately 18 months.

3.2. BMC Opto-electro-mechanical Characterization of Components

After fabrication, twelve 100%-working devices were selected for dynamic mechanical tests. Each component was characterized in three tests at BMC to evaluate mirror surface topography and electromechanical actuator performance. The first test was a measurement of topographic surface maps and root mean square (rms) surface deviation from flatness over the entire mirror, using a wide field interferometer (Zygo Verifire®). This measurement quantified to ~1nm precision any topography in the mirror shape. Mirror non-flatness can be attributed to residual stresses in the thin films or the die, or print-through, so this measurement provides a baseline that is sensitive to changes in

stress that might result from testing. Both the unpowered and filtered (High Pass FFT with $\lambda > 1.66/\text{mm}$) measurements were taken. An example measurement, showing the unpowered surface and the filtered surface (7 nm rms non-flatness on the full active aperture) is shown in Figure 5.

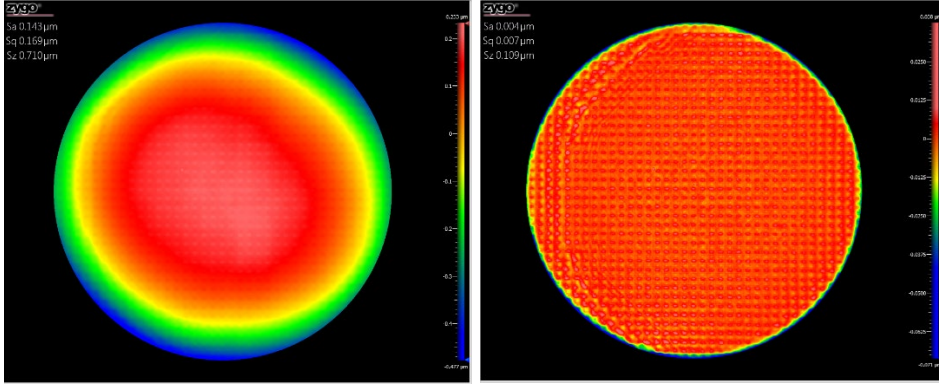


Figure 5: Interferometric measurement of the DM surface(L) unpowered and (R)filtered (High Pass FFT with $\lambda > 1.66/\text{mm}$).

The second test was a quasi-static electromechanical measurement of mirror displacement (measured in surface normal direction directly above each actuator post) in response to a series of applied voltages spanning the operational range of the actuator. In one variation of this test, one actuator was energized at a time, and in another variation, a 4x4 array was energized. All actuators other than the actuator or actuators being energized were held at ground potential. Multi-point displacement curves were measured multiple times for each actuator in the component to establish an error-bounded electromechanical performance baseline. An example of this measurement can be seen in Figure 6.

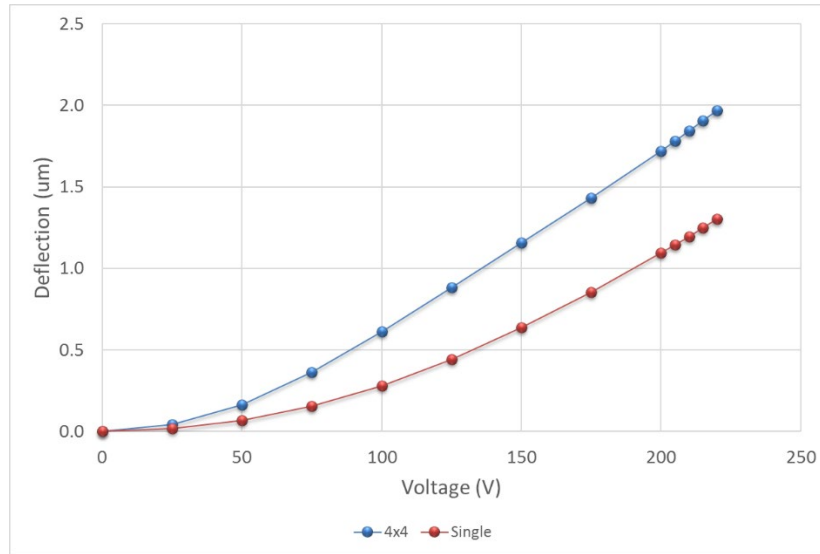


Figure 6: Example of the Quasi-static mirror displacement data

The third test was an active flattening of the surface of the deformable mirror and measurement of the flattened surface using the Zygo Verifire. A closed loop algorithm was used to control the DM surface. The algorithm identified the post locations for each

of the 952 actuators and drove them to a best fit plane. The controller was looped 30 times, which was determined to be the number of loops required to achieve the best flat. An example of the active area of a DM being controlled to flat is shown in Figure 7.

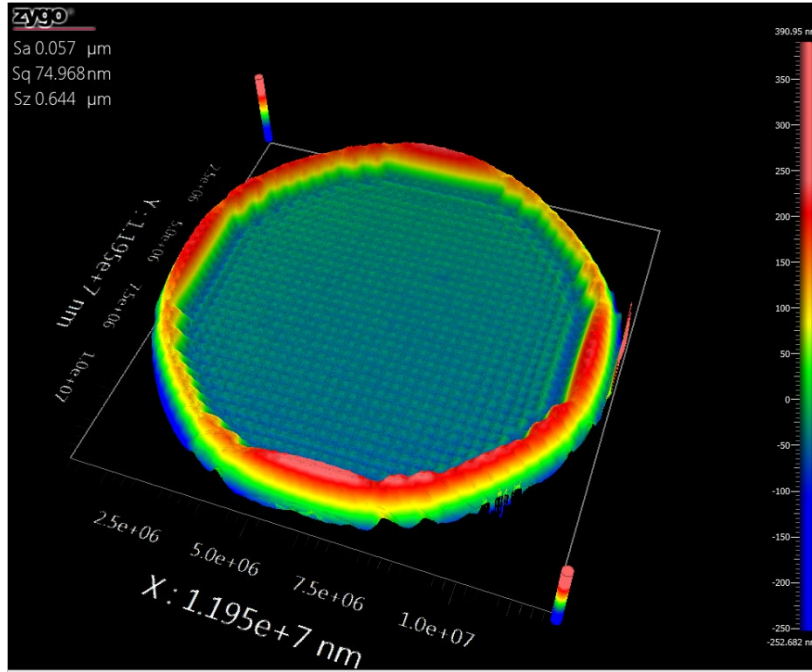


Figure 7: Interferometric measurement of the DM surface actively controlled to flat.

A summary for the characteristics of the 12 deformable mirrors can be seen in Table 2. This includes the serial number, the unpowered RMS surface finish, the unpowered filtered RMS surface finish (High Pass FFT with $\lambda > 1.66/\text{mm}$), the voltage required to actuate a 4x4 array to 1.5um of stroke, and the actively flattened RMS surface finish.

Serial Number	Unpowered RMS (nm)	Filtered RMS (nm)	Voltage required for 1.5μm stroke	Flattened RMS (nm)
25CW011#035	169	6.3	182	6.5
25CW012#015	128	6.4	184	5.6
25CW003#010	160	6.3	175	7.5
25CW003#014	188	6.8	179	7.1
25CW003#013	145	7.6	181	5.8
25CW008#040	167	5.6	176	4.3
25CW011#019	99	5.1	177	5.9
25CW015#017	109	6	183	6.2
25CW018#031	72	5.5	183	5.5
25CW018#033	75	5.9	172	6.2
25CW018#041	80	6.3	180	6.7
25CW019#029	98	6.3	174	5.2

Table 2: Characteristics of the 12 DMs tested in this project.

3.3. Coronagraph Test Bed Component Insertion and Baseline Null Testing

3.3.1 ExEP facilities at JPL

Two DMs were sent to the Exoplanet Exploration Program (ExEP) facilities at JPL and were inserted and tested in the Vacuum Surface Gauge (VSG). The two DMs were serial numbers 25CW012#015 and 25CW011#035, which JPL referred to as DM1 and DM2, respectively. The VSG and its optical layout can be seen in Figure 8.

The tests performed on the VSG included surface measurements, both powered and unpowered. The gains of all actuators were measured at a given offset which was used to produce a flat surface. Also tested at the VSG were position stability and repeatability. These tests were performed by JPL's Frank Greer, Cory Hill, Brian Gordon, and John

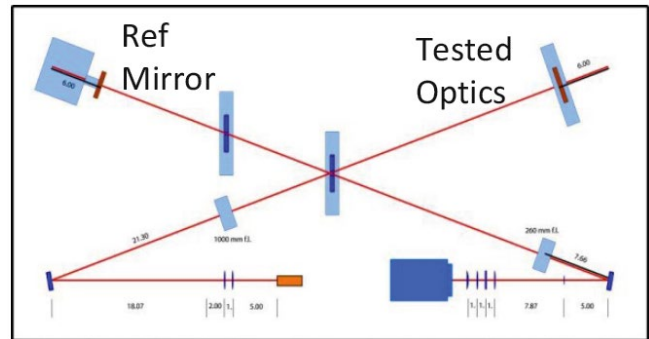
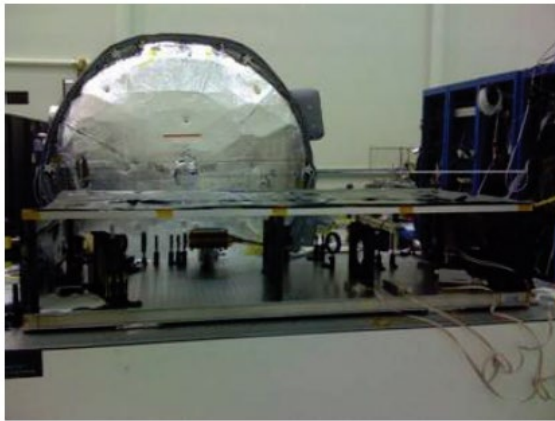


Figure 8: Image of VSG bench (left) and VSG optical layout (right).

Trauger.

1. Measure surface figure of BMC DMs at zero bias and 100V bias

For this test the surface figure of the DM was measured in the unpowered state (zero bias) and with a uniform voltage (100V bias) applied to all actuators. This gave a baseline for future measurements.

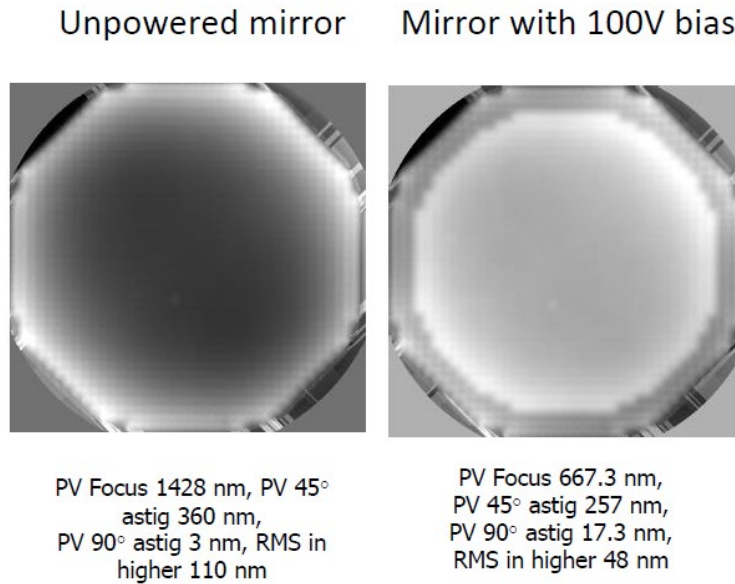


Figure 9: Measurement of surface of DM1, unpowered (left) and powered with 100V bias (right).

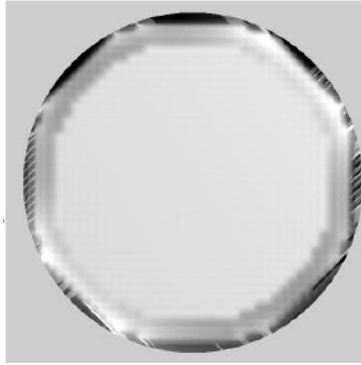
2. Measure actuator gains for all 952 actuators

In this test, a 100V bias was placed on all 952 actuators then +/- 10V pokes were applied to the actuators. These pokes were used to measure the gains and generate a gain map, which was, in turn, used to calculate the voltage map for a flat surface figure. The gains for all actuators in each of the DMs was measured to be in the 5-10nm/V range.

3. Measure surface figure of BMC DMs for flat surface figure

When the voltages for the flat surface figure were calculated, they were then applied to each DM. This resulted in 6.6 nm PV focus and 7.6 nm RMS of the higher high order terms (greater than astigmatism) for DM1 (typical of the other devices).

Flattened DM



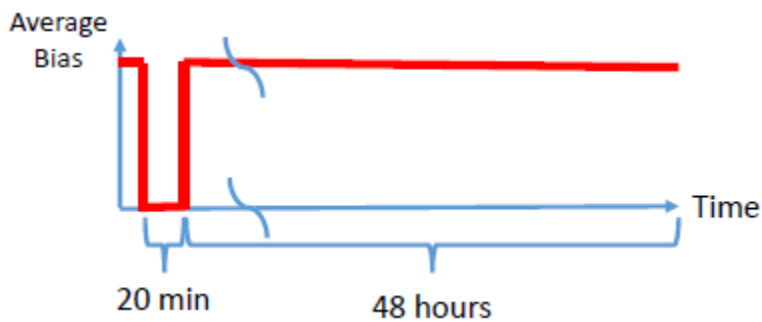
6.6nm PV focus,
2.9nm PV 45 deg astig,
0.3nm PV 90 deg astig,
7.6nm PV higher order
terms

Figure 10: VSG image of flattened mirror surface figure for DM1.

4. Measure drift in surface figure for flat condition

For this test, each DM was left unpowered for ~20 minutes, and then driven to its flat state. The flat surface figure solution was applied, passing through an unpowered state for ~20 minutes prior to the beginning of the experiment. The mirror was then left powered, with no change to the applied voltages, and was characterized frequently over a 48-hour period, to measure any shift or “settling” in the surface of the mirror while being held at a fixed voltage pattern

Phase retrievals completed after the following waiting periods: 20 minutes, 1 hour, 2 hours, 4 hours, 8 hours, 16 hours, 24 hours, 32 hours, 40 hours, and 48 hours.



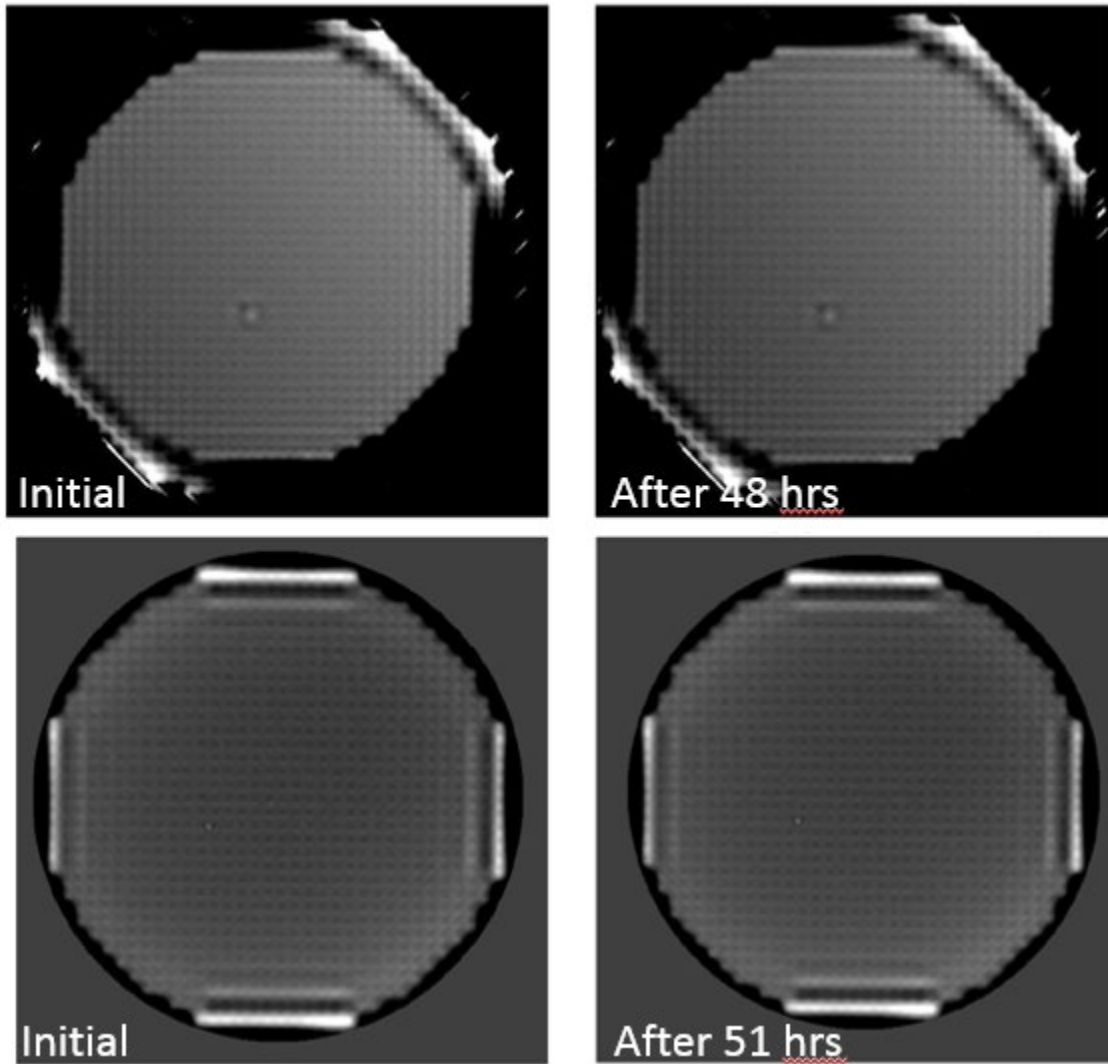


Figure 11: Phase Maps of DMs 1 (top) and 2 (bottom) before (left) and after (right) drift test. Difference for DM1 was 2.1 nm RMS and for DM2 was 0.9nm RMS

5. Repeatability for “flat” solution

This series of tests measured the repeatability of a flat surface figure ten times, passing through an unpowered state each time prior to applying the flat surface figure. Two phase retrievals were completed at the biased and unbiased condition for every repetition

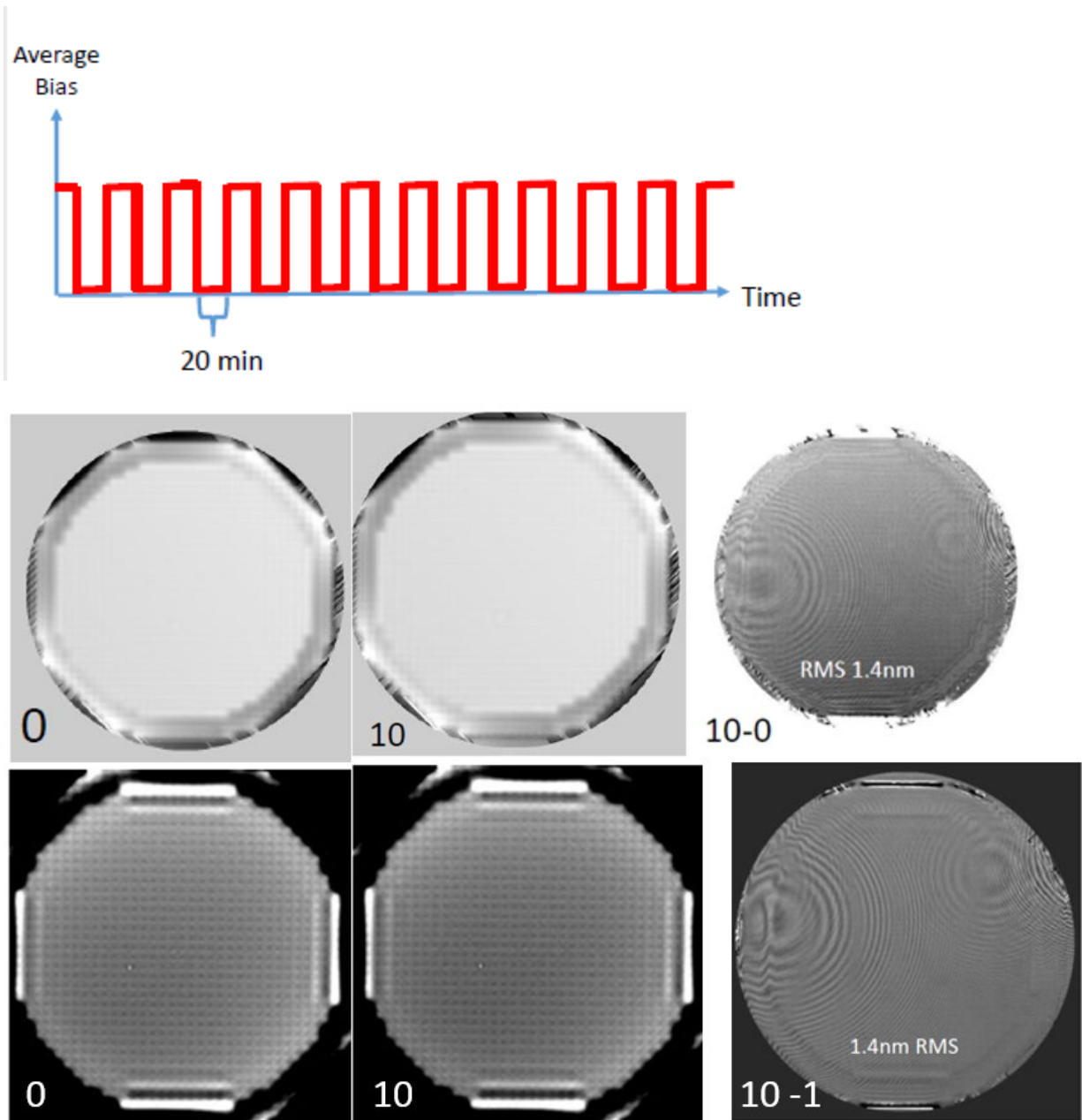


Figure 12: Repeatability test results for DM1 (top) and DM2 (bottom). Left column shows each DM before the 10 cycles; middle column shows each DM after 10 cycles. Right column shows a change of 1.4nm RMS from the “before” measurement for both DM1 and DM2.

Details of these tests can be found in Appendix A.

3.3.2 Princeton High Contrast Imaging Laboratory

Two DMs were sent to the Princeton High Contrast Imaging Laboratory (HCIL), where they were inserted and tested in the HCIL Testbed. Along with each DM, a voltage map

was provided that would produce a flat mirror surface (flat to the level of measurement capable with BMC's Zygo Verifire interferometer). This would allow testing at the HCIL from a relatively flat starting point.

At the HCIL, the DMs were characterized and used in wavefront correction using different algorithms to create a dark hole. An example of the test results can be seen in Figure 13, showing a contrast of 2×10^{-7} over 6 to $11\lambda/D$ and 9×10^{-7} over 5 to $14\lambda/D$. A detailed report of the work performed has been provided by Dr. Jeremy Kasdin and is Appendix B this report.

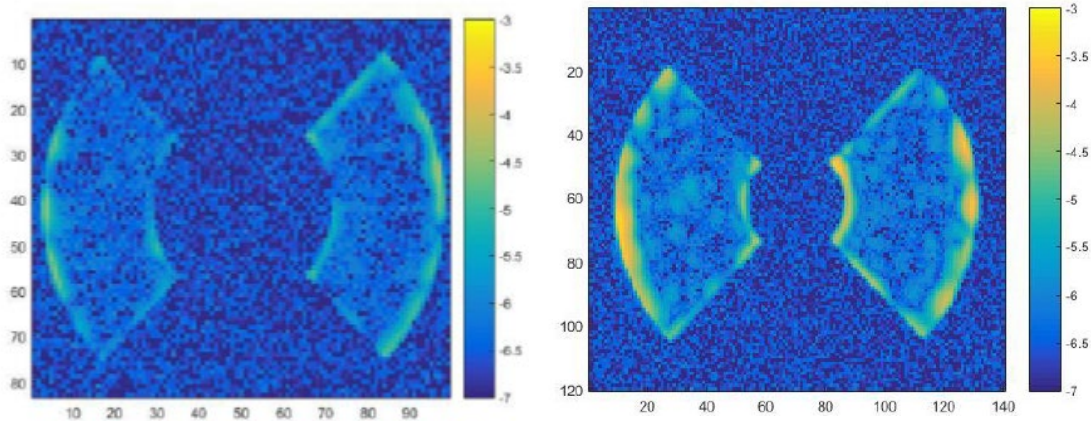


Figure 13: Final camera images after wavefront corrections. (Left) 6 to $11\lambda/D$ and 85 degrees wedged dark holes achieved by the DMs. The measured average contrast is also 2×10^{-7} . (Right) 5 to $14\lambda/D$ and 85 degrees wedged dark holes achieved by the DMs. The measured average contrast is 9×10^{-7} .

3.3.3 BMC Opto-electro-mechanical Characterization of Components after test

Upon return of the 4 DMs from testing (2 from JPL and 2 from Princeton), the quasi-static electromechanical measurement of mirror displacement and the active flattening tests were repeated at Boston Micromachines. For the mirror displacement testing, the variation in deflection for a given applied voltage was calculated. An example of the results can be seen in Figure 14. The average variation in deflection for a given voltage from before testing to after testing was 6.8nm.

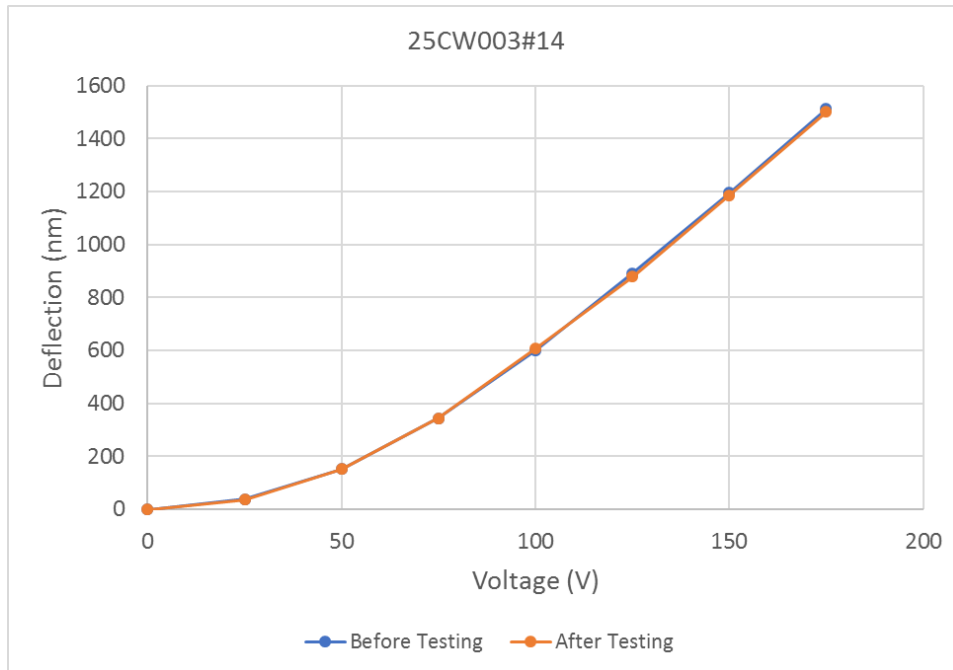


Figure 14: Quasi-static mirror displacement data from before and after testing at Princeton.

Next, all 4 DMs were actively flattened and their surface figures were measured. The variation in RMS from before and after testing was never more than 1nm. An example mirror's before-and-after flattened surfaces can be seen in Figure 15.

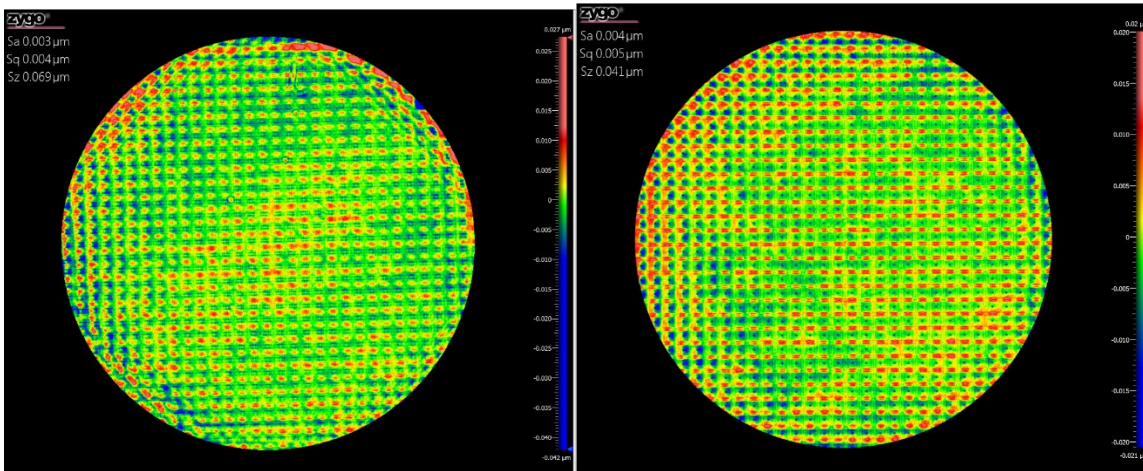


Figure 15: Actively flattened DM (left) before external testing and (right) after external testing. The variation in RMS is 1nm.

3.4. Dynamic Mechanical Testing at ETIF

A Random Vibration Test Plan was developed with Goddard Space Flight Center (Appendix C).

Three deformable mirrors were exposed to three random vibration environments, low medium and high as seen in Table 2 and Figure 16, for a total of nine tested devices. Each level was conducted in all three axes. The low level corresponds to a workmanship level of testing. The medium and high levels correspond to the WFIRST Coronagraph Instrument’s (now Roman Telescope) specifications for the random vibration environment of the deformable mirrors, for Flight Acceptance and Qualification, respectively. Nine packaged, wire-bonded, and tested DM components were delivered to GSFC for this testing. There were also two control DMs: one DM traveled to GSFC and back but was not exposed to vibration and one DM stayed at BMC. Details of the DMs sent can be seen in Table 1.

A test fixture was designed and built to hold the DM during vibration testing. It was mounted to a modified CV-Plat that was provided by Boston Micromachines.

DM#	Vibration Level	DM Serial Number
1	Low	25CW011#035
2	Low	25CW012#015
3	Low	25CW008#040
4	Med	25CW003#010
5	Med	25CW015#017
6	Med	25CW018#031
7	High	25CW003#014
8	High	25CW018#033
9	High	25CW018#041
10	Control/Travel	25CW019#029
11	Control/Home	25CW019#035

Table 1: Deformable mirrors tested at Goddard Space Flight Center with vibration level.

	Low Level	Medium Level	High Level
Frequency (Hz)	PSD Level (g^2/Hz) Three axis test	PSD Level (g^2/Hz) Three axis test	PSD Level (g^2/Hz) Three axis test
	Low-level 1 minute per axis	Medium-level 1 minute per axis	High-level Two minutes per axis
20	0.01	0.08 g^2/Hz	0.16 g^2/Hz
20-50	+3dB/oct	+3dB/oct	+3dB/oct
50–500	0.04	0.40 g^2/Hz	0.80 g^2/Hz
500–2000	-3dB/oct	0.04 g^2/Hz	0.08 g^2/Hz
2000	0.01	-3dB/oct	-3dB/oct

Overall	6.8 g _{rms}	0.01 g ² /Hz	0.02 g ² /Hz
		11.0 g _{rms}	15.6 g _{rms}

Table 2: Frequency spectrum of the three levels

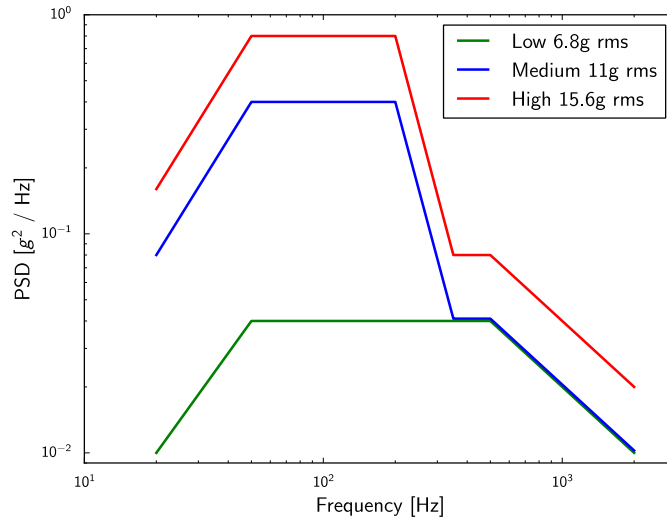
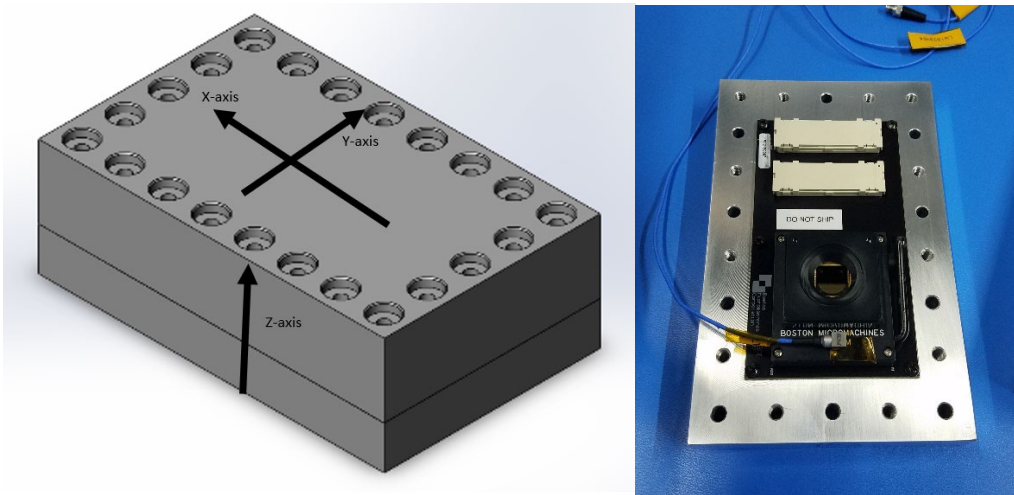


Figure 16 A plot of the three random vbe levels specified in Tables 1 and 2.

A test fixture was designed and built to hold the DM during vibration testing. It consisted of an 8” x 5” x 2.7” aluminum housing surrounding a PCB with a zero-insertion force socket to hold the DM. This was then mounted to a modified CV-Plat that BMC modified and provided. The model of the test fixture and an image of the DM mounted in the PCB can be seen in figure 17.



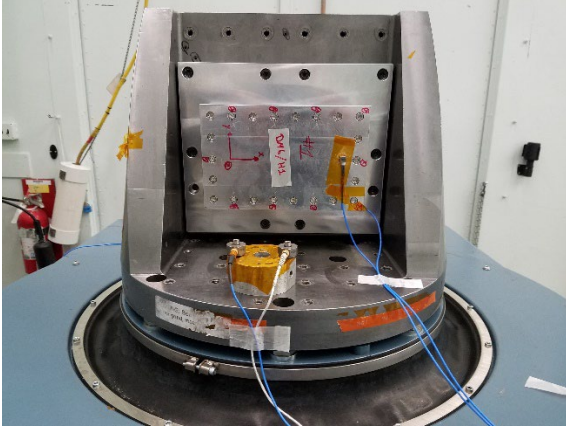


Figure 17. Top Left: Aluminum fixture for holding DM during testing (1inch between holes) Top Right – DM mounted in PCB attached to the test fixture. Bottom – CV Plate and test fixture mounted to shake table.

All DMs went through a detail optical characterization with a custom imaging system at GSFC with a 5x7mm FOV and a resolution of $\sim 1.5 \mu\text{m}/\text{pixel}$ on the detector. The bond pads and wirebonds were imaged before and after vibration to see if there was any initial damage. No damage to bondpads or wirebonds were seen

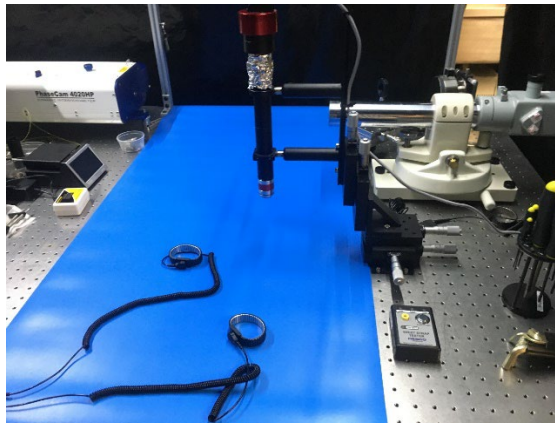


Figure 18: Imaging system to examine the DMs before and after vibration.

Opto-electro-mechanical Evaluation at BMC

After random vibration testing, all devices were fully characterized at BMC using the protocols established in Section 3.3 to ensure that baseline surface quality and actuator function have not been adversely affected. Examples of the results can be seen in Figures 19 and 20



Figure 19: Quasi-static mirror displacement data from before and after vibration exposure at GSFC testing at Princeton.

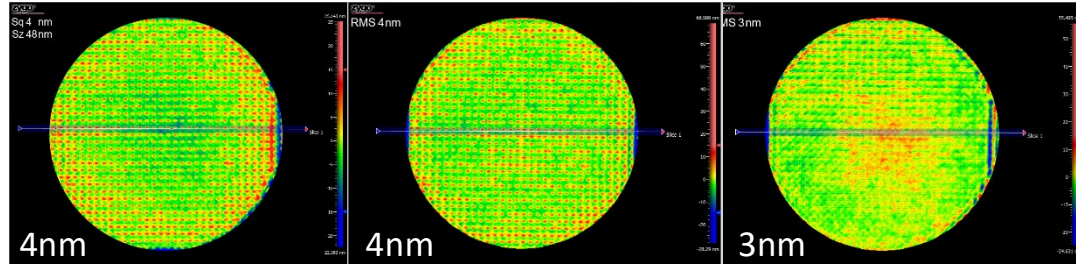
For the active flattening characterization, the same algorithm and equipment used before vibration were used to control the surface to the best fit flat. The flat surface was measured and then subtracted from the pre-vibration measurements. Examples of DMs from each vibration level and the two control DMs can be seen in Figure 20.

Pre-Vibe Flattening

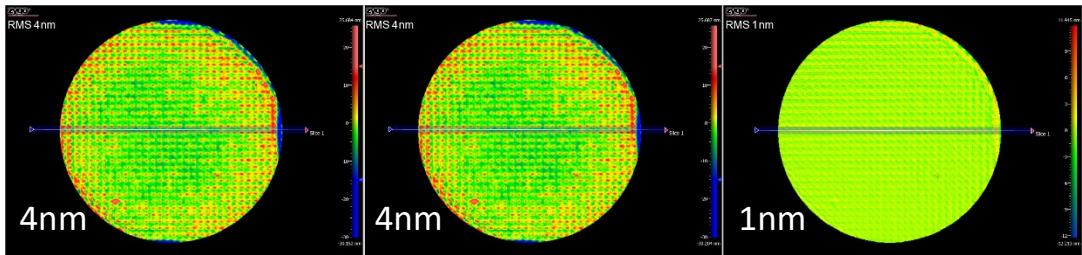
Post-Vibe Flattening

Difference

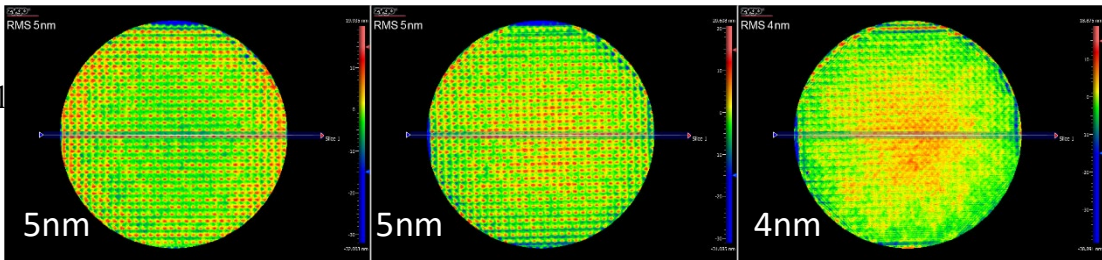
Low-Level



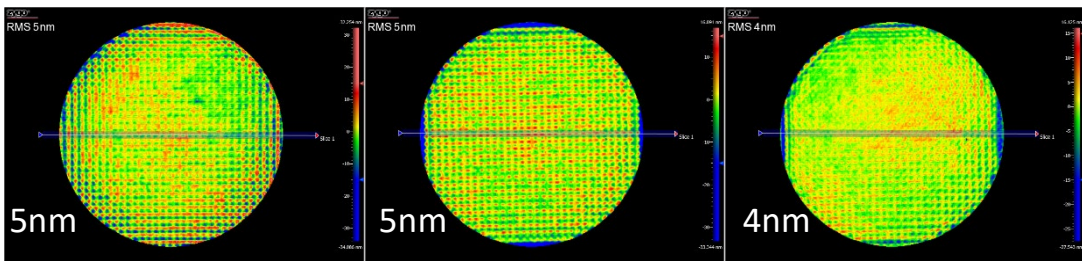
Med-Level



High-Level



Control 1



Control 2

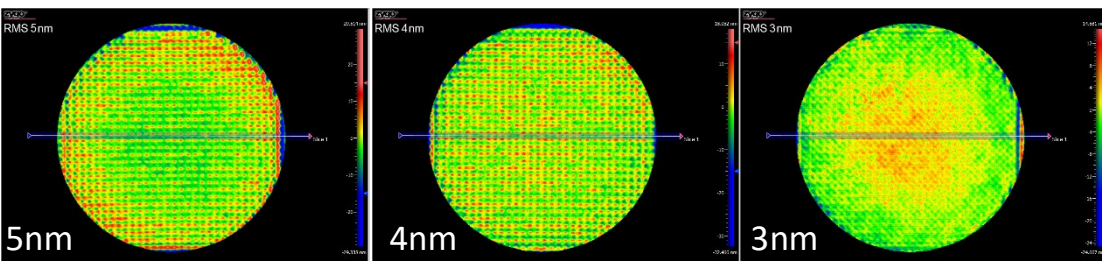


Figure 20: examples of pre and post vibration active flattening for each vibration level and the two controls as well as the difference between pre and post. The RMS value is in the bottom of each in the bottom left corner.

No variations outside the noise floor of the instrumentation were seen in any of the post vibration testing.

3.5. Post-Exposure Coronagraph Test Bed Component Insertion and Null Testing

3.5.1 ExEP facilities at JPL

After vibration testing and re-characterization at BMC, two DMs were sent back to JPL. Two different groups of testing were performed on the DMs. First, testing was performed that was similar to the pre-vide testing discussed in Section 3.3.1 using the VSG. Second, the DMs were testing using a Fizeau interferometer in the High Contrast Imaging Testbed (HCIT) facility one was integrated into a coronagraph testbed in a vacuum chamber. The two DMs were labeled “DM#15” and “DM#35” based on their serial numbers.

Summary of first test:

1. Unpowered surface figure:

VSG measurements were acquired with the DMs in the unpowered state (all actuators at 0V). The magnitude of the first 15 Zernike terms were fitted to the unpowered surface. The residual RMS value after subtracting these 15 Zernike terms was calculated.

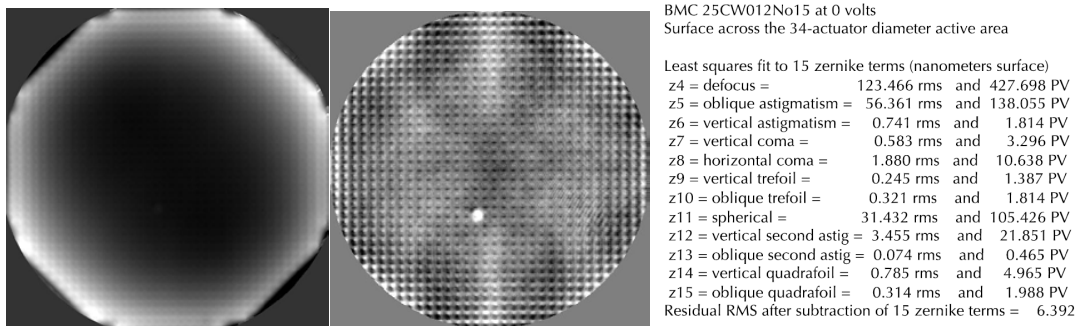


Figure 21: Example of unpowered surface finish measurements. Left unpowered surface, Center surface with 15 Zernike terms removed, Right, magnitude of the Zernike terms fit.

2. Actuator gains and flattening voltage maps:

The actuator gains (nm/V) were measured for each actuator using the following steps:

1. Apply a pre-determined flattening voltage map to all actuators in the DM.
2. Apply alternating +10 and -10 V pokes (deviations from the bias applied in the previous step) to a grid of actuators wherein neighboring bias points are five actuators apart (Figure 22).
3. Apply the above poke pattern with biases reversed.
4. Take the difference of the two surfaces corresponding to the two steps above.
5. Fit an *a-priori* influence function to each individual poke. Each fit coefficient represents the actuator gain per 20V poke.
6. Repeat the steps above with shifted grids until all actuators are characterized.
7. Use the measured gains and surface in Step 1 to solve for a new flattening voltage map.
8. Repeat the steps above until the flattening voltage map solution converges (Figure 22).

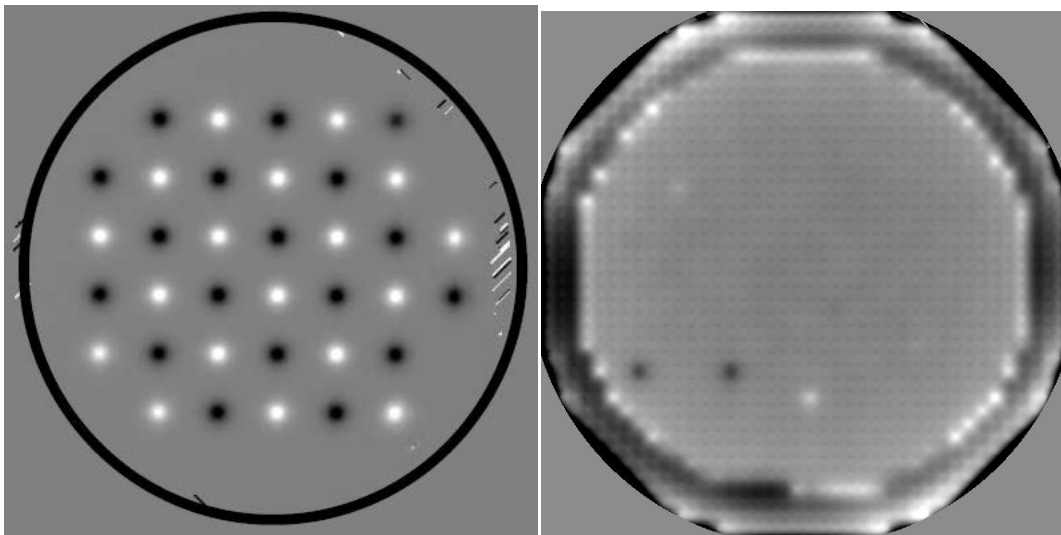


Figure 22. Left- Example poke pattern for gain measurements. The notional circle is drawn for clarity only. Right - Flattened surface figures of DM#35. Darker shades correspond to smaller actuator movement, and lighter shades correspond to larger actuator movement. Abnormally dark spots indicate non-moving actuators due to connector issues external to the DMs. The bright spot in the 6:00 position corresponds to an anomalous actuator, which drifted in position between derivation of the flattening voltage map and acquisition of the interferogram.

3. Repeatability test

Four cycles of successively applying 0V to all actuators, then a voltage map resulting in flat, and then return to 0V were performed. For both DMs, the RMS difference in surface figure between successive settings was < 0.8 nm. VSG instrument noise likely dominates

this number. Therefore, the post-vibe DM's overall surface figures are repeatable to within VSG measurement precision, with one significant exception; an anomalous actuator in DM#35 drifted by 5.8 nm between two successive flat applications, an interval of approximately 9-minutes.

4. Stability test (Applied to DM#35 Only)

Data were continuously acquired with the DM in the powered for 13 hours. Overall, the DM remained stable over the entire 13-hour period to within measurement noise (~ 0.7 nm RMS). However, two actuators, an anomalous actuator and a “non-moving” actuator (due to external connector problems), drifted over a range up to 10 nm during the 13 hours.

Conclusions

Overall, the DMs after random vibrate demonstrated the same performance as pre-vibe regarding actuator gains, cyclic repeatability, and long-term stability with the measurement capabilities of the VSG—with the exception of one high-gain actuator (out of 1904 actuators in two DMs) that appeared to drift. However, there were some interconnect issues external to the DMs that had not been resolved at the time of VSG testing and cannot rule out such issues as the culprit. Full details of this testing can be found in Appendix D.

Summary of second test:

1 - Functionality tests using the Fizeau interferometer

An optical table was set up in the High Contrast Imaging Testbed (HCIT) facility at JPL with a Fizeau interferometer (Zygo Verifire) for DM testing and characterization. A functionality test was performed that consisted of (1) applying a uniform bias to make sure all actuators respond, (2) poking each row and column, and (3) poking each actuator individually. This resulted in confirmation that all actuators were functional (Figure 23)

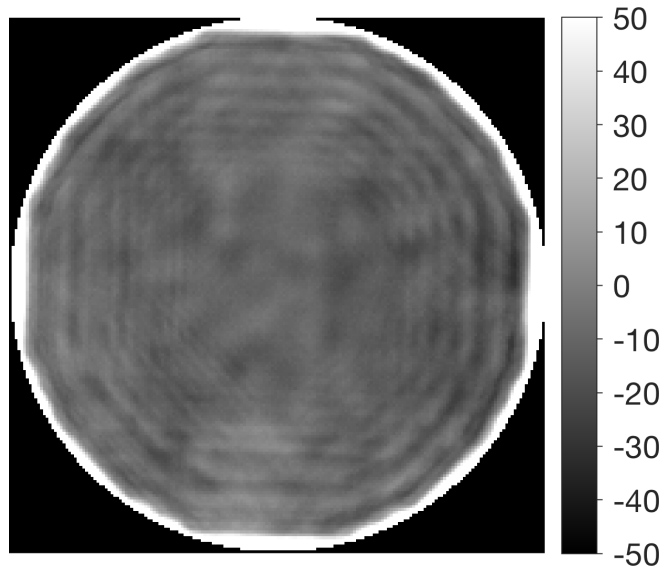


Figure 23: Example of DM surface difference measurements (in nm) between 0% and 50% bias using commercial electronics with the DM#035. Note that all actuators function

2 - Full calibration of DM#15 using the Fizeau interferometer

A complete calibration of every actuator was carried out by flattening the DM and measure the actuator gains (Fig. 24). The voltage map that flattened the DM had peak-to-valley of approximately 85 V and the individual actuator gain coefficients were typically 2-5 nm/V. The DM surface error in the flat state is <10 nm RMS within the spatial frequencies measured by the interferometer (i.e., down to a few pixels per actuator).

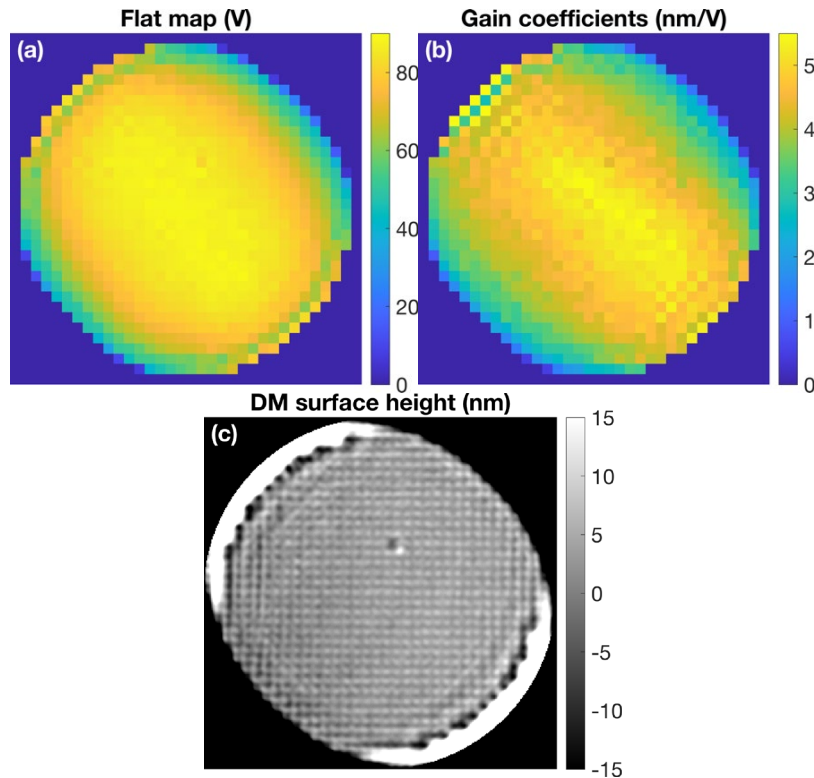


Fig. 24: DM calibration using the interferometer. (Left) The flat map in Volts. (Center) The measured gain coefficients for each actuator. (Right) The DM surface with the flat map applied.

3 -Performance testing using a vacuum coronagraph testbed

DM#15 was installed on a coronagraph testbed in a vacuum chamber at <1 mTorr. The DM was illuminated with a circular beam with a diameter of 9 mm (effectively 30 actuators across).

The optical layout consisted of a vortex coronagraph, which was being tested as part of a different SAT award (PI: Serabyn). After running standard wavefront control procedures, we achieved the dark hole in Fig. 25, which had a normalized intensity on the order of $1e-8$ over $2-12 \lambda/D$ with a 20nm spectral bandwidth centered at 637 nm.

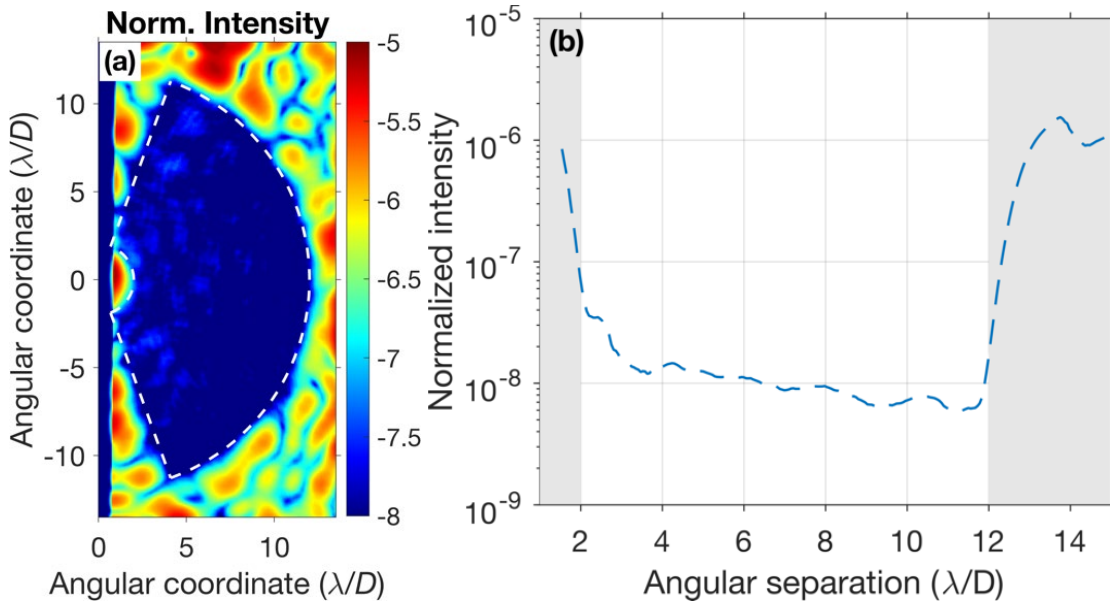


Fig. 25: (Left) Log normalized intensity achieved with DM#15. (Right) Azimuthal average profile within the dark hole region.

The contrast demonstrated is consistent with surface precision on the order of 0.1 nm. Furthermore, this performance is comparable to the contrast we achieved with a Kilo DM that did not undergo environmental testing, and therefore the testbed performance may or may not be limited by the DM and/or its electronics. This test demonstrated that a BMC DM can achieve high contrast after flight-relevant environmental testing.

Full details of this testing can be found in Appendix E.

3.5.2 Princeton High Contrast Imaging Laboratory

After vibration testing and re-characterization at BMC, two DMs were sent back to Princeton's HCIL. There were initial problems with the testing in that a number of actuators were not responding. This could be seen with the naked eye when tested. An engineering DM was inserted into the system and the same actuators were not working; thus, it was determined that the issue was the drive electronics. New high voltage driver cards were installed, and the issue was resolved. The DMs were then tested in the testbed. During these tests a single DM command produced varying surfaces. The surface variation could be determined by measuring the variation in the intensity over time for a set voltage command. Figure 26 shows this instability. The gap between each image is ~ 1 seconds. The variations seen corresponded to nanometer instabilities of the DM surface or $\sim 0.5V$ variations in the DM voltage control. The best contrast achieved was $\sim 2 \times 10^{-6}$ and the contrast varied by a similar amount. A series of tests were performed with engineering DMs that had not left Princeton and then same contrast was achieved as in previous tests. These results can be seen in Figure 27

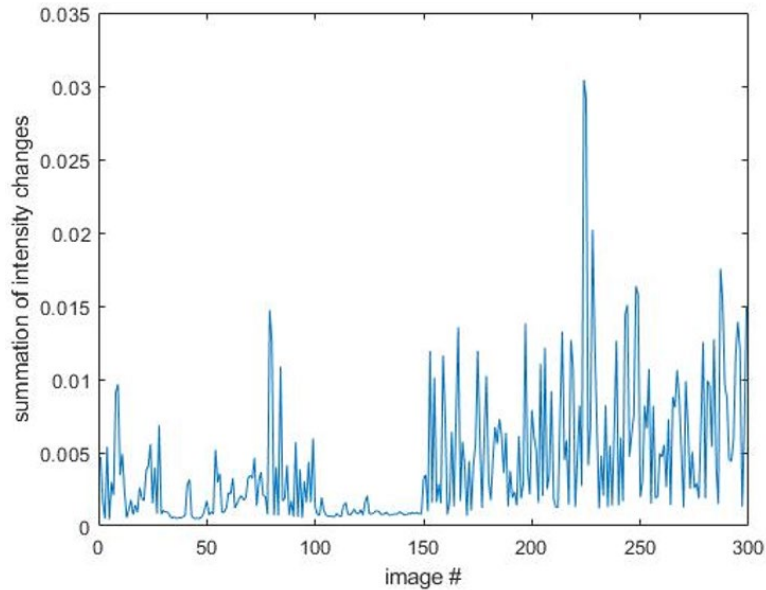


Figure 26: Intensity variation over time for a set voltage command

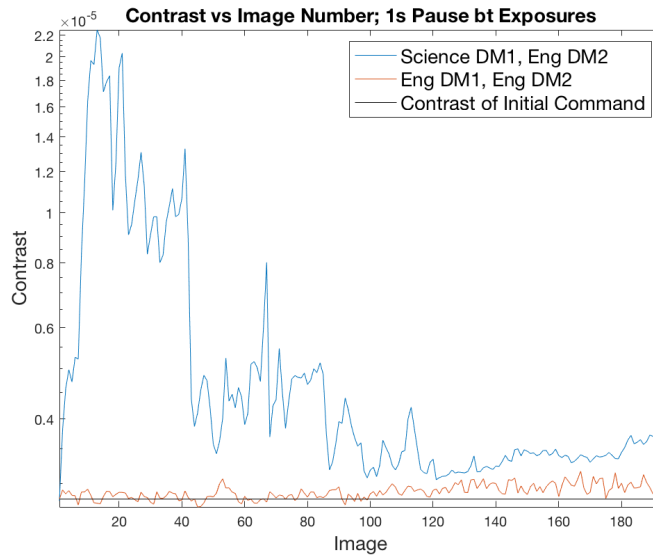


Figure 27: Plot comparing the contrast variations for the two cases where the blue line is the science/engineering DM combination, the red line is the two engineering DMs, and the black line is the initial contrast achieved by the DM command.

The project team tried to determine the cause of this instability in the DM actuators. The devices were returned to BMC for evaluation and characterization. A fishbone diagram was developed to evaluate potential causes. The surfaces were measured using a Zygo Verifire interferometer and no fluctuation or variation could be seen, but the projected variation ($\sim 1\text{nm}$ over $\sim 1\text{ sec}$) would not be measurable with that instrument. A careful inspection of the device, package and wirebonds did not show any cracks, delamination,

missing wirebonds, or other mechanical failures. One thing that was noticed was that there was contamination in different areas of the devices. Figure 28 shows a black residue on the pin grid array and underneath some of the wirebonds. This contamination was not seen previously on these devices. It does potentially look like residue from the packaging in which the DMs were transported. We were not able to determine if this contamination or some other instance that happened during testing was the cause of the instability in the actuators before the program ended.

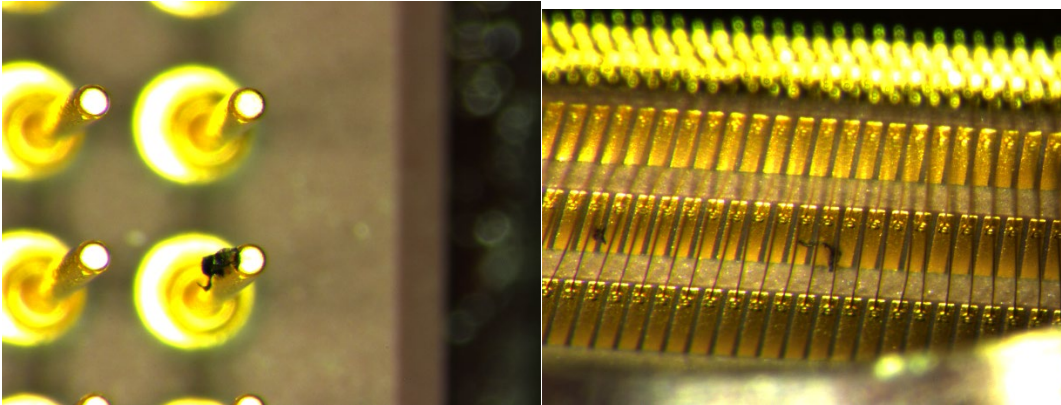


Figure 28: Examination of DM returned from Princeton showing an unknown residue

4. Conclusion

The objective of this project was to achieve a technology development milestone that demonstrates the capacity of the MEMS DMs to survive dynamic mechanical environmental stresses associated with launch and deployment in space. This objective was met. All steps proposed in this project were performed and results were presented. The MEMS DMs were fabricated to a predetermined specification and were exposed to a random-vibration level matching that of a launch load for a space telescope. Various tests were performed that showed that the random-vibration exposure did not affect the performance of the device in a surface characterization tools or in testbeds. There were tests that were determined to be inconclusive where the cause of unrepeatability was not confirmed to be caused by the environmental exposure.

4.1. Lessons Learned

MEMS fabrication: We experienced the sensitivity to micro-contamination in the fabrication process. In previous runs that we have performed, the micro-contamination did not pose a significant issue, as the performance criteria was not as stringent as those needed for a high contrast space-based program. BMC has put procedures in place to resolve these issues in future runs. Also, in MEMS fabrication we learned how sensitive the process was to the thermal budget applied to the phosphosilicate glass and the effects of phosphorus segregation on yield. By modifying this process we were not only able to

apply this process to the devices in this fabrication run, but to all other runs the company has produced going forward and increase the yield or reliability of DM produced.

Handling/Contamination: With a project of this nature, where devices were shipped all over the country and handled by many groups, procedures need to be in place for all handling and storage of devices. While there is no conclusive evidence that this has caused problems, it is a leading culprit. Steps have already been taken in projects after this program was completed in terms of careful documentation of handling, storage and transportation of BMC's MEMS DMs.

4.2. Future Work

Future work for the development of deformable mirrors for space-based exoplanet detection would involve two areas. First is the testing of MEMS devices after exposure to other environmental conditions. This project tested random-vibration, which was expected to be the most probable cause of failure of these DMs. There are other tests that can be performed such as shock, thermal vac, and radiation. Second, these tests could be performed on DMs with higher actuator counts. JPL has already performed the random-vibe testing on a 2000+ actuator device (see Appendix F) where "*BMC's 2K continuous face sheet MEMS deformable mirrors have passed 3-axis random vibration environmental testing at bounding launch loads encompassing those of future launch vehicles.*", and more tests could be performed with different environmental conditions or when a larger device is fabricated.

5. Abbreviations, acronyms, and symbols

BMC	Boston Micromachines Corporation
CDM	Continuous Surface Deformable Mirror
DM	Deformable Mirror
ESD	Electrostatic Sensitive Device
ExEP	Exoplanet Exploration Program
FFT	Fast Fourier Transform
FG	Force Gage
FOV	Field of View
GSFC	Goddard Space Flight Center
HCIL	High Contract Imaging Laboratory, Princeton University
HCIT	High Contrast Imaging Testbed, JPL
Hz	Hertz
in	inch
JPL	Jet Propulsion Laboratory
kg	kilogram
LTO	Low Temperature Oxide
m	meter
MEMS	Micro-electrical-mechanical
mm	millimeter
N/A	Not applicable
PCB	Printed Circuit Board
PSD	Power Spectral Density
RMS	Root-Mean-Square
S/N	Serial number
um	micrometer
VSG	Vacuum Surface Gauge

6. References

[1] Levine M, Soummer R, "Overview of Technologies for Direct Optical Imaging of Exoplanets," submission to ASTRO 2010 Science White Paper, <http://planetquest.jpl.nasa.gov/TPF-C/TechnologyAstro2010WP-VisiblePlanetImagingFinal.pdf>, (2009)

[2] National Academies of Sciences, Engineering, and Medicine 2021. Pathways to Discovery in Astronomy and Astrophysics for the 2020s. Washington, DC: The National Academies Press. <https://doi.org/10.17226/26141>

[3] http://exep.jpl.nasa.gov/files/exep/3-TDEM_Infrastructure_2012.pdf

[4] Lawson, P.R., Aguayo, E., Bierden, P., Helmbrecht, M., Levine, M., Lyon, R., O'Connell, M., and Trauger, T. "Environmental Testing Requirements for TDEM Deformable Mirror Technology," Jet Propulsion Laboratory, Doc, XXXX, 2013.

7. Appendix

7.1. Appendix A: Pre-Vibe JPL Testing

7.2. Appendix B: Initial Princeton Testing

7.3. Appendix C: Random-Vibe Test Plan

7.4. Appendix D: Post-Vibe JPL Testing in VSG

7.5. Appendix E: Post-Vibe JPL Testing in HCIT

7.6. Appendix F: 50 x 50 Testing

BMC DM Testing Progress and Results

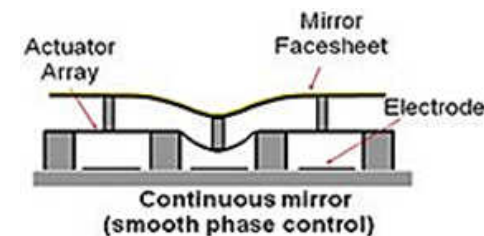
Frank Greer, Cory Hill, Brian Gordon, John Trauger

Background

- Boston Micromachines (BMC) DMs sent to JPL under TDEM for characterization
- Milestone Whitepaper (dated 12/9/2013) involving BMC, Boston University, Princeton University, and JPL written to outline tests for BMC MEMS DMs that:
 - “Demonstrate survivability and functional performance repeatability of the BMC 952-actuator MEMS CDM (Continuous Surface Deformable Mirror to within the noise floor of the various test equipment after exposure to dynamic mechanical environments representative of a range expected in coronagraph launch.”
 - Characterize the degree of degradation in CDM optical and electromechanical performance through functional test and interferometric surface mapping.
 - “The level of measurement repeatability in this series of tests will be 5nm using the BMC interferometer and <100pm using the JPL Vacuum Surface Gauge.” (currently measured to be ~50pm for VSG)
 - 33 μm per pixel resolution promised (VSG has been modified to 13.5 $\mu\text{m}/\text{pixel}$)
- DM model to be tested: BMC Kilo 32x32 (952-active actuators)

Table 1: Characteristics of MEMS Deformable Mirror

Mirror architecture	952 actuator continuous facesheet
Active aperture	9.9 mm Circular, 34 actuators across diameter
Actuator pitch	300 μm
Fill Factor	99.6%
Surface figure error	<5nm RMS, λ <400 μm
Surface Roughness	<2nm RMS
Mirror segment material	Silicon, 1000 Å gold coating
Actuator stroke	2 μm



Agreed upon VSG tests to be completed

1. Measure surface figure of BMC DMs at zero bias
2. Measure surface figure of BMC DMs for flat surface figure
3. Measure actuator gains for all 952 actuators for small up/down pokes about the flat surface figure condition
4. Measure drift in surface figure for "flat" condition for 48 hour period
5. Measure repeatability for "flat" and BMC/JPL solution for 10 repeats
6. Send mirror for environmental testing
7. Repeat VSG tests

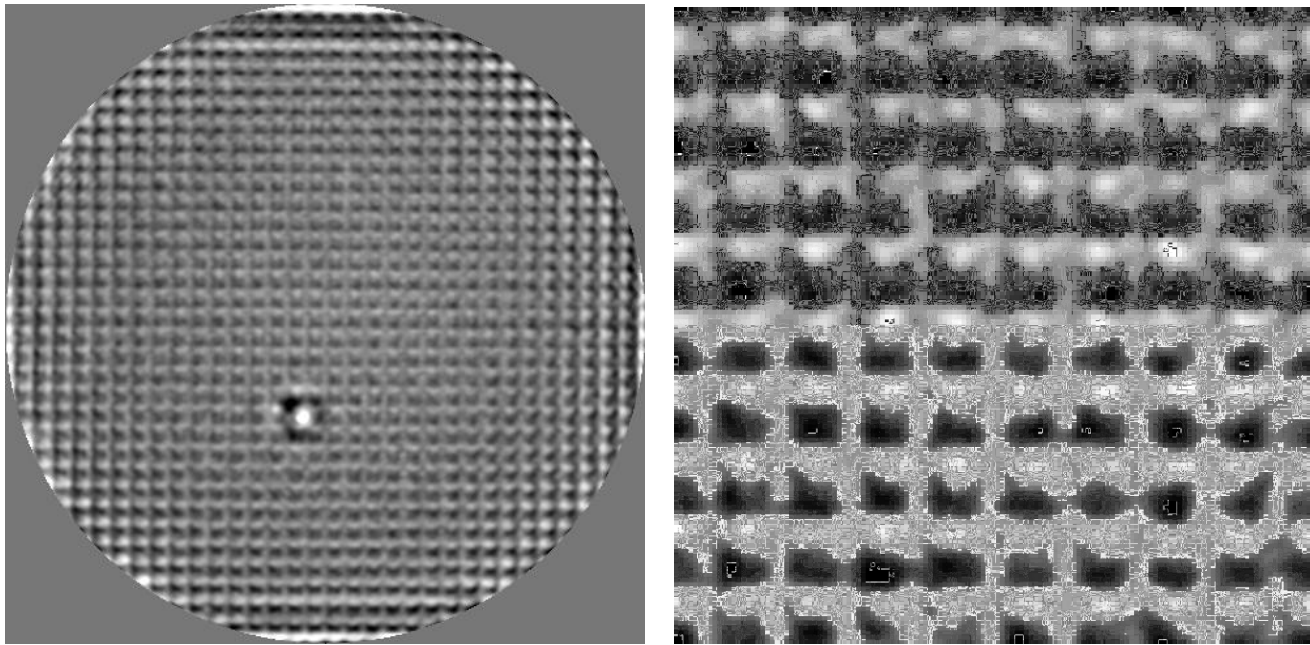
All of the above is complete for both mirrors. In addition, ZeMapper scans have been made of both mirrors in an unpowered state. ZeMapper measurements are consistent with VSG, and have proven useful in understanding anomalies observed by the VSG. Objective of today is to review the data and decide on next steps.

Protocols

- **Flattened BMC DM1 in the VSG to the following standards:**
 - 6.6nm PV focus, 2.9nm PV 45 deg astig, 0.3nm PV 90 deg astig, 7.6nm PV higher order terms
 - BMC reports 6.4 nm RMS for the flattened mirror in BMC measurements
- **Tested repeatability of a flat surface figure solution ten times, passing through an unpowered state each time prior to applying the “flat surface figure solution”.**
- **Tested settling time for the BMC mirror when applying the “flat surface figure solution” passing through an unpowered state for ~20 minutes prior to the beginning of the experiment.** The mirror was left powered for with this solution and was characterized frequently over a 48 hour period.

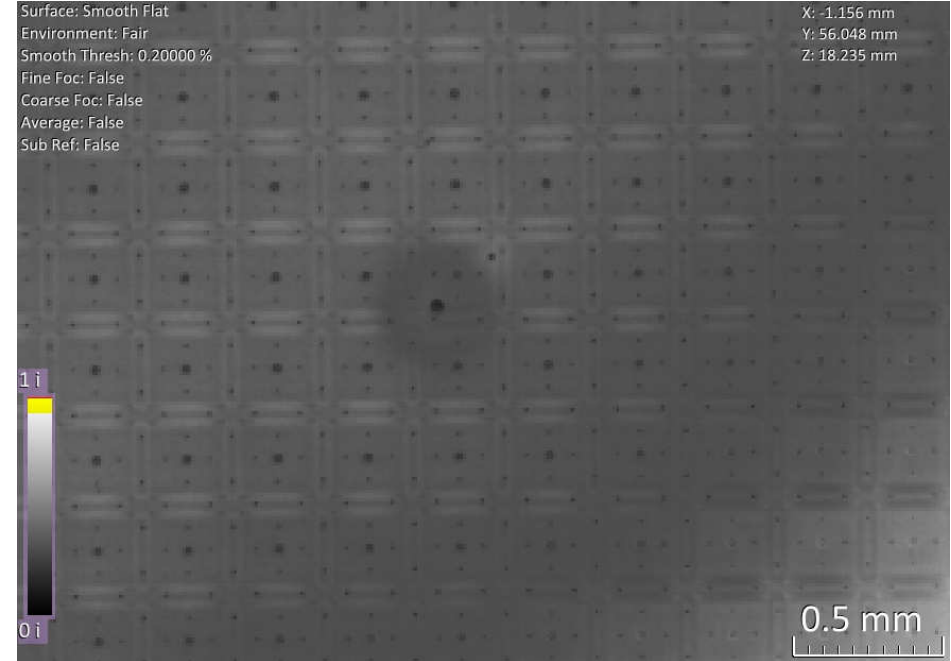
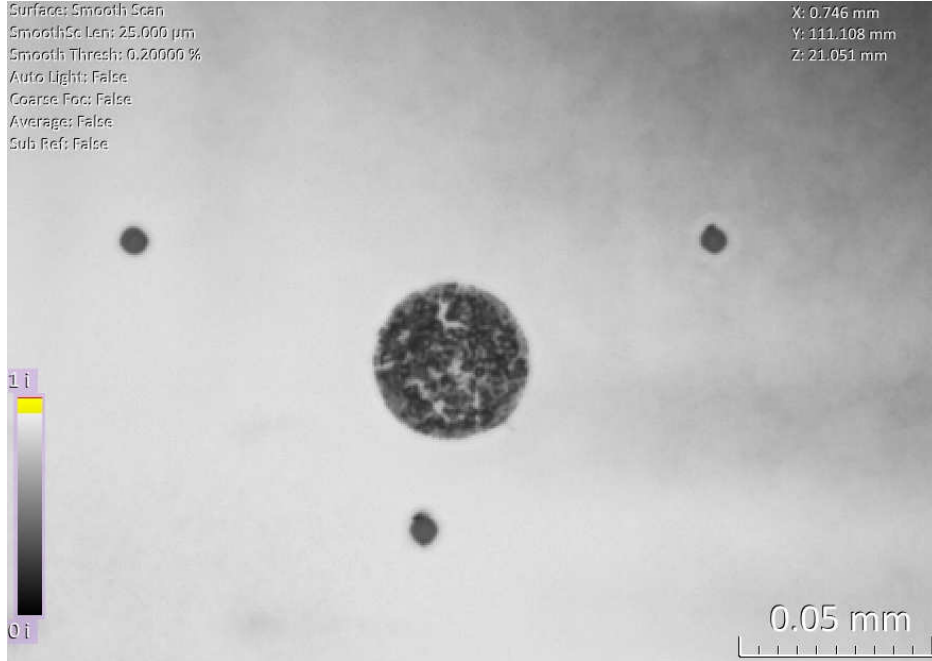
DM1 Mirror Surface after Flattening

Focus and astigmatism removed



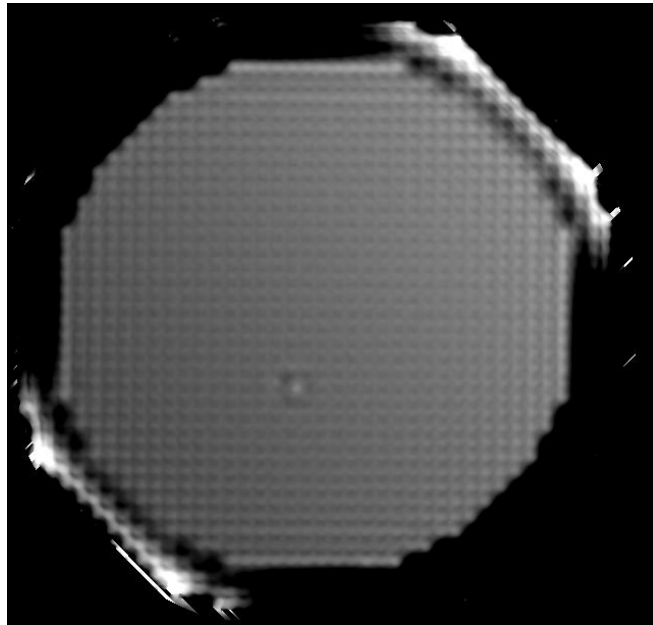
VSG measurement = 7.5 nm RMS residual due to actuator shape
Defect observed

Visual Images of Defects on DM1

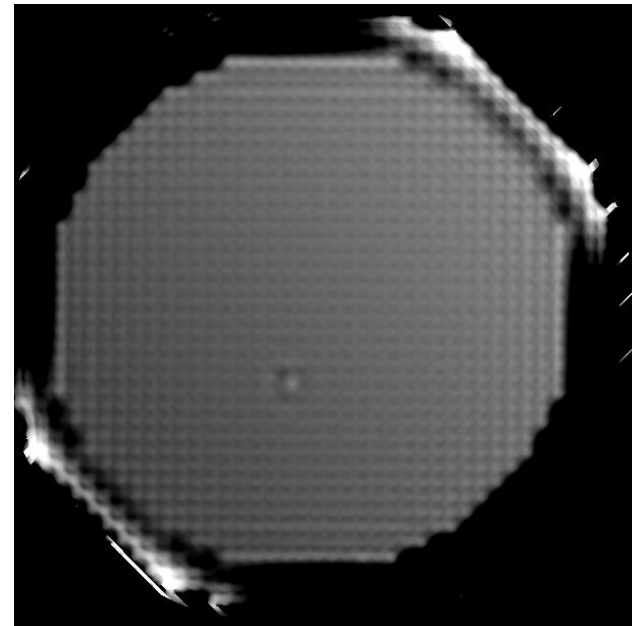


Comparison of first phase map and last phase map from repeatability test

Beginning of repeatability test



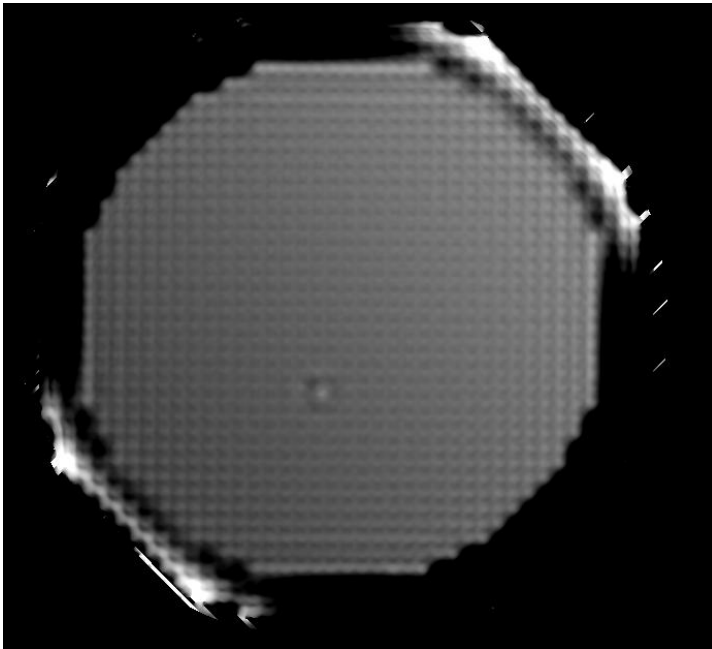
10th iteration



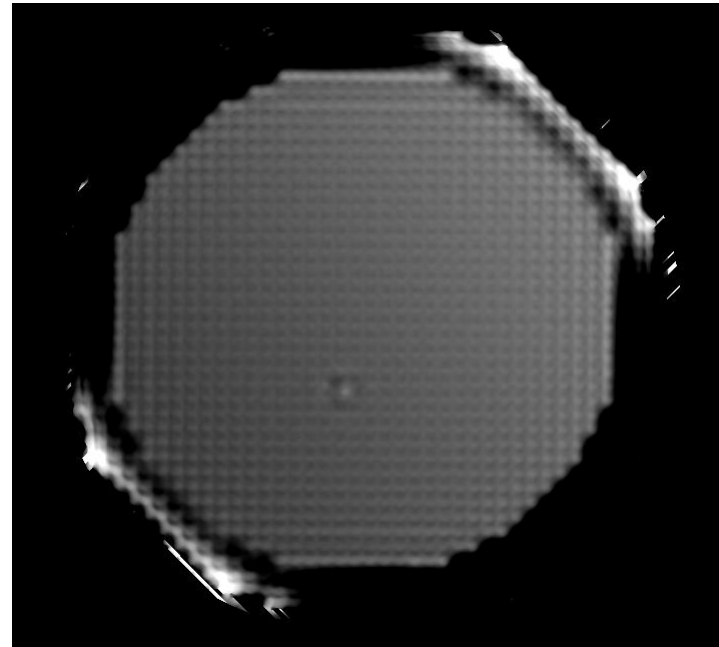
No significant changes observed in the repeatability test (difference map 1.4nm RMS)

Phase maps before and after settling test

**Phase map before
DM1 settling test**



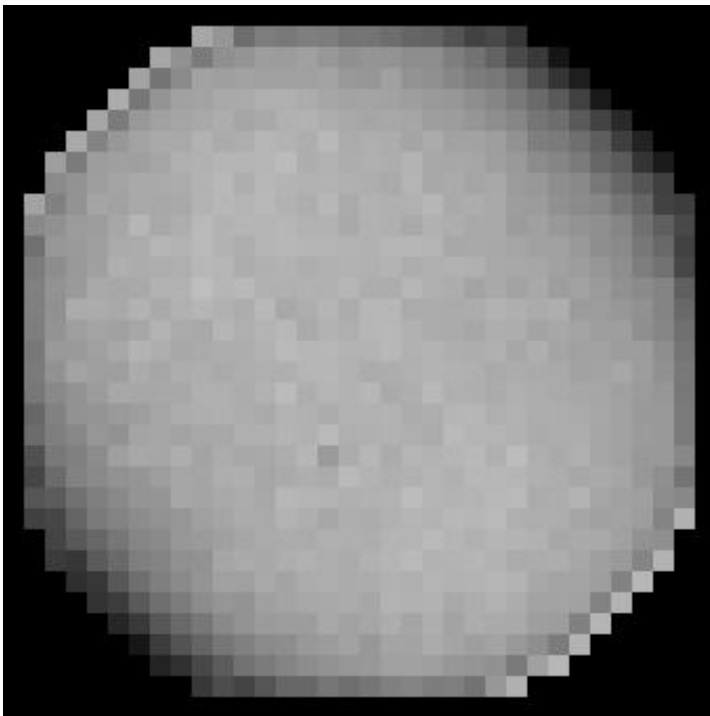
**Phase map after
DM1 settling test**



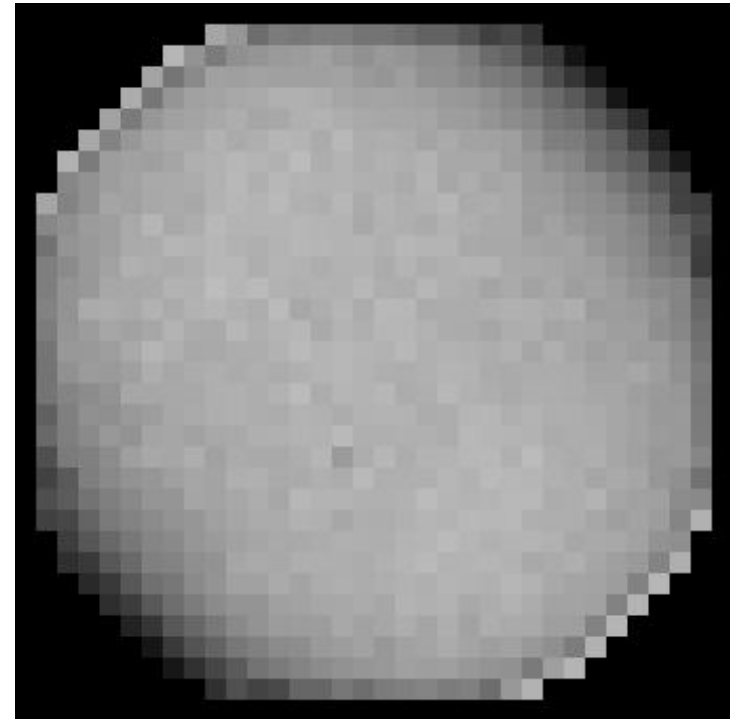
No significant changes observed in the settling time test (difference map is 2.1nm RMS)

Gain Maps Collected Before and After Settling Tests

Gain map before settling test

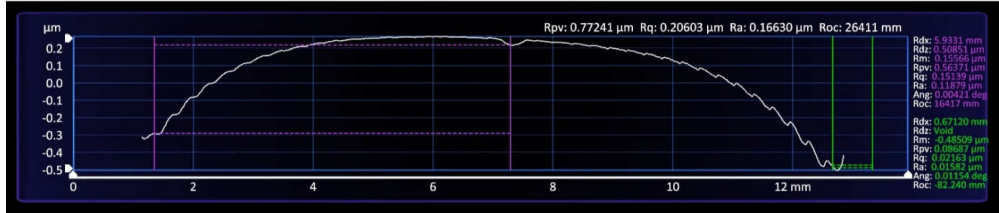
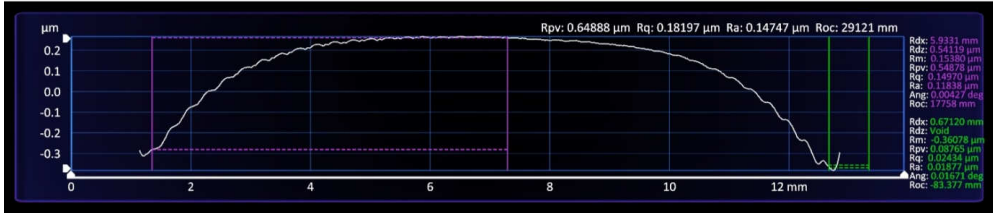
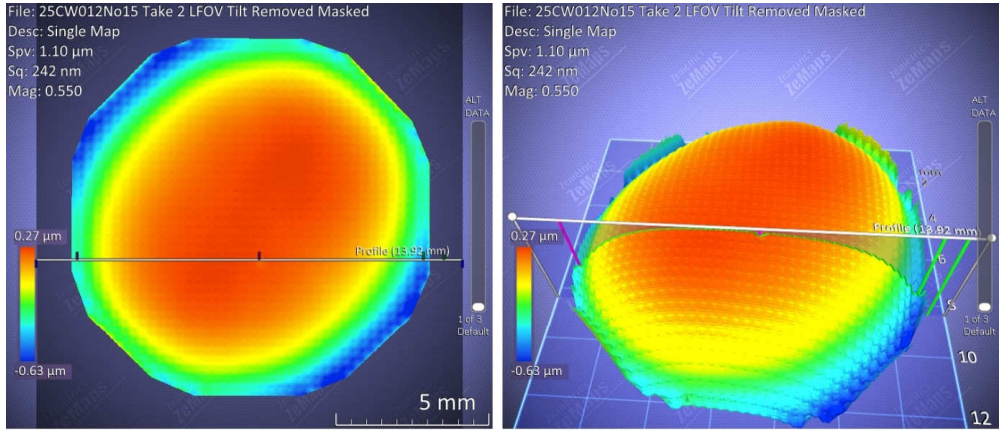
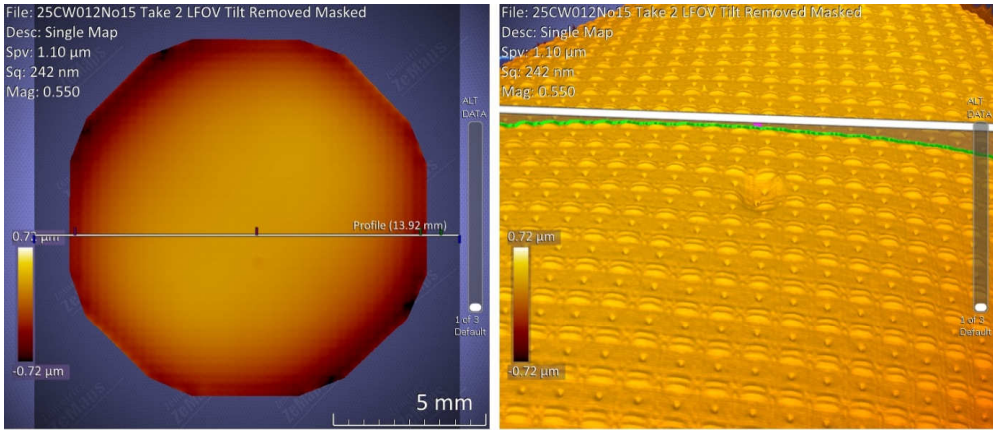


Gain map after settling test

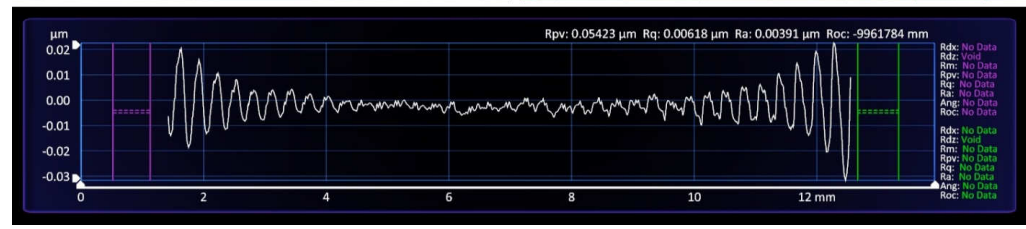
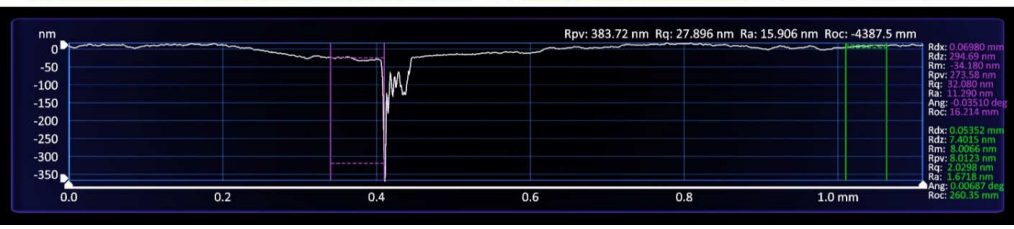
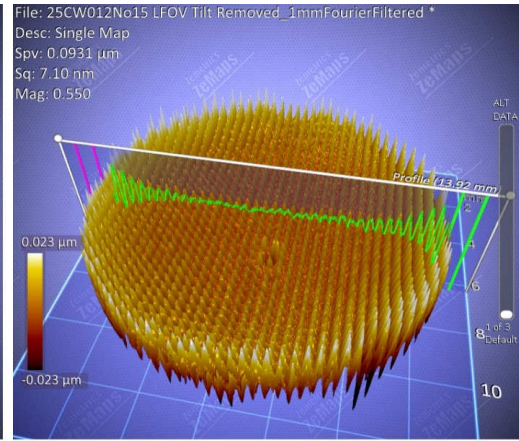
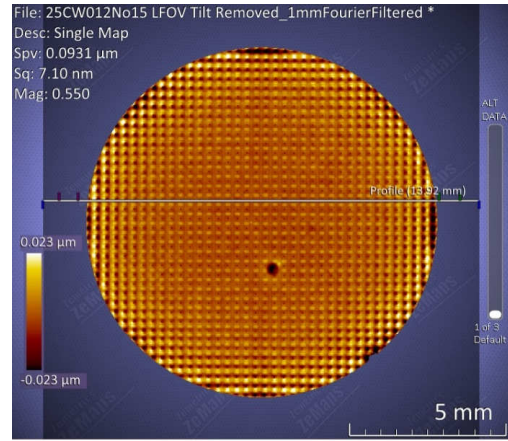
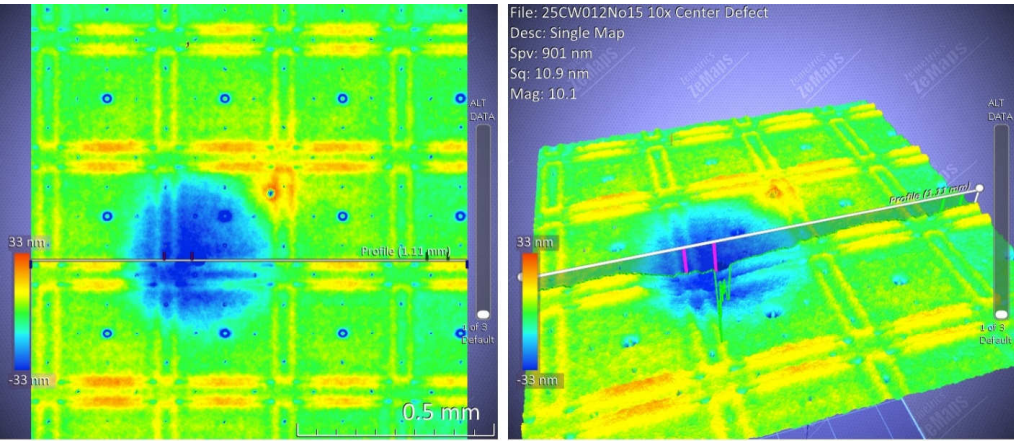


5 – 10 nm/V
stretch

Measurement of DM1 with MDL ZeMapper – Done After Testing

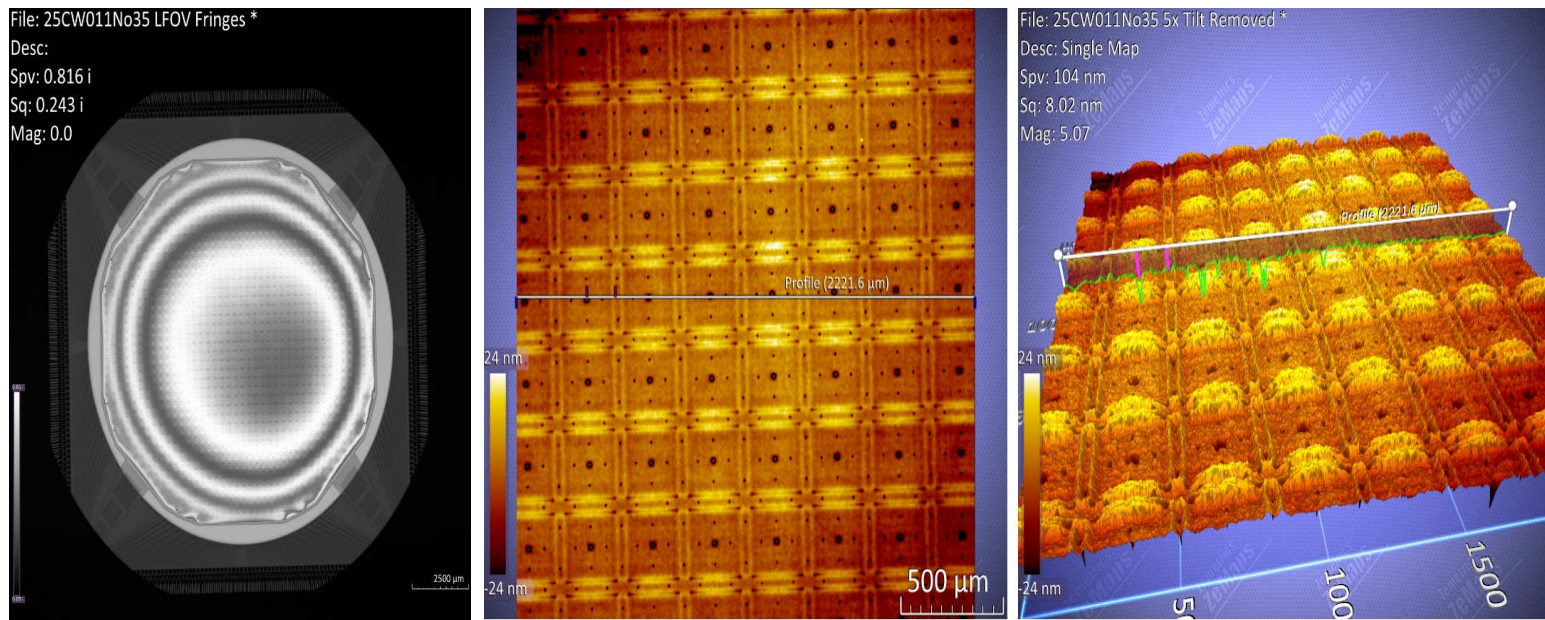


Measurement of DM1 with MDL ZeMapper – Done After Testing



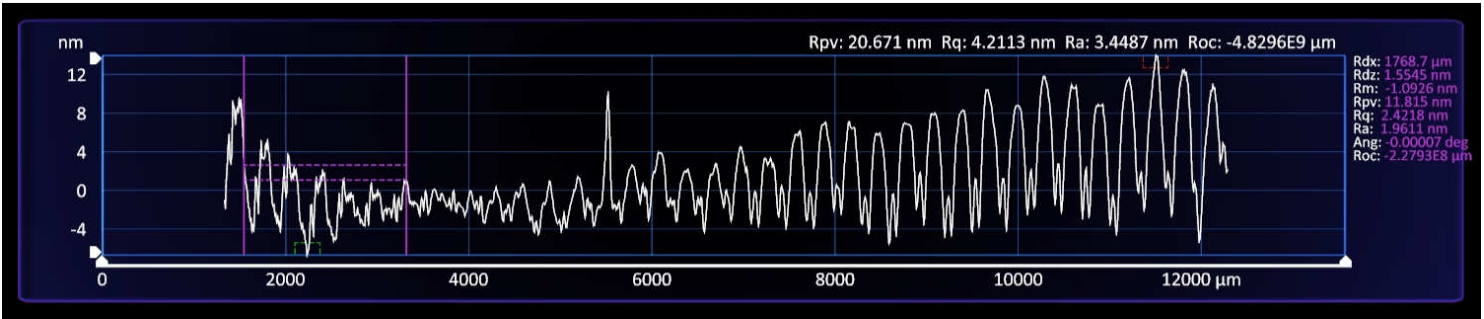
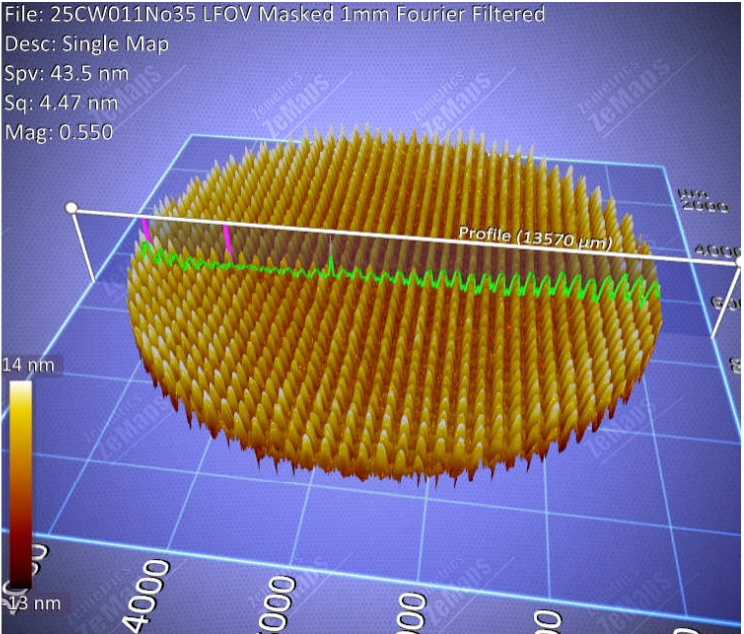
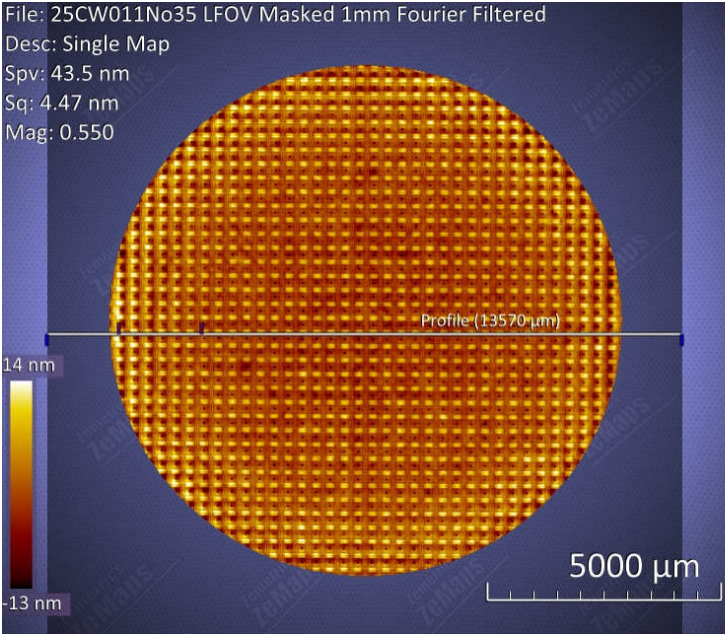
DM2

Measurement of DM2 with MDL ZeMapper – Done Before Testing

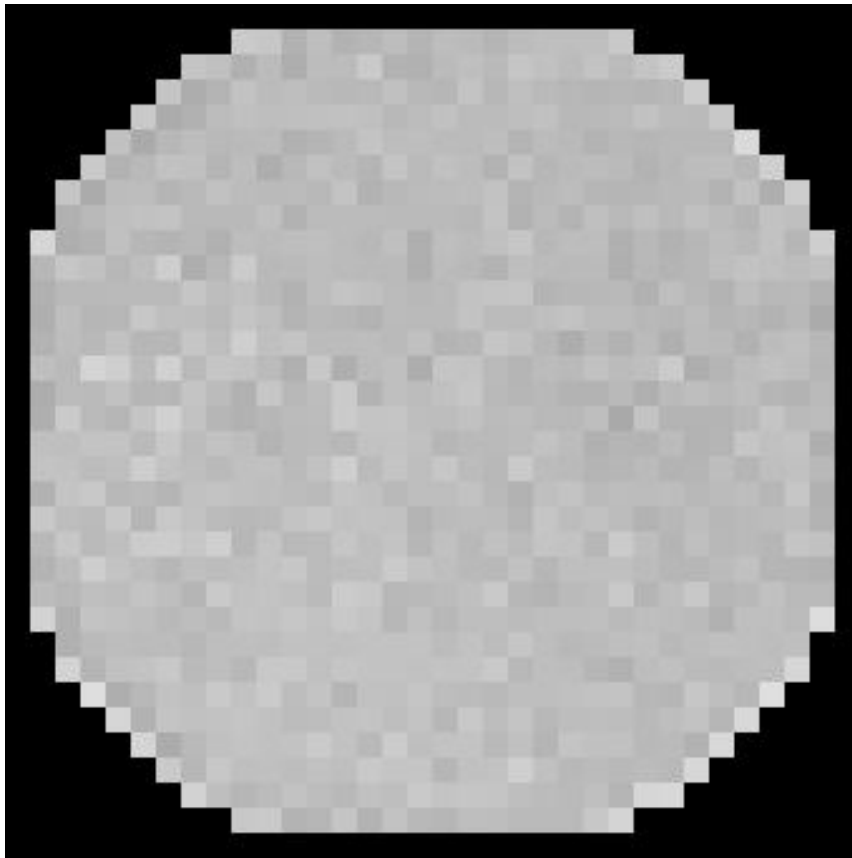


ZeMapper measurement: 7.3 nm RMS residual due to actuator shape

Measurement of DM2 with MDL ZeMapper – Done Before Testing



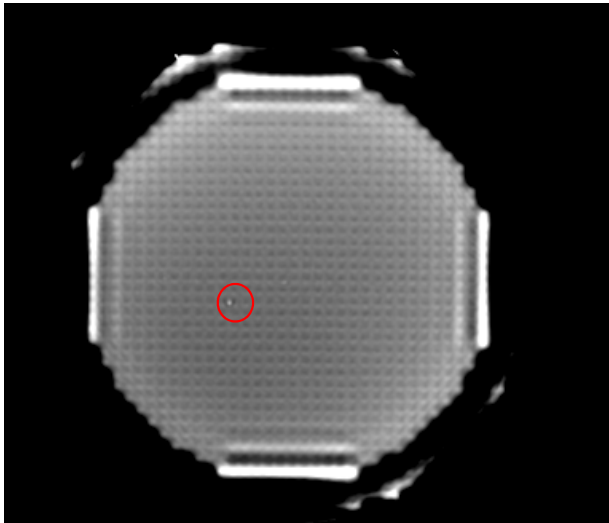
DM2 Actuator Gain from First 5x5 Poke Experiment



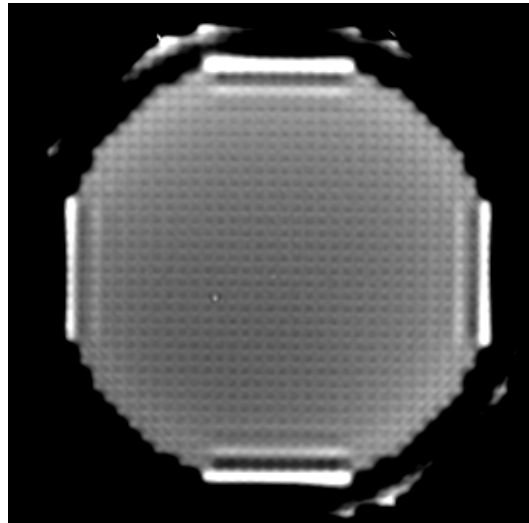
Scale 5 -10 nm/Volt

Repeatability Test for DM2

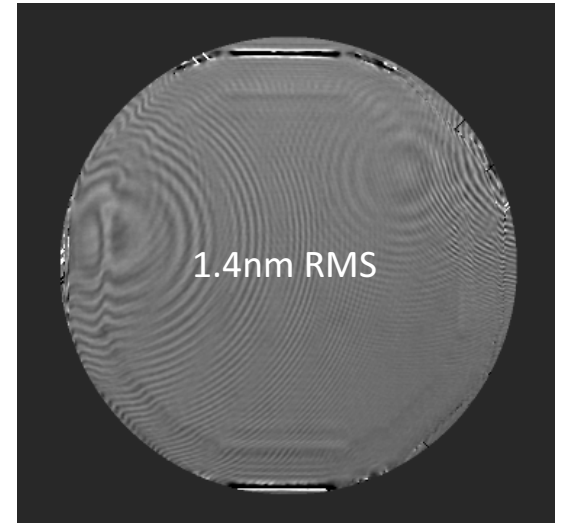
“Flat” solution after ~5 days of bias



“Flat” solution 10 iterations
of zero volts to “flat”



Difference Phase Map

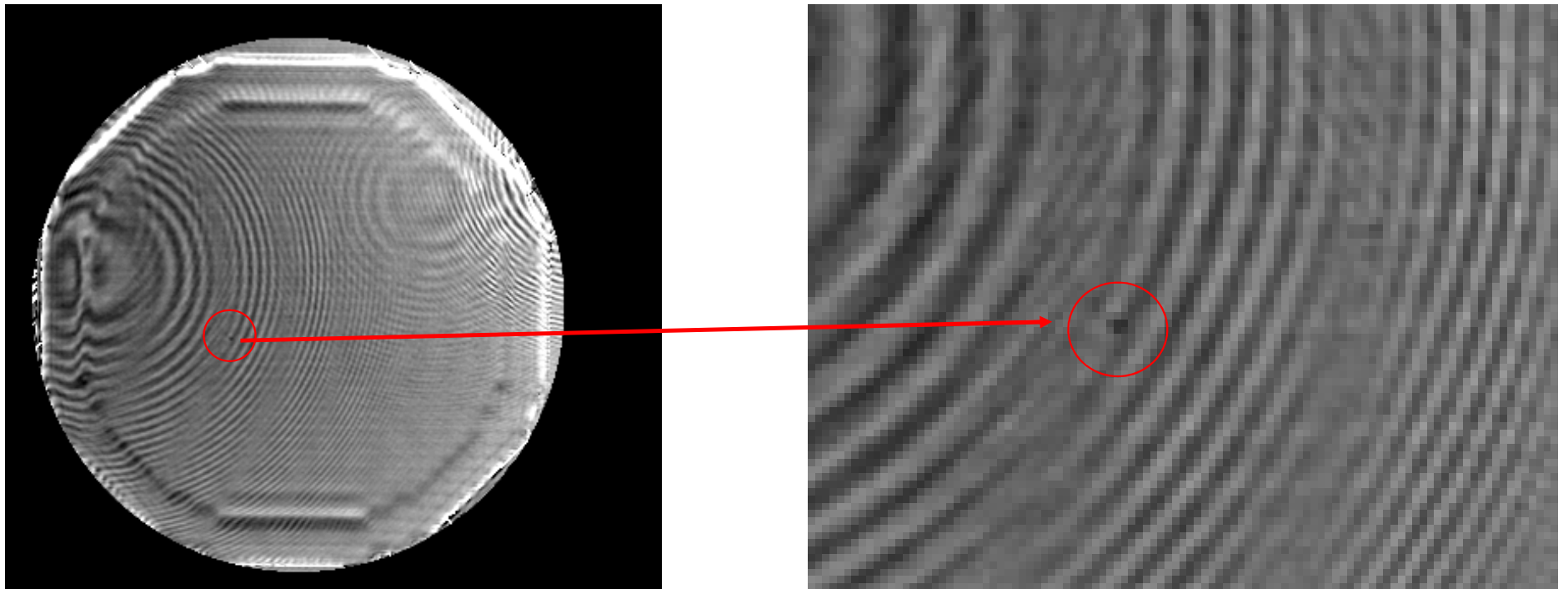


No obvious differences between maps. Encouraging sign for most actuators that needs to be confirmed with quantitative calculations

New potential defect has appeared on the mirror. Need to recheck ZeMapper after DM2 is removed.

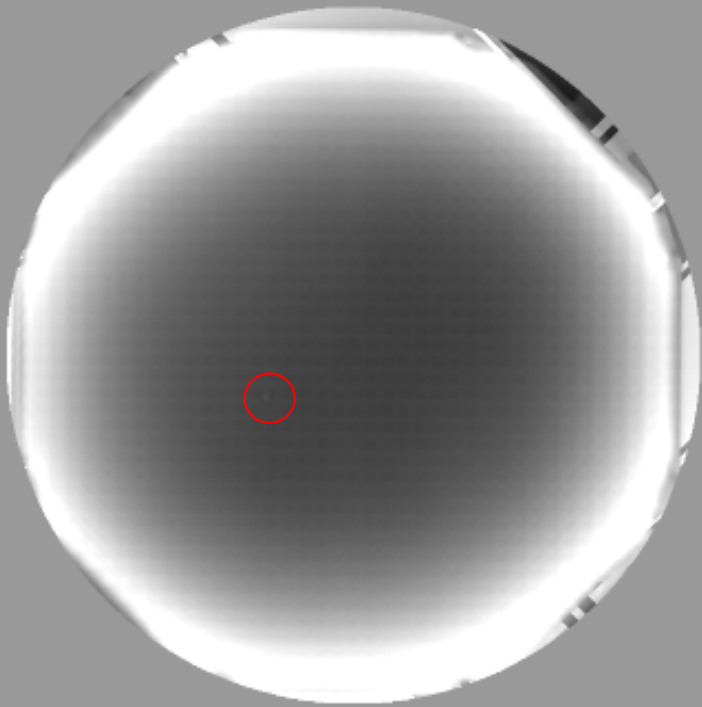
Difference phase map from beginning repeatability test to end of DM2 settling test

After 68 hours, defect appears to be getting worse, but otherwise, drift appears minimal. Needs quantitative validation

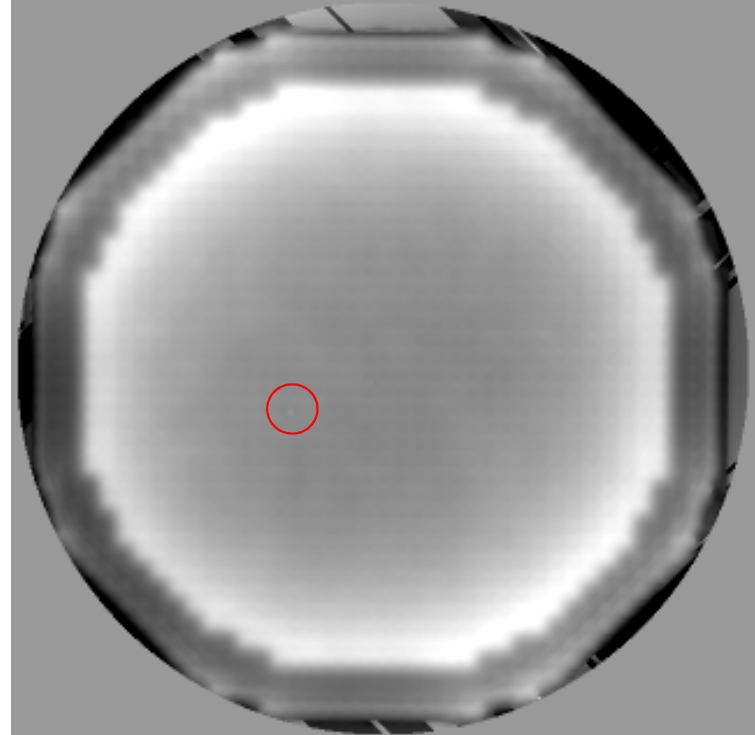


Defect status at beginning of DM2 testing

First unpowered phase map



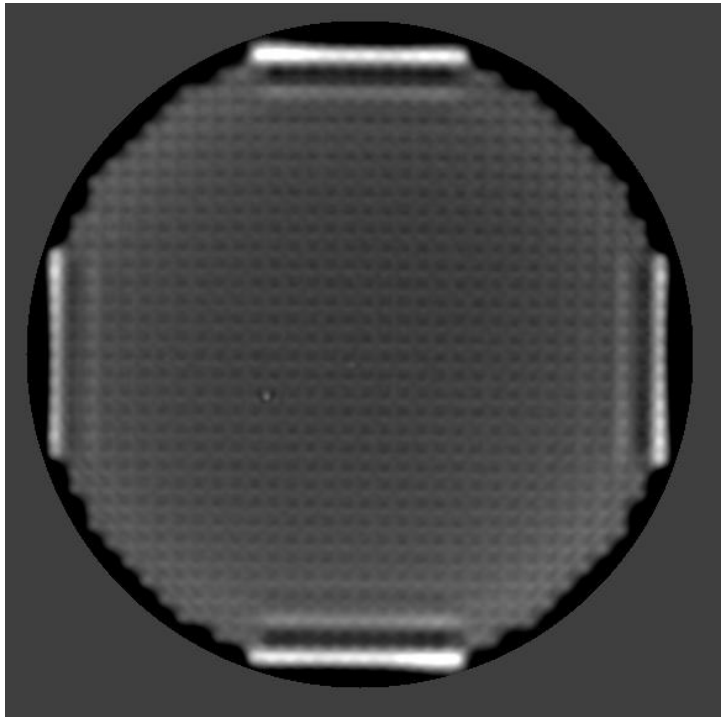
First 100V flat voltage phase map



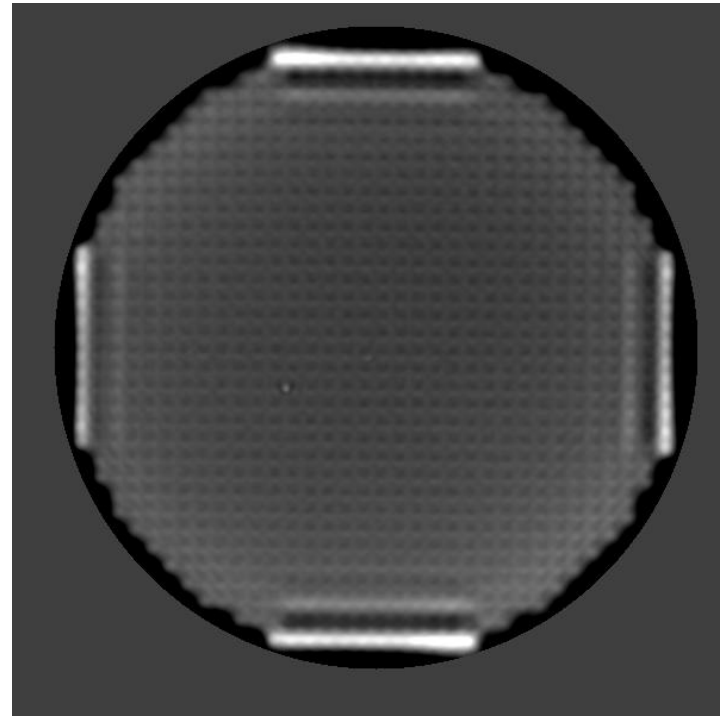
Defect present at very beginning of testing before power was applied. Did vacuum cause it?

Comparison of flats from DM2 settling test

First map



Last map (51 hours total)



No significant changes observed in the settling time test (difference map is 0.9nm RMS)

Remaining analysis and experimental tests

- Sine wave application to test linearity of influence function
- ZeMapper post measurement
- Others?

Test Report of the BMC Dual Kilo-C-DM Deformable Mirror System in HCIL

He Sun^a and N. Jeremy Kasdin^a

^aPrinceton University, Princeton, NJ, the United States.

1. INTRODUCTION

This document explains the various testing activities of the Boston Micromachines Corporation (BMC) 2nd generation continuous facesheet kilo deformable mirror (DM) systems. The objective of the testing is to verify the performance of the DMs in a real high precision adaptive optics/wavefront control and estimation system. All the experiments were conducted in the High Contrast Imaging Lab (HCIL) at Princeton University.

In this report, we start by introducing the setup of the HCIL testbed. Then we explain the procedure to characterize some DM properties which are necessary for wavefront control and estimation experiments. Some of them are not perfectly in accord with the information on the user manual. Then, we check the inner working angle (IWA) and the outer working angle (OWA) of the system, which defines the largest effective working region of the DM in the image plane. Some wavefront correction experiments using different algorithms are reported in the following section and we also show the recovered DM gains and compare them with the data from BMC. Finally, we report accidents that occurred during the testing period and conclude the testing results.

2. HIGH CONTRAST IMAGING LAB AT PRINCETON UNIVERSITY

The HCIL is designed to study state of the art technologies for exoplanet direct imaging. Usually, an earth-like exoplanet is 10^{-10} times fainter than its parent star. Considering the finite aperture of the telescope, as shown in Fig. 1 (a), the planet image is covered by the star's Airy pattern. One solution to that problem is a coronagraph. Consisting a series of masks and stops, a coronagraph modifies the point spread function (PSF) of the imaging system and creates regions with extremely high contrast, as shown in Fig. 1 (b), so the exoplanet can be detected in the so-called dark holes. However, a weakness of the coronagraph is its fundamental sensitivity to optical aberrations. Even small aberrations bring significant starlight leakage (Fig. 1 (c)), so deformable mirrors (DMs) are necessary in this system to actively compensate the wavefront errors.

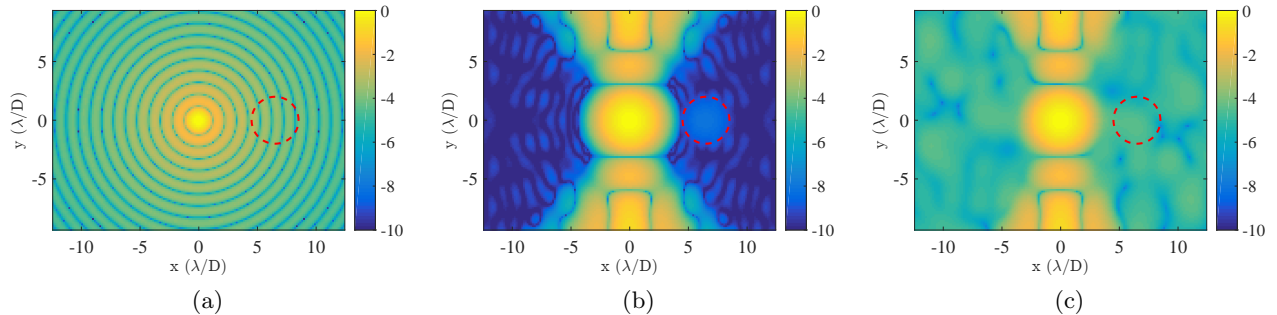


Figure 1. Right circles indicate the planet locations. (a) Planet 10^{-8} times fainter disappears in the star light Airy pattern. (b) Exoplanet is detected in the high contrast regions by coronagraph. (c) Optical aberrations cause contrast degradation in the dark regions, so the faint planet disappears again.

Figure 2 shows the layout of the HCIL testbed. The laser source is used to simulate the light from the star and/or exoplanet. After collimation by an off-axis parabola (OAP), the light arrives at the BMC DMs under test. The wavefront after corrections then passes the shaped pupil mask, reflects off another imaging OAP (simulating the primary mirror of the telescope), and is imaged in the focal plane. A focal plane mask (FPM) is placed in front of the stars image to block the bright parts of the PSF, avoiding saturation of the camera. Instead of

classical adaptive optics based on pupil wavefront sensors, a focal plane wavefront correction procedure is applied in the HCIL system. As the left part of Figure 2 suggests, the focal plane electric field is directly estimated from the final images, and then the DM commands are computed by model based optimization.

For convenience, the frequently used concepts and notations in the following statement are pre-defined here. The contrast of a pixel is defined as the ratio of the local intensity and the central intensity of the PSF. The star light wavelength is denoted as λ and the aperture diameter is denoted as D . In the image plane, the distance is usually measured using the unit of λ/D , which physically represents the angular separation between objects.

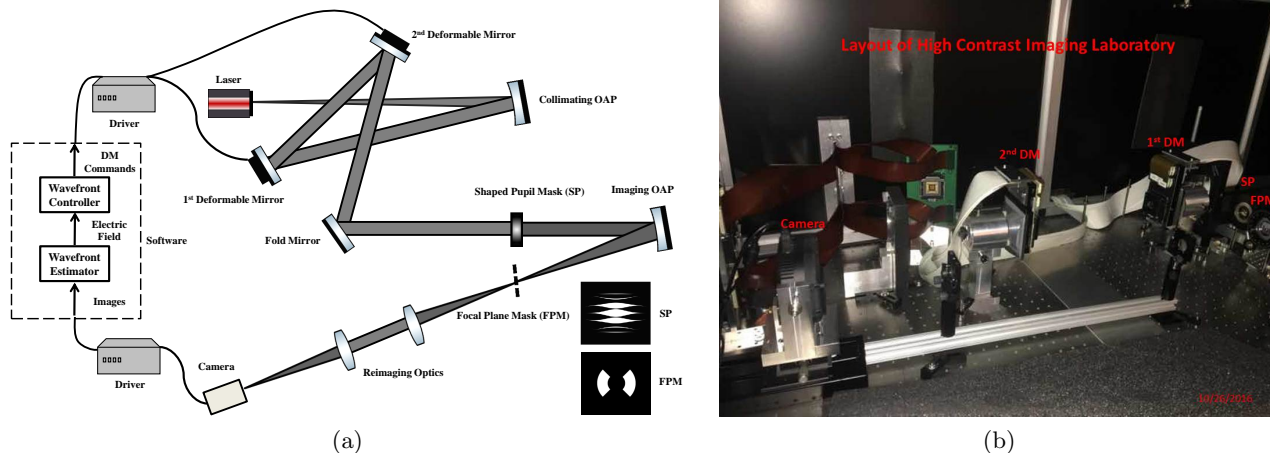


Figure 2. (a) Concept diagram of HCIL layout. (b) HCIL testbed image after implementing new DMs.

3. CHARACTERIZATION OF DM PROPERTIES

In this section we describe a few of the characteristics of the DMs that are critical to their use for high-contrast imaging and what we found in working with the specific mirrors.

3.1 DM surface

To achieve dark holes with high contrast, the correction scheme requires a good initial starting contrast; i.e., the nominal aberrations in the system need to be small enough that the control system will converge. This implies the need for a reasonably flat initial surface on the DM. Our approach to testing the DM surface flatness is by imaging the PSF of the system. Such a test is shown in Fig.3 with the BMC supplied DMs.

Figure 3 (a) is the measured PSF in the HCIL after replacing both DMs with flat mirrors. The average contrast in the 5 to $11\lambda/D$ wedged areas is 4×10^{-5} . Figure 3 (b) shows the PSF after replacing the flat with the two unpowered DMs; the resulting contrast degrades to 1×10^{-3} . The highly distorted PSF that results can only be corrected by the wavefront control algorithm to a contrast of at best 1×10^{-5} . After applying a flattening voltage map, the DM surface can be brought to flatness that corresponds to a contrast of roughly 1×10^{-4} , slightly worse than the flats but good enough to achieve a final average contrast after control of 2×10^{-7} . Figure 3 (c) is an example of the measured PSF after control starting with a flat voltage map. Note that this PSF has a slightly worse contrast of around 3×10^{-4} in the dark hole. That is because this particular image was taken after the failure of one actuator resulting in higher light leakage into the dark hole. However, the final achievable contrast changes little with only one dead actuator because the focal plane wavefront correction does not require the DM shapes to exactly conjugate the pupil aberrations.

3.2 Actuator pitch

Another key characteristic of the DM that factors into the control model is the actuator pitch. This needs to be known so that the proper spatial frequencies are commanded by the controller. The quoted actuator pitch in the user manual is $300\mu m$. However, that number does not match our calculations made from camera images. In

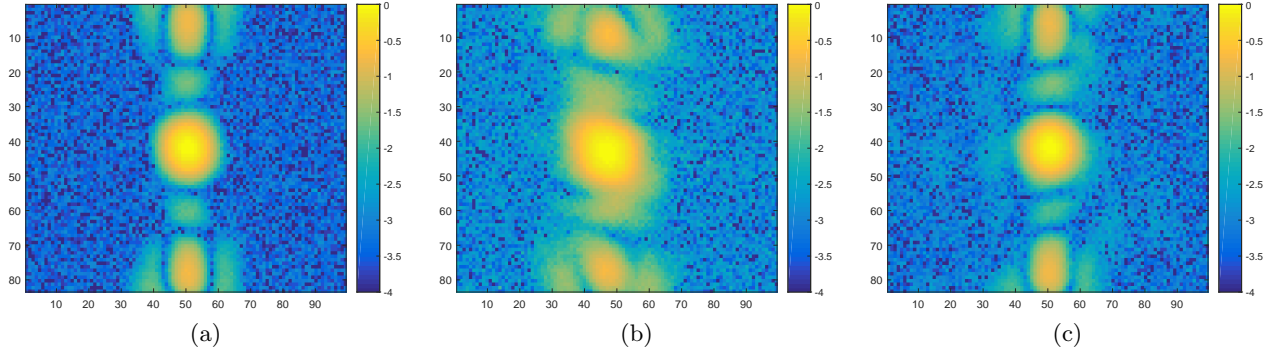


Figure 3. The pixel size of the camera images above is around $0.24 \lambda/D$ (a) Measured PSF with flat mirrors replacing the DMs. Contrast in the working areas is around 4×10^{-5} . (b) Measured PSF without flattening the DM surfaces. The PSF is strongly distorted and the average contrast in the working areas is around 1×10^{-3} . (c) Measured PSF after flattening the DM surfaces. There are some star light leaks because of one dead actuator, and the average contrast is around 4×10^{-4} .

particular, the actuator pitch can be found by placing a known spatial frequency on the DM and observing the location of the mapped PSFs. Since the relationship between the image plane and pupil plane (approximately the location of the DM) is a Fourier transform, placing a sinusoid on the DM creates two copies of the PSF at the corresponding spatial frequency locations in the image (by the Fourier shift theorem).

The separation of the PSF copies can be used to calculate the DM pitch size, since it depends on the spatial frequency of the sine wave. By alternately giving the DM actuator columns $+1$ or -1 volt commands, we create a sine wave with the angular frequency $\omega = D/(2 \times p_{act})$ cycles, where p_{act} is the pitch size of an actuator. The measured PSF separation in the image plane is around $17.8\lambda/D$ and the aperture diameter D is $10mm$, so the calculated actuator pitch is

$$p_{act} = 10mm / (2 \times 17.8) = 0.281mm = 281\mu m. \quad (1)$$

This calculated pitch size is 6.3% smaller than the reference value, $300\mu m$, which is enough to affect the control capability. For the experiments described below we used this measured value of the pitch.

We note that other effects can create an apparent change in pitch size. For example, if the laser source is not well collimated by the first off-axis parabola (OAP) (that is, is slightly off focus), a converging beam results in shrinking the pupil at the DM. Likewise, a residual curvature on the DM will also lead to a converging beam. Both of these result in an apparent reduction in DM pitch from the measurement above. An accurate measure of the curvature of the DM can help determine the source of the pitch error.

4. WAVEFRONT CONTROL AND ESTIMATION

In this section, we display the results of our experiments using the DMs in the focal plane wavefront control system.

4.1 Inner and Outer Working Angles

The IWA and OWA define the controllable regions in the image plane. By gradually increasing the size of desired dark holes and running focal plane wavefront control, the largest OWA and smallest IWA achievable with the DMs are determined. According to Fourier optics, the IWA and OWA in fact reflect the ability of the DMs to create shapes with different spatial frequencies, so the IWA and OWA also partly reflect the inter-actuator coupling of the DM.

As mentioned in the previous section, to correct a bright spot in the image plane, a sine wave with specific spatial frequency is applied to the DM. The further the spot is from the PSF center, the higher the spatial frequency needed to correct. The second generation DMs consist of a 34×34 array of actuators, so the largest spatial frequency achievable is $34/2 = 17$ cycles/aperture. Consequently, the theoretical limit of the OWA is

$17\lambda/D$. The designed IWA of the shaped pupil coronagraph on our testbed is $4\lambda/D$, so the smallest IWA the system can achieve is also $4\lambda/D$.

Previously, with two 1st generation BMC DMs ($32 \times 32 = 1024$ actuators on each), high contrast was only achieved in two small rectangular dark holes from $7\lambda/D$ to $10\lambda/D$ horizontally and $-2\lambda/D$ to $2\lambda/D$ vertically (Fig. 4(a)). The new second generation DMs allowed us to significantly enlarge the size of the effective working regions, achieving almost the same limiting contrast (2×10^{-7}) in two wedged regions of 85 degrees from $6\lambda/D$ to $11\lambda/D$. Of note is that this is the first time we demonstrated successful dark holes with more pixels than actuators on the DM. Fig. 4(c) shows an even larger dark hole (85 degrees, $5\lambda/D$ to $14\lambda/D$, 3572 pixels) but at a lightly reduced contrast of roughly 10^{-6} . The IWA and OWA of the system are now approaching their theoretical limits.

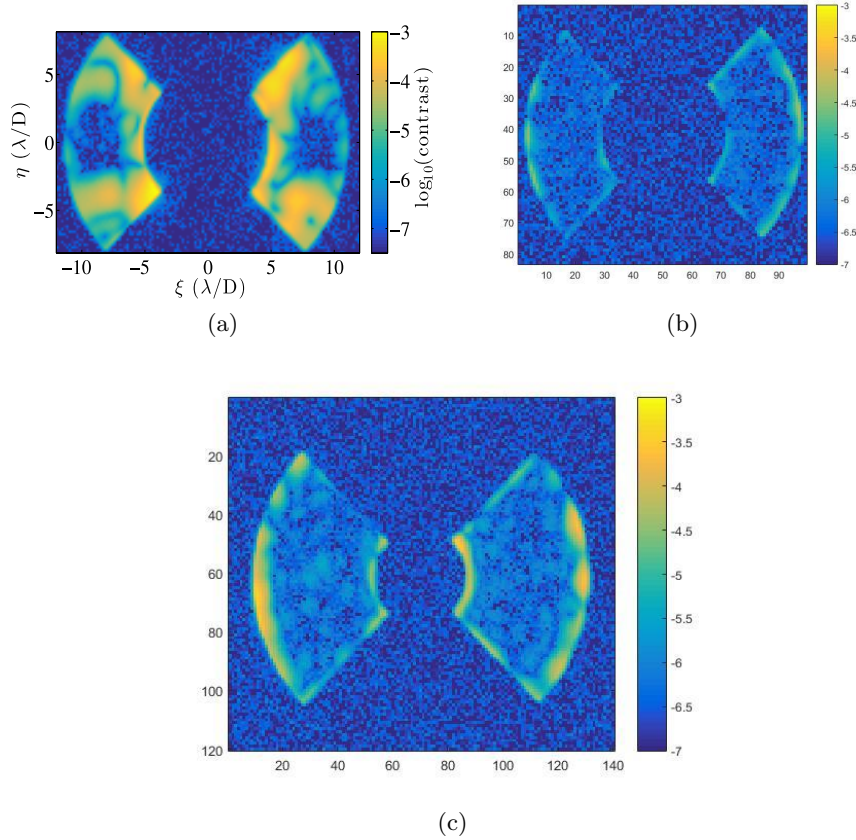


Figure 4. Final camera images after wavefront corrections. (a) The largest dark holes achieved by the old DMs. Dark hole regions are from 7 to $10\lambda/D$ horizontally and -2 to $2\lambda/D$ vertically. The measured average contrast in the dark holes is 2×10^{-7} . (b) 6 to $11\lambda/D$ and 85 degrees wedged dark holes achieved by the second generation DMs. The measured average contrast is also 2×10^{-7} . (c) 5 to $14\lambda/D$ and 85 degrees wedged dark holes achieved by the second generation DMs. The measured average contrast is 9×10^{-7} .

4.2 DM gains and Correction speed

Correction speed is defined as the number of wavefront control iterations used to reach a desired contrast. Since model predictive control is applied in the lab, there is a direct relationship between the correction speed and the quality of the DM model. Using common practice, we model the DM as the linear superposition of influence functions. In that ideal case, none of the actuators are coupled and the DM height is proportional to the input

voltages. Mathematically, the DM surface shape is represented as

$$\Delta\phi(x, y) = \sum_k u_k \alpha_k f(x, y), \quad (2)$$

where $\Delta\phi(x, y)$ is the DM surface shape, u_k is the input voltage of the k -th actuator, α_k is the corresponding actuator gain and $f(x, y)$ is the normalized influence function of a single actuator. The DM gain is defined as the maximum height change given a unit command.

For our control we use the same influence function for each actuator. The influence function shown in Fig. 5 (a) was measured by Remi Soummer’s group at the Space Telescope Science Institute. Based on the voltage-deflection relations from BMC, the DM gain is quasi-linear with the voltages. The initial flattening voltages are quite uniform in the central region, so the gains of the center actuators are almost the same. Based on several trials of wavefront correction experiments, the best gains for DM1 and DM2 are respectively $5.1nm/v$ and $6.3nm/v$, which is a little smaller than the calculation from provided data. Although we don’t know the exact values, given those calculations, the wavefront correction converges and reaches a measured contrast limit of 7×10^{-7} in around 25 iterations (black curves Fig. 6).

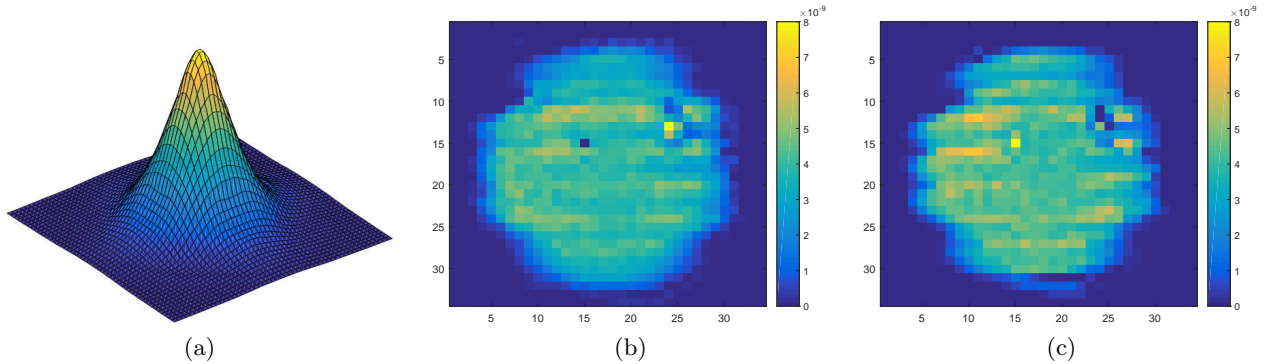


Figure 5. (a) The influencing function of a single actuator. (b) The recovered gains of the first DM. (c) The recovered gains of the second DM.

Recently, we conducted system identification on the system and directly estimated the image plane response to DM commands. Using the estimated model, the wavefront correction speed increased significantly and reached a lower contrast limit as indicated in Fig. 6. The different curves represent different estimation approaches, including a batch process, Kalman filter and extended Kalman filter. Fitting the DM actuator gains to the estimated image plane response, we get an estimated gain map as shown in Figs. 5 (b) and (c). Since the surrounding actuators are blocked by the shaped pupil, it seems that we cannot recover the gains of those actuators. Some dead spots (actuators with zero or negative gains) are also observed in the estimated gain map. Apart from those, the fitted DM gains of the central area are also not as uniform as we expected. That partly verifies our concerns that different actuators on the DMs may have slightly different influence functions and/or voltage-deflection relations. It is clear that a better influence and voltage-deflection map for each actuator could significantly improve performance.

5. PROBLEM DURING TESTING

During the testing period, we in total encountered 4 problems or accidents. Dead actuators were observed three times in the one year period. In each case the failed actuators were fixed by replacing the mounting boards or unplugging and plugging back the cables several times. One serious accident occurred in January 2017. One of the four driver boards was burned after continuous experiments for 3 days. It turned out that we inappropriately placed the driver box directly on the table, which made the driver board not well cooled by the air flow. Now the driver box has been elevated.

Another issue worth mentioning is the flattening voltages. According to our observations, the wavefront corrections using both DMs always converged slower than the experiments using only DM1. Recently, we

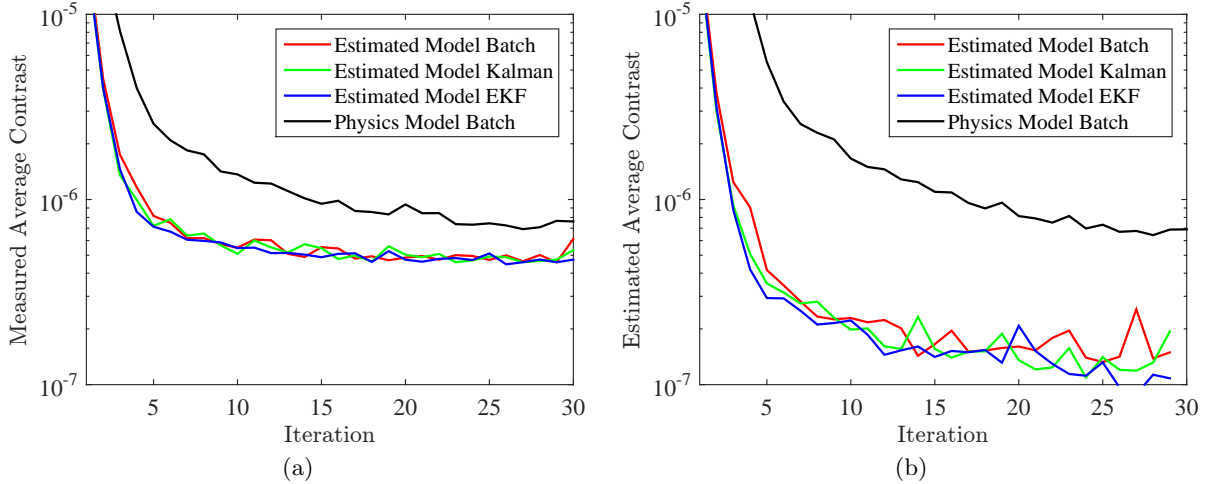


Figure 6. The correction curves of different cases. (a) shows the measured average contrast in the dark holes versus iterations and (b) shows the estimated coherent contrast in the dark holes. Theoretically, the measured contrast is the summation of the coherent contrast and incoherent contrast. The incoherent intensities for those test cases are around 3×10^{-7} .

realized that this problem came from the large flattening voltages of DM2. The average flattening voltage on DM2 is 175 volts, which is too close to the safe operating voltage limit (180 volts). As a result, the command voltages were sometimes clipped resulting in poor control coverage. A new flat map with smaller offset should be made for further wavefront correction experiments.

6. CONCLUSION

The BMC dual Kilo-C-DM deformable mirror system was carefully tested in HCIL focal plane wavefront correction system and it performed well in the real-time wavefront control loops.

The DM properties, including the surface flatness and DM pitch size, were characterized based on camera images. There are some differences between our calculations and the user manual information. It would be helpful in the future if the DM pitch can be re-measured and the DM curvature after flattening can be characterized. Based on our wavefront control experiments, the IWA and OWA achievable with the new DMs was significantly increased, which is indicative of their better surface properties and smaller inter-actuator coupling than the old DMs. The actuator gains and influence functions of different actuators may differ slightly. Better measurements of each actuator's gain and influence function will help improve the correction speed and estimation accuracy.

During our test period, the mounting boards of the DMs and their connections to the cables seem to be the most sensitive parts in the system.

**Boston Micromachines Corporation MEMS Deformable
Mirror Random Vibe Test Plan**

BMC-PLAN-001

Revision - 001

Effective Date:

July 12, 2018

Prepared by:

Paul Bierden

Goddard Space Flight Center

**National Aeronautics and
Space Administration**

Review/Approval Page (for Revision -)

Names

Date

MMS Stack Sine Test Plan
DOCUMENT CHANGE RECORD

Sheet: 1 of 1

REV/ VER LEVEL	DESCRIPTION OF CHANGE	APPROVED BY	DATE APPROVED
Revision -	Xxx	NAME	DATE

Table of Contents

1	SCOPE.....	1
1.1	OVERVIEW	1
1.2	OBJECTIVES/REQUIREMENTS.....	1
1.3	TEST OVERVIEW	1
1.4	PERSONNEL	1
1.5	ROLES AND RESPONSIBILITIES.....	1
2	APPLICABLE DOCUMENTS.....	2
2.1	GOVERNMENT DOCUMENTS.....	2
2.1.1	National Aeronautics and Space Administration (NASA).....	2
2.1.2	Drawings.....	2
3	TEST INFORMATION.....	2
3.1	GENERAL	2
3.1.1	Description of Test Article.....	2
3.1.2	Precautions.....	4
3.2	TEST FACILITIES	5
3.3	TEST PREPARATIONS.....	5
3.3.1	Test Instructions	5
3.3.2	Test Equipment	5
3.4	TEST CONDITIONS.....	5
3.4.1	Environment.....	5
3.4.2	Test Tolerances	6
3.4.3	Read-out Accuracy	6
3.5	TEST INSTRUMENTATION	6
3.6	TEST LEVELS	8
3.7	OUTPUT DATA.....	11
3.8	TEST FLOW.....	12
4	QUALITY ASSURANCE PROVISIONS	2
4.1	RESPONSIBILITY FOR INSPECTION	2
4.2	ACCEPT-REJECT CRITERIA	2
4.3	TEST FAILURES	2
5	ABBREVIATIONS, ACRONYMS, AND SYMBOLS	3

List of Figures

Figure 3.1.1-1 Fixture for holding DM during testing (1inch between holes)..... 2
Figure 3.1.1-2 Modified CV-Plate with holes to mount fixture. 3
Figure 3.5-1: Location of Accelerometers 7

List of Tables

Table 1.4: Personnel 1
Table 2.1.1: Documents..... 2
WFIRST Coronagraph Instrument Environmental Requirements Document 2
Table 2.1.2: Drawings 2
Table 3.3.2: Equipment List..... 5
Table 3.4.2: Test Tolerances 6
Table 3.5-1: Instrumentation..... 6
Table 3.5-2: Accelerometers 7
Table 3.8-1: Required Output Data 12

1 SCOPE

1.1 Overview

This document presents the information required by the test facilities to perform the random vibration testing of MEMS deformable mirrors (DMs) provided by Boston Micromachines Corporation (BMC).

This testing is in support of the NASA Exoplanet Exploration Program’s goals to mature deformable mirror technology for future missions (such as HabEx and LUVOIR) that will use a coronagraph to direct-image Earth-like exoplanets orbiting Sun-like stars. The Coronagraph Instrument (CGI) on the WFIRST mission, currently ending Phase A, includes a deformable mirror as an essential component, and the project is interested in exploring MEMS technology as a possible solution.

1.2 Objectives/Requirements

The objective is to verify the MEMS deformable mirror in three levels of random vibration: low, medium, and high. The low level corresponds to a workmanship level of testing. The medium and high levels correspond to the WFIRST Coronagraph Instrument’s specifications for the random vibration environment of the deformable mirrors, for Flight Acceptance and Qualification, respectively.

1.3 Test Overview

Three deformable mirrors will each be exposed to three random vibration environments, low medium and high, for a total of nine tested devices. Each level will be conducted in all three axes.

The MEMS DM shall only be directly handled in the B34 C138 laboratory. The accelerometers will be attached in the B7 test facility by the facility engineer prior to installation of the MEMS DM by the Boston Micromachines engineer in B34 C138. The Boston Micromachines engineer will close the DM fixture (Fig. 3.1.1) in B34 C138 and return the test fixture back to B7 for the environmental test. The DM fixture shall only be opened in the B34 C138 laboratory by the Boston Micromachines engineer. There will be three test fixtures, and the DMs will be installed and tested in batches of three, one batch per test level.

1.4 Personnel

Table 1.4: Personnel

Title	Name	Org	Contact Info

1.5 Roles and Responsibilities

Test directors are responsible for the overall coordination of all the activities related to the vibration testing. The test directors are responsible for generating/maintaining the WOA coordinating these activities.

The dynamic analyst is responsible for ensuring vibration testing is performed to appropriate levels and the hardware is instrumented sufficiently to ensure its safety.

Facility engineer is responsible for scheduling the test, facility test procedure, conducting the actual vibration test, delivering of test data, and delivering the facility test report. The Boston Micromachines engineer is responsible for installing, removing, and inspecting the MEMS DMs from the test fixture in B34 C138. The facility engineer is responsible for verifying the test fixture fasteners meet torque requirements prior to testing.

Applicable Documents

1.1 Government documents

1.1.1 National Aeronautics and Space Administration (NASA)

Table 2.1.1: Documents

WFIRST Coronagraph Instrument Environmental Requirements Document	Preliminary version April 2018

1.1.2 Drawings

Table 2.1.2: Drawings

Drawing Title	Drawing No.
MEMS DM Holding fixture	
Modified CV-Plate with holes to mount fixture.	
Location of Accelerometers	

2 TEST INFORMATION

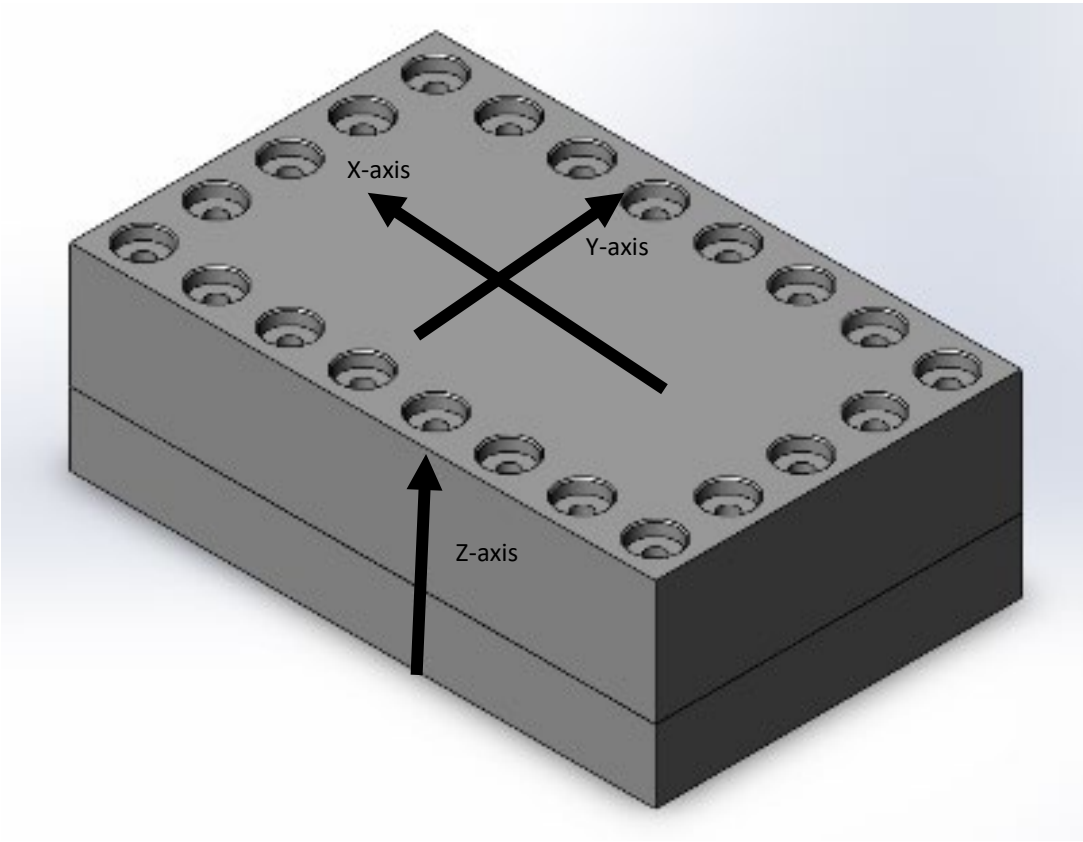
2.1 General

This is the test plan for the three-axis random vibration test of the MEMS deformable mirror.

2.1.1 Description of Test Article

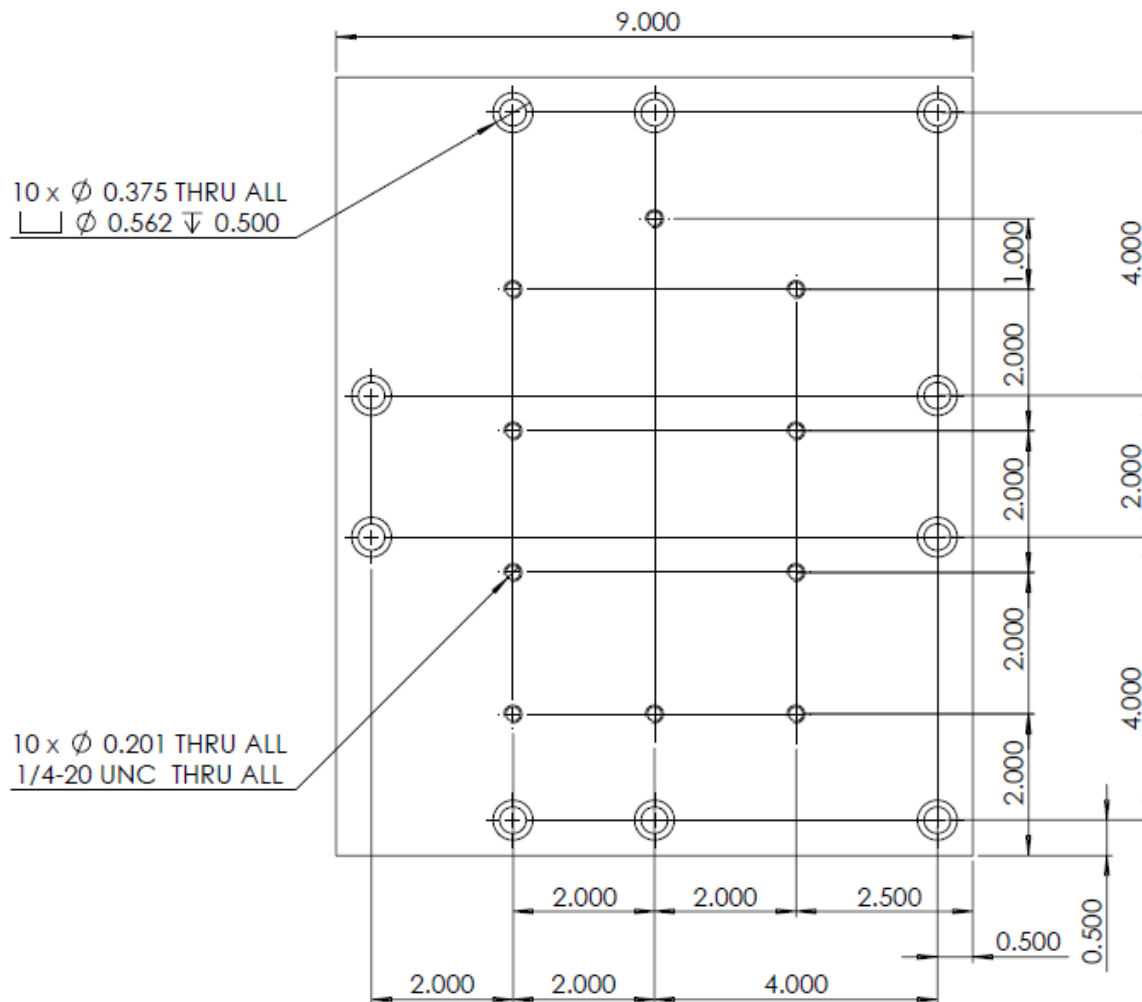
The test article is 8" x 5" x 2.7" aluminum housing surrounding a MEMS deformable mirror. It will weigh 10 lbs. The actual configuration will be documented in assembly drawings and the test report.

Figure 3.1.1-1 Fixture for holding DM during testing (1inch between holes)



It will be mounted to a modified CV-Plat that will be provided by Boston Micromachines.

Figure 3.1.1-2 Modified CV-Plate with holes to mount fixture.



Precautions

2.1.1.1 Device Power

MEMS DMs will not be powered during testing.

2.1.1.2 ESD Control Program Requirements

The MEMS DM is ESD-sensitive. Proper ESD precautions must be followed at all times by anyone within 1 meter (3.3 feet) of any hardware. Daily checked wrist straps or continuous monitored wrist straps are to be connected and worn during all contact with the hardware.

If contamination bagging is opened then ESD Smocks or bunny suits and ESD gloves must be worn by personnel while working within the 1 meter proximity of flight hardware.

The MEMS DM shall only be directly handled in the B34 C138 laboratory. The accelerometer attached to the ZIF socket (Fig. 3.5-1) will be installed onto the ZIF socket in the B7 test facility by the facility engineer and taken to B34 C138 for installation of the MEMS DM by the Boston Micromachines engineer. The Boston Micromachines engineer will close the DM fixture (Fig. 3.1.1) in B34 C138 and delivered back to B7 for the environmental test. The DM fixture shall only be opened in the B34 C138 laboratory by the Boston Micromachines engineer.

2.1.1.3 Contamination Control Program Requirements

The MEMS DM will be bagged when not being tested.

The MEMS DM shall only be directly handled in the B34 C138 laboratory. The accelerometer attached to the ZIF socket (Fig. 3.5-1) will be installed onto the ZIF socket in the B7 test facility by the facility engineer and taken to B34 C138 for installation of the MEMS DM by the Boston Micromachines engineer. The Boston Micromachines engineer will close the DM fixture (Fig. 3.1.1) in B34 C138 and delivered back to B7 for the environmental test. The DM fixture shall only be opened in the B34 C138 laboratory by the Boston Micromachines engineer.

2.2 Test facilities

Unless otherwise specified, the examinations and tests described shall be conducted at Goddard Space Flight Center in Greenbelt, MD.

2.3 Test Preparations

2.3.1 Test Instructions

All personnel directly concerned with the conduct of the test shall become familiar with the entire content of this document before beginning the test. Each step, including all notes, warnings, and cautions, shall be understood thoroughly before commencing the test. In addition, personnel should become familiar with the operation of the equipment identified in Table 3.3.2. The sequence of X, Y and Z-axis tests is at the discretion of the test conductor.

2.3.2 Test Equipment

All measurements shall be made using the test equipment specified in Table 3.3.2, or its equivalent. All inspection, measurement, and test equipment that are used shall be currently calibrated to certified standards.

Table 3.3.2: Equipment List

Manufacturer	Model	Description
???	???	Electrodynamic Vibration Shaker
Endevco (or equiv)	Per facilities	Accelerometers for Control and Fail-Safe
Endevco (or equiv)	Per facilities	Accelerometers for Responses

2.4 Test Conditions

The following paragraphs shall apply to all testing described in this document.

2.4.1 Environment

Unless otherwise specified in a detailed method paragraph, all handling and testing shall be performed under the following ambient atmospheric conditions:

Temperature:	24 ± 5 °C
Relative humidity:	30-70%
Barometric pressure:	N/A

2.4.2 Test Tolerances

The tolerances allowed on test conditions are intended only to provide for accuracy of items such as instrumentation and controls. Conditions shall be as close as possible to the nominal or center values specified, and in no instance shall they exceed the tolerances specified.

Table 3.4.2: Test Tolerances

Test Condition	Test Tolerance
Random Vibration	
Spectral shape	±3dB when measured in frequency bands no wider than 25Hz percent
Wideband level	±1.0 dB (true RMS)
Test Duration	+10, -0 percent

2.4.3 Read-out Accuracy

Parameters are specified either as limits or as nominal values with plus-or-minus tolerances. These limits and tolerances shall be regarded as absolute, and the inaccuracies of measuring equipment shall not be interpreted as part of measured values in such a way that out-of-limit measurements may appear in-limit.

2.5 Test Instrumentation

Accelerometers used during random vibration testing are documented Table 3.5-1

If, during the testing, there are instrumentation problems the Test Conductor, Structural Analyst, Dynamic Analyst, and Mechanical PDL, and facility engineer will consult on how to proceed.

The instrumentation count in table 3.5-1 and the list in Table 3.5-2 include all possible instrumentation envisioned for this test. Some instrumentation may be eliminated from those requested for output in actual testing.

Table 3.5-1: Instrumentation

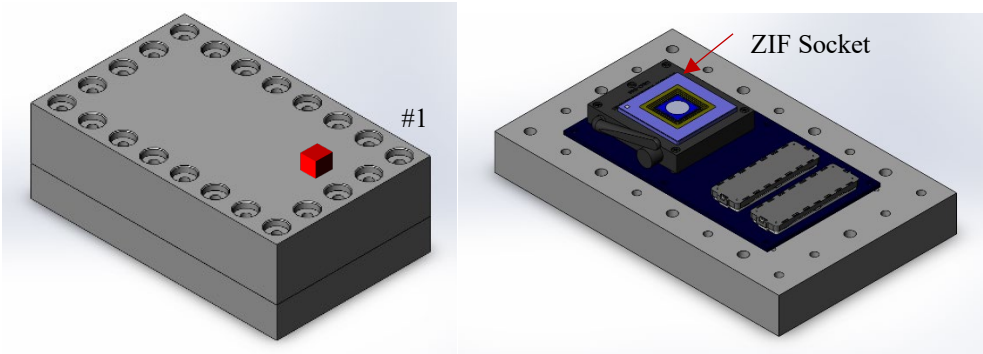
Type	Total Locations	
Accelerometers	2	
Total		

* - Does not include any instrumentation that facility may desire on slip table or head expander

Table 3.5-2: Accelerometers

Location No.	Location	Axis	Channels
1	Top of mounting block	XYZ	3
2	Next to zero insertion force (ZIF) socket in mounting block	XYZ	3

Figure 3.5-1: Location of Accelerometers



 = accelerometer

2.6 Test levels

The MEMS DM random vibration testing includes three axes of low, middle and high levels of random vibration, each of which are specified in Tables 3.6.1, 3.6.2 and 3.6.3.

Table 3.6.1. Frequency spectrum of the Low-Level vibration test.

Frequency (Hz)	PSD Level (g^2/Hz) Three axis test
	Low-level 1 minute per axis
20	0.01
20-50	+3dB/oct
50-500	0.04
500-2000	-3dB/oct
2000	0.01
Overall	6.8 g_{rms}

Table 3.6.2. Frequency spectrum of the Medium-Level vibration test.

Frequency (Hz)	PSD Level (g^2/Hz) Three axis test
	Medium-level 1 minute per axis
20	0.08 g^2/Hz
20-50	+3dB/oct
50-200	0.40 g^2/Hz
350-500	0.04 g^2/Hz
500-2000	-3dB/oct
2000	0.01 g^2/Hz
Overall	11.0 g_{rms}

Table 3.6.3. Frequency spectrum of the High-Level vibration test.

Frequency (Hz)	PSD Level (g^2/Hz)
	Three axis test
	High-level Two minutes per axis
20	0.16 g^2/Hz
20-50	+3dB/oct
50-200	0.80 g^2/Hz
350-500	0.08 g^2/Hz
500-2000	-3dB/oct
2000	0.02 g^2/Hz
Overall	15.6 g_{rms}

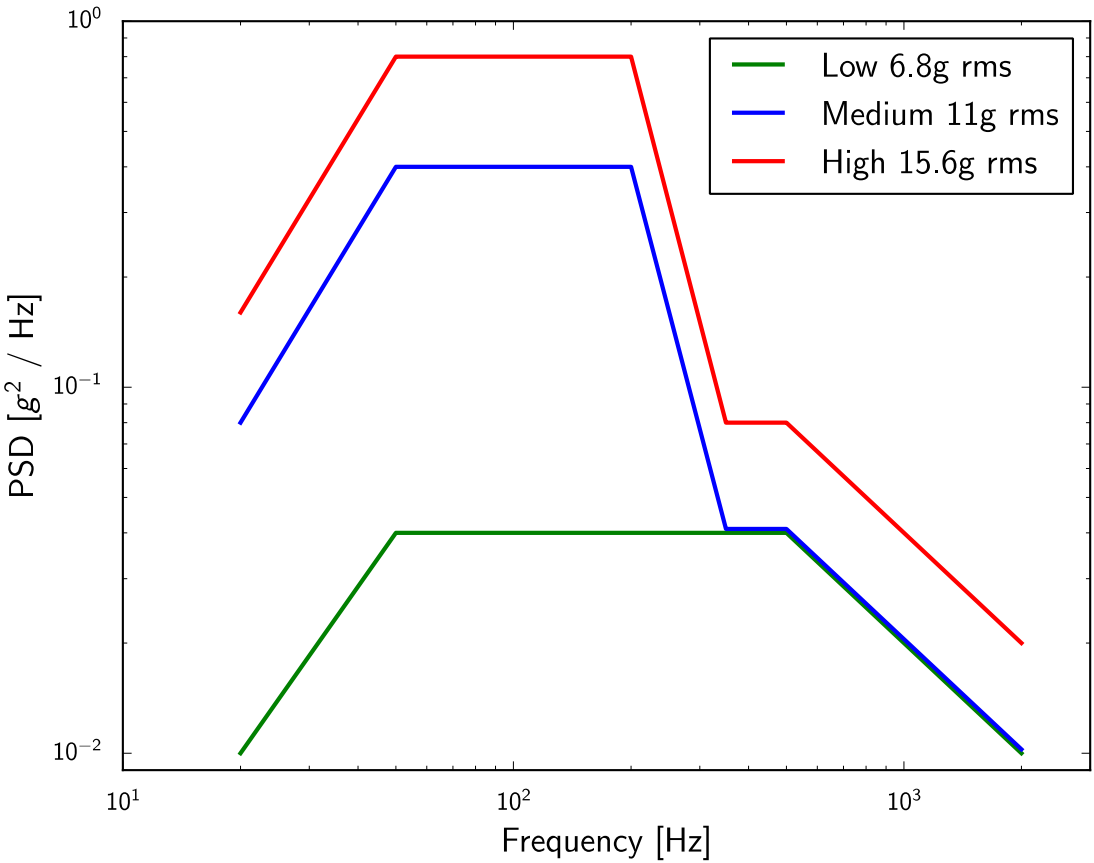


Figure 3.6.1 A plot of the three random vibs levels specified in Tables 1 and 2.

Nine DMs will be tested. Three DMs will be tested at each level on three axis. .

For the low level of random vibration test, we adopt the “Component Minimum Workmanship” test level stipulated in the General Environmental Verification Standard (GEVS) page 2.4-19, which is as follows:

Low level: $0.04 \text{ g}^2/\text{Hz}$, 80–500 Hz, $6.8 \text{ g}_{\text{rms}}$ overall

with a 3 dB/octave roll-off at higher and lower frequencies. The low level of random vibration is specified in Table 1.

The WFIRST/CGI project provide the medium and high levels, shown in Tables 3.6.6 and 3.6.3 . They are based on a finite element model of the preliminary instrument design and encompass the vibration levels expected at the location of the deformable mirrors inside CGI.

2.7 Output Data

All response data described in Table 3.8-1 will be required after each test in MSEXcel and Adobe PDF format at the conclusion of each test run (PDF may be provided after test series). Prior to testing, the lab shall provide the DM dynamic analyst with the programmed channel ordering for all channels, including computed forces/moments so that pretest analysis can be structured in same format.

A photograph of the DM before and after each vibration run shall be taken and included in the output data.

Table 3.8-1: Required Output Data

Test Type	Required Data Printouts For All Channels
Random Vibe	Acceleration Spectral Density (g^2/Hz) vs. Frequency (Hz)

2.8 Test Flow

The MEMS DMs will be subjected to random vibration tests (as defined in section 3.6) performed on the T4000 shaker at GSFC.

The envisioned sequence of events is outlined below.

1. Accelerometers are fastened to the three test fixtures in B7 as shown in Fig. 3.5-1
2. DMs #1,2,3 are installed into the test fixtures in B34 C138
3. DM #1
 - a. X-Axis
 - i. Signature sweep
 - ii. -6 dB random Low-Level
 - iii. 0 dB random Low-Level
 - iv. Signature sweep
 - b. Y-Axis
 - i. Signature sweep
 - ii. -6 dB random Low-Level
 - iii. 0 dB random Low-Level
 - iv. Signature sweep
 - c. Z-Axis
 - i. Signature sweep
 - ii. -6 dB random Low-Level
 - iii. 0 dB random Low-Level
 - iv. Signature sweep
4. DM #2
 - a. X-Axis
 - i. Signature sweep
 - ii. -6 dB random Low-Level
 - iii. 0 dB random Low-Level
 - iv. Signature sweep
 - b. Y-Axis
 - i. Signature sweep
5. DM #3
 - a. X-Axis
 - i. Signature sweep
 - ii. -6 dB random Low-Level
 - iii. 0 dB random Low-Level
 - iv. Signature sweep
 - b. Y-Axis
 - i. Signature sweep
 - ii. -6 dB random Low-Level
 - iii. 0 dB random Low-Level
 - iv. Signature sweep
 - c. Z-Axis
 - i. Signature sweep
 - ii. -6 dB random Low-Level
 - iii. 0 dB random Low-Level
 - iv. Signature sweep
6. DMs #1,2,3 are removed from the test fixtures in B34 C138 and evaluated
 - i. -6 dB random Low-Level
 - iii. 0 dB random Low-Level
 - iv. Signature sweep

7. DMs #4,5,6 are installed into the test fixtures in B34 C138
 - ii. -6 dB random Medium -Level
 - iii. 0 dB random Medium -Level
 - iv. Signature sweep
8. DM #4
 - a. X-Axis
 - i. Signature sweep
 - ii. -6 dB random Medium-Level
 - iii. 0 dB random Medium -Level
 - iv. Signature sweep
 - b. Y-Axis
 - i. Signature sweep
 - ii. -6 dB random Medium -Level
 - iii. 0 dB random Medium -Level
 - iv. Signature sweep
 - c. Z-Axis
 - i. Signature sweep
 - ii. -6 dB random Medium -Level
 - iii. 0 dB random Medium -Level
 - iv. Signature sweep
9. DM #5
 - a. X-Axis
 - i. Signature sweep
 - ii. -6 dB random Medium -Level
 - iii. 0 dB random Medium-Level
 - iv. Signature sweep
 - b. Y-Axis
 - i. Signature sweep
10. DM #6
 - a. X-Axis
 - i. Signature sweep
 - ii. -6 dB random Medium -Level
 - iii. 0 dB random Medium -Level
 - iv. Signature sweep
 - b. Y-Axis
 - i. Signature sweep
 - ii. -6 dB random Medium -Level
 - iii. 0 dB random Medium -Level
 - iv. Signature sweep
 - c. Z-Axis
 - i. Signature sweep
 - ii. -6 dB random Medium -Level
 - iii. 0 dB random Medium -Level
 - iv. Signature sweep
11. DMs #4,5,6 are removed from the test fixtures in B34 C138 and evaluated
12. DMs #7,8,9 are installed into the test fixtures in B34 C138
 - ii. -6 dB random High -Level
 - iii. 0 dB random High -Level
 - iv. Signature sweep
13. DM #7
 - a. X-Axis
 - i. Signature sweep
 - ii. -6 dB random High -Level
 - iii. 0 dB random High -Level
 - iv. Signature sweep
 - b. Y-Axis
 - i. Signature sweep
 - ii. -6 dB random High -Level
 - iii. 0 dB random High -Level
 - iv. Signature sweep
 - c. Z-Axis
 - i. Signature sweep
 - ii. -6 dB random High -Level
 - iii. 0 dB random High -Level
 - iv. Signature sweep
14. DM #8
 - a. X-Axis
 - i. Signature sweep
 - ii. -6 dB random High -Level
 - iii. 0 dB random High-Level
 - iv. Signature sweep
 - b. Y-Axis
 - i. Signature sweep
15. DM #9
 - a. X-Axis
 - i. Signature sweep
 - ii. -6 dB random High -Level
 - iii. 0 dB random High -Level
 - iv. Signature sweep
 - b. Y-Axis
 - i. Signature sweep
 - ii. -6 dB random High -Level
 - iii. 0 dB random High -Level
 - iv. Signature sweep
 - c. Z-Axis
 - i. Signature sweep
 - ii. -6 dB random High -Level
 - iii. 0 dB random High -Level
 - iv. Signature sweep
16. DMs #7,8,9 are removed from the test fixtures in B34 C138 and evaluated

3 QUALITY ASSURANCE PROVISIONS

3.1 Responsibility for inspection

3.2 Accept-reject criteria

1. Test inputs achieved within specified tolerances
2. Pre/Post signature overlays show no significant differences (<5% frequency difference for fundamental mode, <10% frequency difference for higher order modes)
3. No visible sign of damage post-test

3.3 Test failures

In the event of failure during any phase of this test procedure, the testing shall be stopped and the test set-up remain undisturbed until a complete description of the observed anomaly failure is documented and implemented to preclude loss of information that may facilitate determining the failure cause.

4 ABBREVIATIONS, ACRONYMS, AND SYMBOLS

DM	Deformable Mirror
ESD	Electrostatic Sensitive Device
FFT	Fast Fourier Transform
FG	Force Gage
G (or g)	Gravitational Units
GSFC	Goddard Space Flight Center
GSE	Ground Support Equipment
Hz	Hertz
in	inch
kg	kilogram
m	meter
mm	millimeter
MEMS	Micro-electrical-mechanical
N	Newton
N/A	Not applicable
P/N	Part Number
PSD	Power Spectral Density
RMS	Root-Mean-Square
RSS	Root-Sum-Square
SA	Solar Array
S/N	Serial number
SG	Strain Gage
TBD	To be determined
TDS	Test Data Sheet
TRR	Test Readiness Review
UUT	Unit Under Test
WOA	Work Order Authorization

Post-Vibe Testing of the Boston Micromachines (BMC) Kilo Deformable Mirrors in the Vacuum Surface Gauge

John Trauger, Pin Chen

Measurement Facility: The Vacuum Surface Gauge (VSG)

VSG is a Michelson interferometer designed and built for the purpose of characterizing DM surface figure with **high spatial resolution** and **ultrahigh (30-picometer) actuator-height resolution**.

Figure 1 shows VSG's basic layout. The entire optical setup is inside a vacuum chamber operating at pressures ~ 1 mtorr. Light from a frequency-stabilized He-Ne laser enters the chamber via a single-mode fiber. Inside the chamber, it propagates through a folding mirror, and a 1000 mm focal-length lens collimates the light. A beamsplitter then transmits 50% of the incident light toward the DM (test object) and reflects the other 50% toward a flat reference mirror. Reflected light from the reference mirror and DM return to the beamsplitter, which directs the combined beam to the imaging system comprising a 400 mm focal-length lens, an iris, a neutral-density filter, and a CCD camera. The camera captures interferograms as the reference mirror steps through a sequence of OPDs (optical path differences). Data-processing algorithms remove tip-tilt and perform a global fit of interferograms to retrieve phase maps of the DM surface.

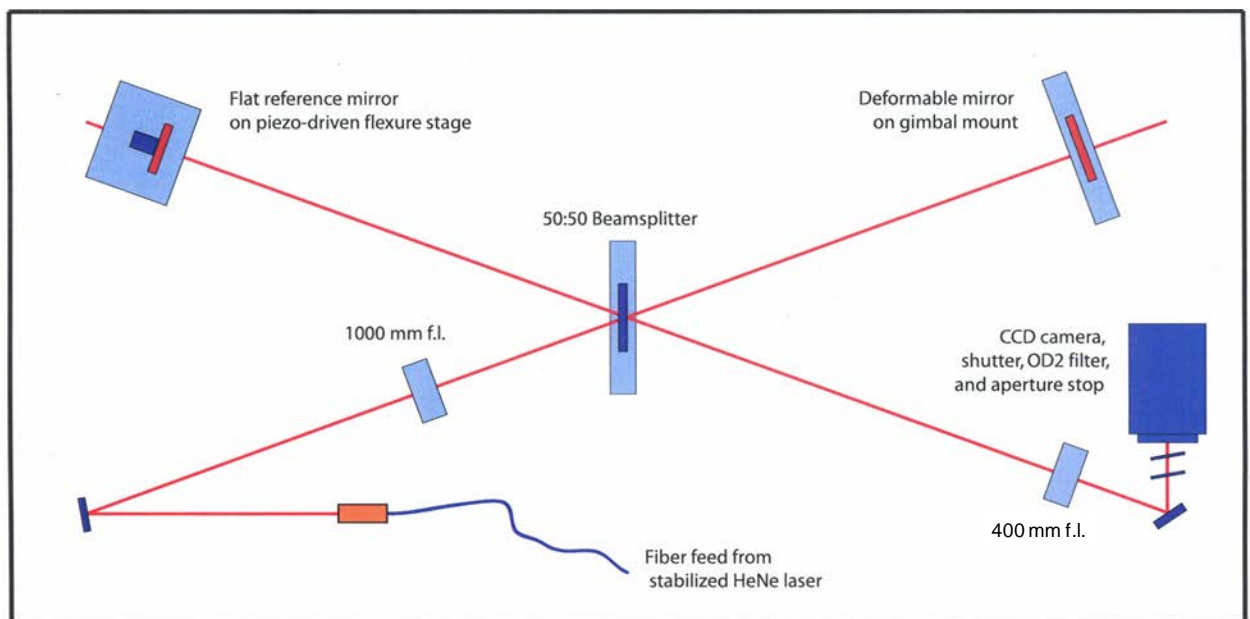


Figure 1. Optical layout of the vacuum surface gauge.

Key measurement specifications are as follows:

- **Spatial resolution:** ~ 15 pixels per actuator spacing
- **Actuator height precision:** ± 30 pm (in measuring individual actuator height/gain)
- **Acquisition time:** ~ 8 min./measurement

Overview of Test Procedures

We tested two BMC Kilo DMs that have experienced random-vibe testing. Their serial numbers are as follows: “25CW012#015” and “25CW011#035.” For convenience, we will refer to them by the last three characters of their serial numbers: “DM#15” and “DM#35.” We performed four procedures to both DMs and one additional procedure to DM#35 only.

Tests Applied to Both DMs

1. **Unpowered surface figure:** measured DM surface figures as described above the actuators at 0V bias.
2. **Actuator gains:** measured the gain (nm/V) of every actuator on each DM.
3. **Flattening voltage map:** applied voltages to flatten the DM surface.
4. **Repeatability test:** applied four cycles of Procedure 1 followed by Procedure 3 to measure repeatability of surface figures.

Tests Applied to DM#35 Only

5. **Stability test:** recorded surface figure of the DM at zero bias over 13 hours.

A superset of the procedures listed above were performed before vibe. Frank Greer et al.’s April 2017 report summarizes the pre-vibe test results. **Comparison of pre- and post-vibe results revealed only one substantive, possible degradation in performance: one actuator in DM#35 showed a 5.7 nm movement during Procedure 4 and excursion up to 10 nm over 13 hours. However, the cause of this observed movement need not be in the DM; for example, connector issues external to the DM module can cause such behavior.**

Sections below describe the test procedures in more detail and present results.

Unpowered Surface Figure

VSG measurements were acquired with the DMs in the unpowered state (with actuators grounded). Figures 2 and 3 summarized results for DM#15 and DM#35, respectively. These results are nominal.

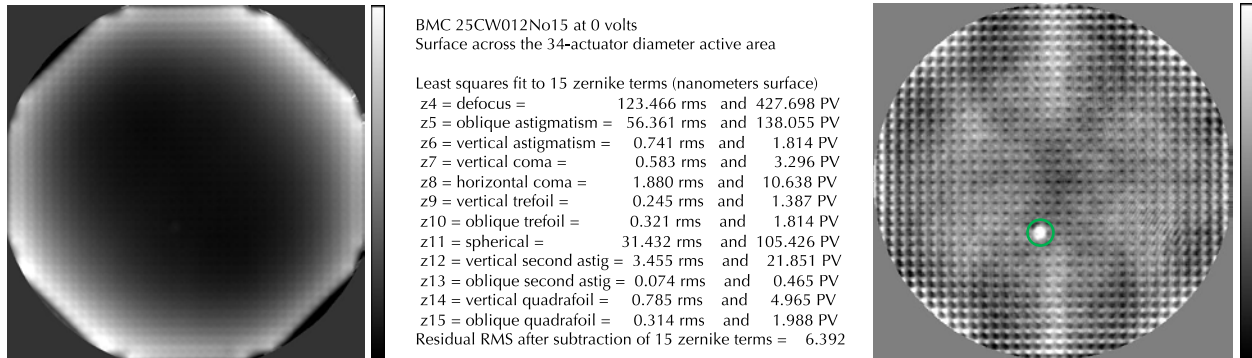


Figure 2. Left panel: Grey-scale plot of **DM#15** surface figure in the unpowered state. Middle panel: magnitudes of Zernike terms fitted to the surface figure. Right panel: surface figure with 15 Zernike terms removed. The green circle marks a structural defect that appeared during pre-vibe testing.

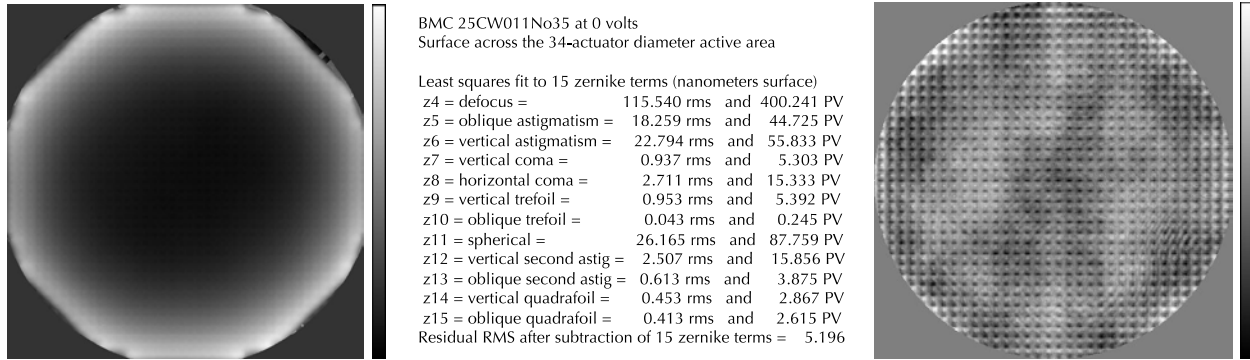


Figure 3. Left panel: Grey-scale plot of **DM#35** surface figure in the unpowered state. Middle panel: magnitudes of Zernike terms fitted to the surface figure. Right panel: surface figure with 15 Zernike terms removed.

Actuator Gains

We measured actuator gains and derived flattening voltage maps using the following steps:

1. Apply a pre-determined flattening voltage map to all actuators in the DM.
2. Apply alternating +10 and -10 V pokes (deviations from the bias applied in the previous step) to a grid of actuators wherein neighboring bias points are five actuators apart.
3. Apply the above poke pattern with biases reversed.
4. Take the difference of the two surfaces corresponding to the two steps above.
5. Fit an *a-priori* influence function to each individual poke. Each fit coefficient represents the actuator gain per 20V poke.
6. Repeat the steps above with shifted grids until all actuators are characterized.
7. Use the measured gains and surface in Step 1 to solve for a new flattening voltage map.
8. Repeat the steps above until the flattening voltage map solution converges.

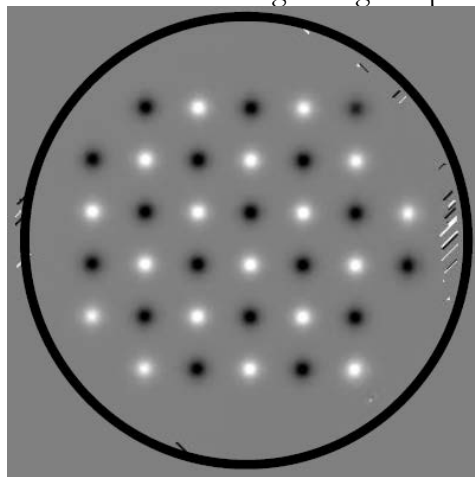


Figure 4. Example poke pattern for gain measurements. The notional circle is drawn for clarity only.

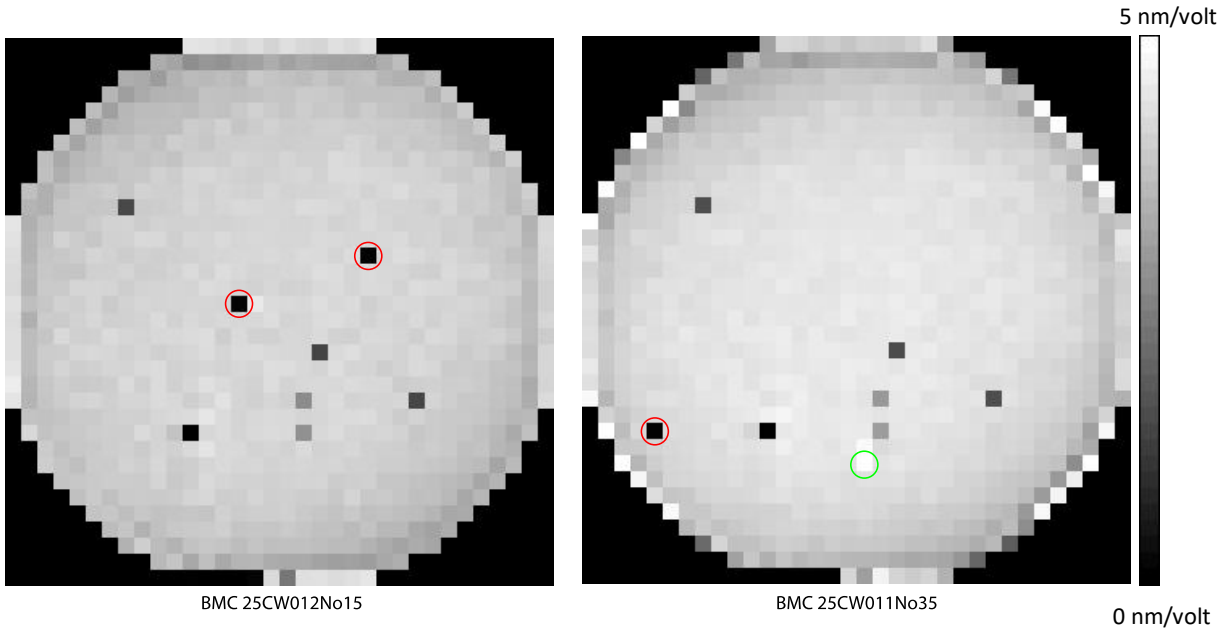


Figure 5. Measured post-vibe actuator gains for DM#15 (left) and DM#35 (right). Anomalous actuators show up as unusually dark or light pixels (with anomalies on the perimeter pixels being data artifacts). A number of low-gain (grey pixels) and non-moving (black pixels) actuators occurred in the same positions in both DMs, we attribute these anomalies to faulty electrical connections external to the DM. DM#15 had two unique non-moving actuators (marked by red circles). DM#35 had one unique non-moving actuator (red circle) and one actuator with gain 40% higher than its neighbors (green circle).

Figure 5 shows the measured actuator gains. We observed the following anomalies where inherent DM flaws could not be ruled out *at the time*:

- A. DM#15 had two unique non-moving actuators, and DM#35 had one unique non-moving actuator (marked by red circles).
- B. DM#35 had one actuator with gain 40% higher than its neighbors (marked by the green circle).

Subsequent HCIT testing proved that all actuators in both DMs are responsive, and therefore, we attribute Anomaly A to faulty connections external to the DMs. On the other hand, **the actuator associated with Anomaly B also showed a degree of instability (see discussion below), whose cause remains to be fully resolved.**

Flattening Voltage map

Steps 1 – 8 in the preceding section describes how we derive a DM’s flattening voltage map. In this segment of the VSG test, we applied slightly different procedures to the two DMs. For DM#15, we applied an *a priori*, pre-vibe flattening field, whereas for DM#35, we solved for and applied a post-vibe field. The left panel of Figure 6 shows DM#15’s surface figure with the pre-vibe voltage map applied. Other than fine corrugations in the facesheet surface, the DM was flat to within a few nm, showing resilience of actuator gains vis-à-vis random vibe. DM#35 demonstrated nominal flatness as well, except for one actuator area caused by a drift in the above-mentioned “Anomaly-B” actuator (see below for further discussion of the drift).

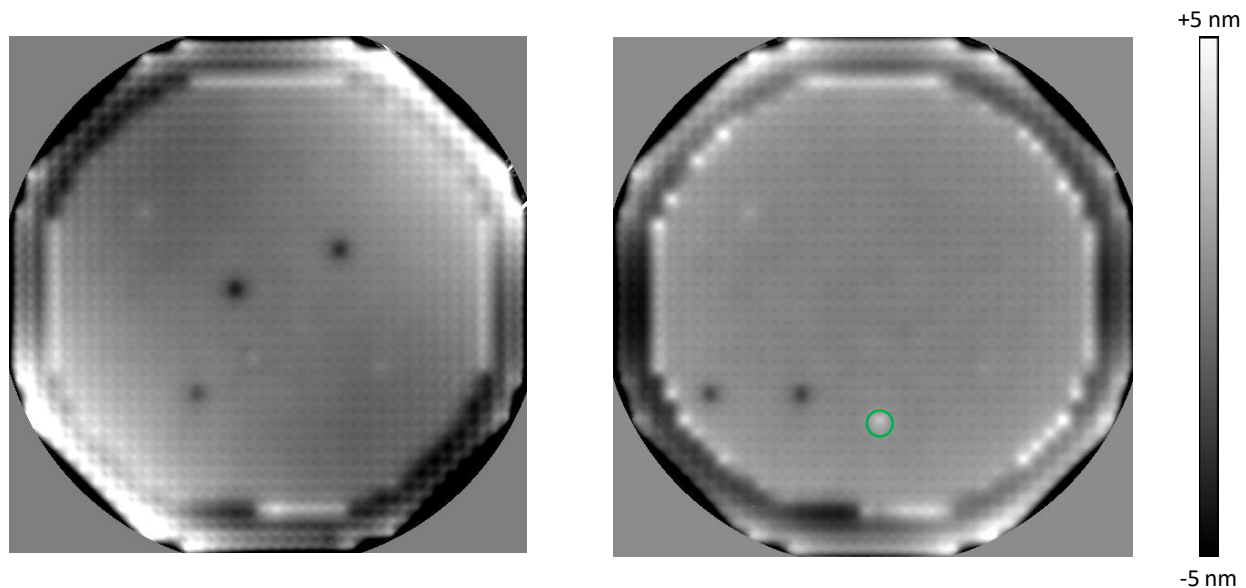


Figure 6. Flattened surface figures of DM#15 (left) and DM#35 (right). Darker shades correspond to smaller actuator movement (higher surface elevation), and lighter shades correspond to larger actuator movement (lower surface elevation). For DM#15, the pre-vibe voltage map was applied. For DM#35, we derived and applied a post-vibe voltage map. Abnormally dark spots indicate non-moving actuators due to connector issues external to the DMs. The green-circled bright spot corresponds to the Anomaly-B actuator, which drifted in position between derivation of the flattening voltage map and acquisition of the interferogram.

Repeatability Test

To characterize the repeatability of DM surface figures after gross transitions of states, we exercised four cycles of sequentially applying 0V to all actuators, then the flattening voltage map, and then return to zero bias. Figures 7 and 8 displays test data for DM#15 and DM#35, respectively. For both DMs, the RMS difference in surface figure (of the DM's active area) between successive settings is < 0.8 nm. VSG instrument noise likely dominates this number. Hence, **the post-vibe DM's overall surface figures are repeatable to within VSG measurement precision, with one significant exception; the Anomaly-B actuator in DM#35 drifted by 5.8 nm between two successive flat applications, an interval of approximately 9-minutes.**

Stability Test

To test the inherent stability of the DM actuators/surface, we continuously acquired data with DM#35 unpowered for 13 hours. Figure 9 shows an hourly sampling of surface figures. **Overall, the DM remained stable over the entire 13-hour period to within measurement noise (~ 0.7 nm RMS). However, two actuators, the Anomaly-B actuator and a "non-moving" actuator (due to external connector problems), drifted over a range up to 10 nm during the 13 hours.**

Conclusions

Overall, the DMs after random vibe demonstrated the same performance as pre-vibe regarding actuator gains, cyclic repeatability, and long-term stability—with the exception of one high-gain actuator (out of 1904 actuators in two DMs) that appeared to drift. However, we had not fully resolved interconnect issues external to the DM modules at the time of VSG testing, and cannot rule out such issues as the culprit.

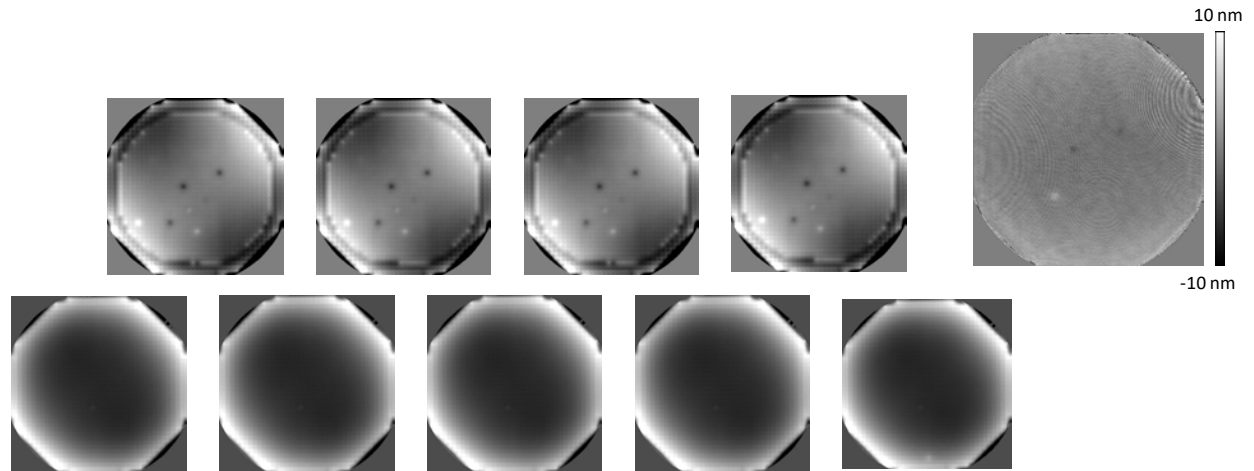


Figure 7. Measured surface figures during repeatability testing, involving four cycles starting from unpowered to flat and then back to unpowered. The upper right panel shows the difference between the second and fourth flattened surfaces, with an RMS value of 0.75 nm over the DM's active area.

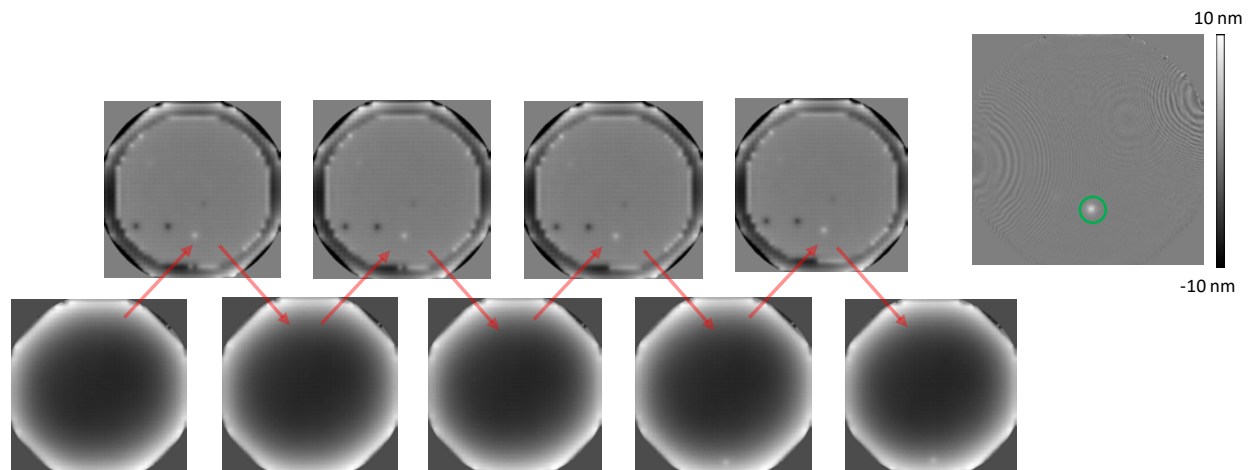


Figure 8. Measured surface figures during repeatability testing, involving four cycles starting from unpowered to flat and then back to unpowered. The upper right panel shows the difference between the third and fourth flattened surfaces, RMS = 0.70 nm over the active area. The bright spot inside the green circle indicates that the Anomaly-B actuator moved by 5.8 nm between the two successive flats.

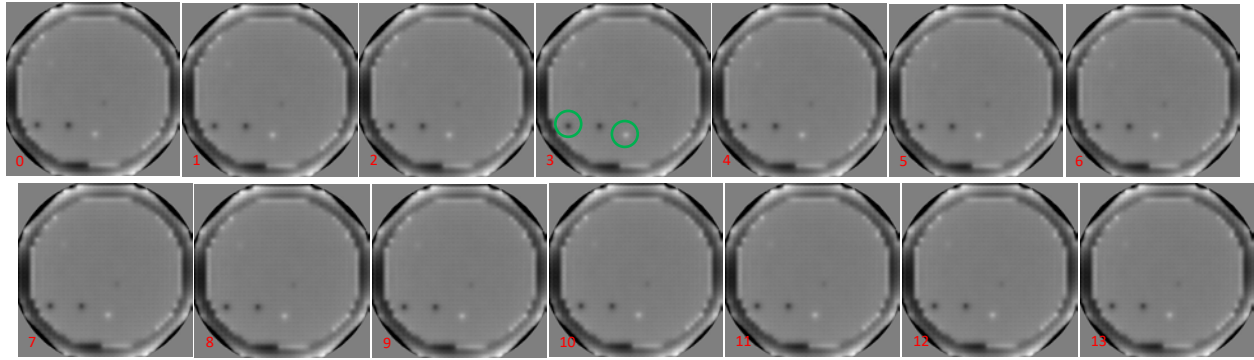


Figure 9. Measured surface figures during the 13-hour testing of unpowered DM#35, only one figure per hour is shown. The difference between the first and each subsequent measurement is ~ 0.7 nm RMS, accountable by fringe artifacts in the data. However, two individual actuators, marked by green circles moved by up to 10 nm over the 13-hour period.

Post-environmental testing of the Boston Micromachines (BMC) Kilo DMs in the High Contrast Imaging Testbed (HCIT) facility

G. Ruane (garreth.ruane@jpl.nasa.gov), C. Mejia Prada, E. Bendek
March 9, 2020

DM serial numbers: 25CW012#015 and 25CW011#035 (DMs from Bierden's TDEM)

Summary

We carried out post-environmental testing of the Boston Micromachines (BMC) Kilo DMs (serial numbers 25CW012#015 and 25CW011#035; herein DM#15 and DM#35). We demonstrated that the both DMs have 100% functioning actuators after environmental testing using a Fizeau interferometer in the High Contrast Imaging Testbed (HCIT) facility at JPL. Furthermore, we integrated DM#15 into a coronagraph testbed in a vacuum chamber and demonstrated $1e-8$ contrast, which suggests the DM is stable and allows high-precision wavefront control with DM surface controlled to within 0.1 nm.

Functionality tests using the Fizeau interferometer

We set up an optical table in the High Contrast Imaging Testbed (HCIT) facility at JPL with a Fizeau interferometer (Zygo Verifire) for DM testing and characterization. The DMs were placed inside of a plastic enclosure that was purged with a continuous flow of dry air to maintain a relative humidity of $<30\%$ during operation. We used two types of control electronics available in HCIT: the commercial electronics provided by BMC and the USB-connected electronics manufactured by Teilch (Bendek et al, in prep.).

Our standard functionality tests consist of (1) applying a uniform bias to make sure all actuators respond, (2) poking each row and column, and (3) poking each actuator individually. Here, we show the results to (1), but the measurements from steps (2) and (3) are available upon request.

The first DM: 25CW012#015

Our initial tests showed a single anomalous actuator on DM#15 using the commercial electronics (see Fig. 1). In cases like this, the anomaly could be caused by a malfunctioning actuator on the DM, the DM electronics, or an issue with the connectors. If the DM has a malfunctioning actuator, rotating the DM in the zero insertion force (ZIF) socket should cause the position of the anomalous actuator to rotate with the DM. However, the location appeared to be the same regardless of the DM orientation. We concluded that the actuator actually corresponded to a broken electrical connection and tracked the missed connection to a bent pin on the MEG-Array connector on the interface board (i.e. the PCB with ZIF socket and MEG-Array connectors), which was later replaced.

In the meantime, we switched to the Teilch controller and thereby recovered control of the anomalous actuator (see Fig. 1, right). Note that the Teilch controller had a known bug that prevents it from controlling actuators at the left and right edges. Together, these measurements demonstrate 100% actuator functionality.

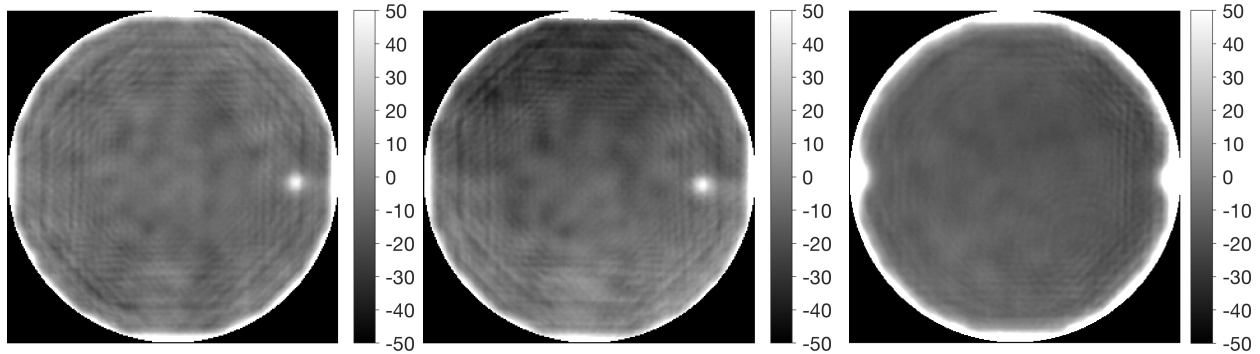


Fig. 1: DM surface difference measurements in nm. (left/middle) Surface difference between 0% and 50% bias using the commercial electronics with the DM (left) vertical and (middle) rotated by 90°. The consistent location of the anomalous actuator suggests it was caused by a connectivity problem. (right) Switching to the Teilch controller recovered control of the anomalous actuator.

The second DM: 25CW011#035

We used the commercial electronics with the replacement interface board to test DM#35. We confirmed that 100% of the actuators respond normally. To demonstrate this, Figure 2 shows no anomalous actuators when applying a uniform bias (compare to Figs. 1a or 1b).

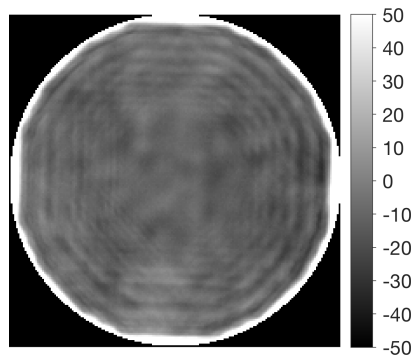


Fig. 2: DM surface difference measurements (in nm) between 0% and 50% bias using the commercial electronics with the DM#035.

Full calibration of DM#15 using the Fizeau interferometer

We carried out the complete calibration steps needed to use the DM#15 in vacuum coronagraph testbed; i.e. to flatten the DM and measure the actuator gains (see Fig. 3). The voltage map that flattened the DM had peak-to-valley of approximately 85 V and the individual actuator gain coefficients are typically 2-5 nm/V. The DM surface error in the flat state is <10 nm RMS within the spatial frequencies measured by the interferometer (i.e. down to a few pixels per actuator). There is a small surface defect near the center of the mirror, but actuators at that location respond normally. Figure 4 shows an example

grid pattern we used to measure the gain coefficients. One out of 16 actuators in a 4×4 grid was poked up and down by 5 V, then we fit the difference to a model of the DM surface to determine the actuator gains.

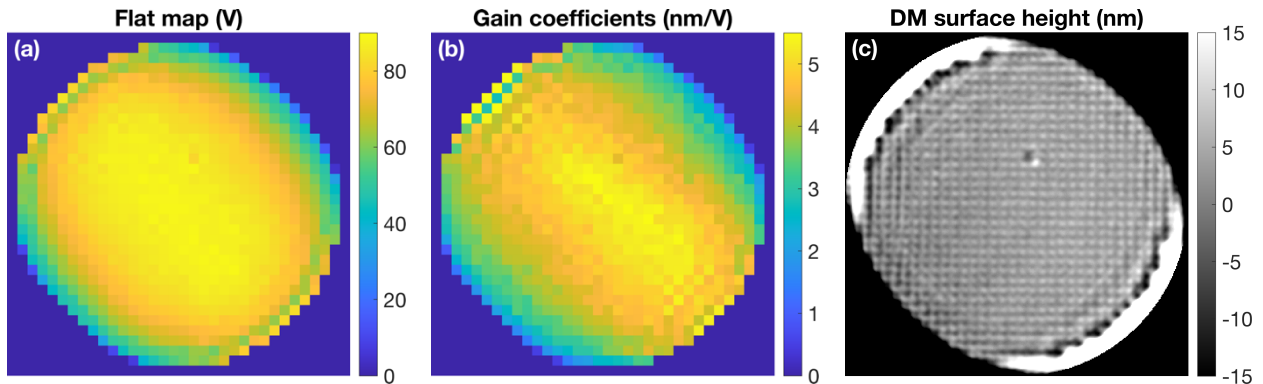


Fig. 3: DM calibration using the interferometer. (a) The flat map in Volts. (b) The measured gain coefficients for each actuator. (c) The DM surface with the flat map applied.

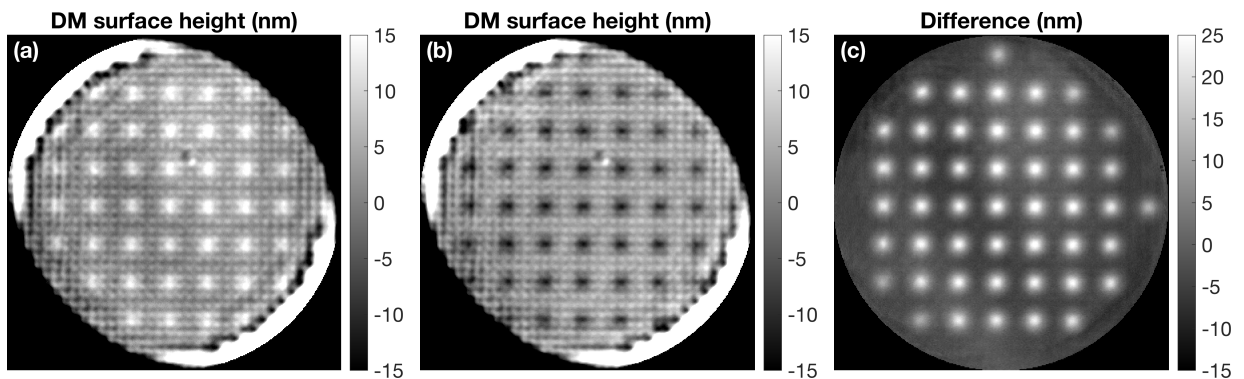


Fig. 4: Example grid pattern used to measure the DM actuator gain coefficients (i.e. Fig. 2, middle). The grid of actuators is poked (a) up and (b) down by 5 V. (c) The difference is represents the effect of applying 10 V to each actuator. Each actuator is measured after 16 pairs of surface measurements.

Performance testing using a vacuum coronagraph testbed

We installed DM#15 and the Teilch controller on a coronagraph testbed in a vacuum chamber at <1 mTorr. Figure 5 shows a schematic of the optical layout. The DM was illuminated with a circular beam with a diameter of 9 mm (effectively 30 actuators across). The optical layout consisted of a vortex coronagraph, which was being tested as part of a different SAT award (PI: Serabyn). After running standard wavefront control procedures, we achieved the dark hole in Fig. 6, which had a normalized intensity on the order of $1e-8$ over 2-12 λ/D with a 20nm spectral bandwidth centered at 637 nm.

The contrast we have demonstrated is consistent with surface precision on the order of 0.1 nm. Furthermore, this performance is comparable to the contrast we achieved with a Kilo DM that did not undergo environmental testing, and therefore the testbed performance may or may not be limited by the DM and/or its electronics. We nonetheless have demonstrated that a Kilo DM can achieve high contrast after flight-relevant environmental testing.

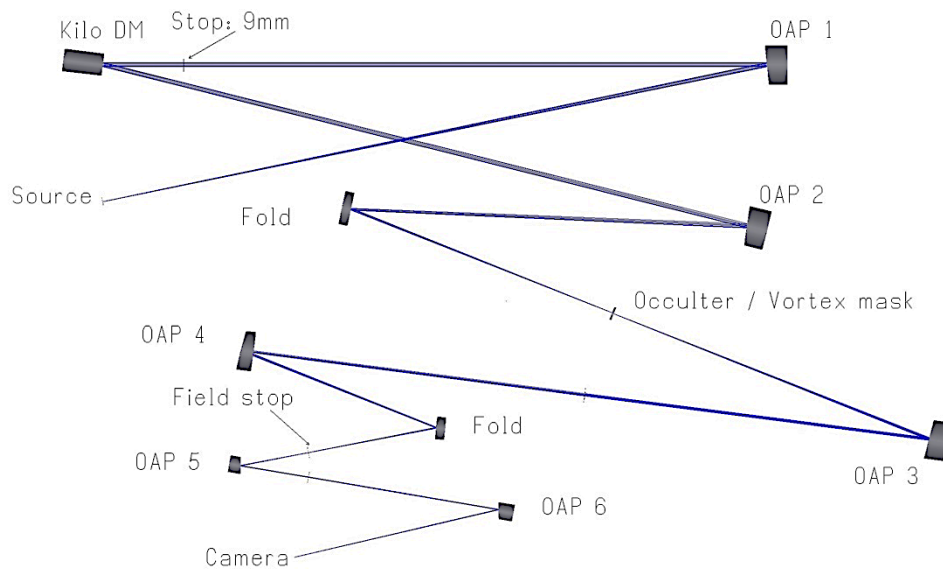


Fig. 5: Optical layout of the coronagraph testbed. OAP: Off-axis parabolic mirror.

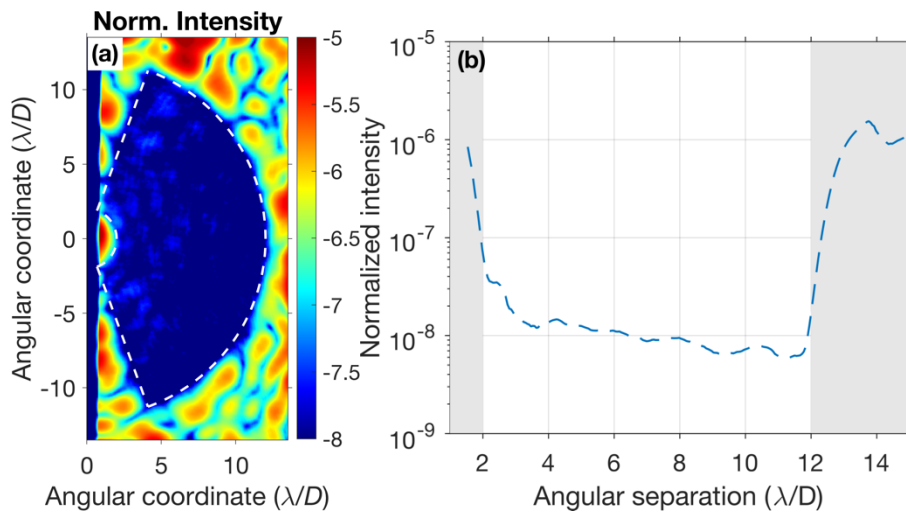


Fig. 6: (a) Log normalized intensity achieved with DM#15. (b) Azimuthal average profile within the dark hole region.



Robustness of MEMS Deformable Mirrors to rocket launch

(MEMS = Micro-Electro Mechanical Systems)

Axel Potier^a, Camilo Mejia Prada^a, Hong Tang^a, Duncan Liu^a,
Garreth Ruane^a, Wesley Baxter^a, A J Eldorado Riggs^a, Phillip
Poon^a, Eduardo Bendek^a, Nick Siegler^a, Mary Soria^a, Mark
Hetzl^a, Charlie Lam^b, Paul Bierden^b

^aJet Propulsion Laboratory, California Institute of Technology

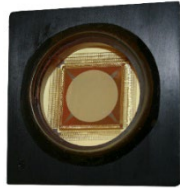
^bBoston Micromachines Corporation

MEMS deformable mirrors rocket launch survivability

INTRODUCTION

Technology Overview (1 of 2)

- The deformable mirror (DM) is the key hardware component for all high-contrast coronagraphs, essential to achieving the wavefront control future direct imaging exoplanet missions require. There are two major DM vendors - AOX and BMC (Adaptive Optics Xinetics and Boston Micromachine Corp). Both vendors' DMs are used on ground based telescopes and MEMS are the most common devices.
- NASA does not currently have a known DM technology capable of directly imaging Earth-size planets orbiting Sun-like stars aboard a future direct-imaging flagship mission. The aforementioned two candidates have shown important issues to be resolved.
- NASA's ExEP HCIT has had significant success with AOX DMs (electrostrictive PMNs) for over ten years and ROMAN baselined them for CGI. In August 2019, the CGI team, conducted random vibrate test on MEMS DM (BMC's electrostatic device). In September 2019, mainly for funding reasons, dropped development of its back-up.
- However, it was only until CGI started flight qualifying the AOX DMs that connectorizing the DMs to their flight driver electronics and surviving a launch environment became important challenges. They are still working these challenges today.



Technology Overview (2 of 2)



- **However, no one is currently working the environmental and anomaly issues on the MEMS DM as CGI ceased further work on this back-up technology.**
- **The ExEP requested NASA's APD fund BMC MEMS DM development for possible application to future exoplanet space missions as an alternative DM technology.**
- **APD agreed and has funded the request.**
- **The recommended plan to assess MEMS DM viability is to:**
 - 1) **continue to conduct coronagraph performance testing in the HCIT with MEMS DMs (50 actuators across the effective aperture).**
 - 2) **conduct a flight-level random vibe and actuator anomaly investigation for these MEMS devices.**
- **This test plan addresses the latter objective.**

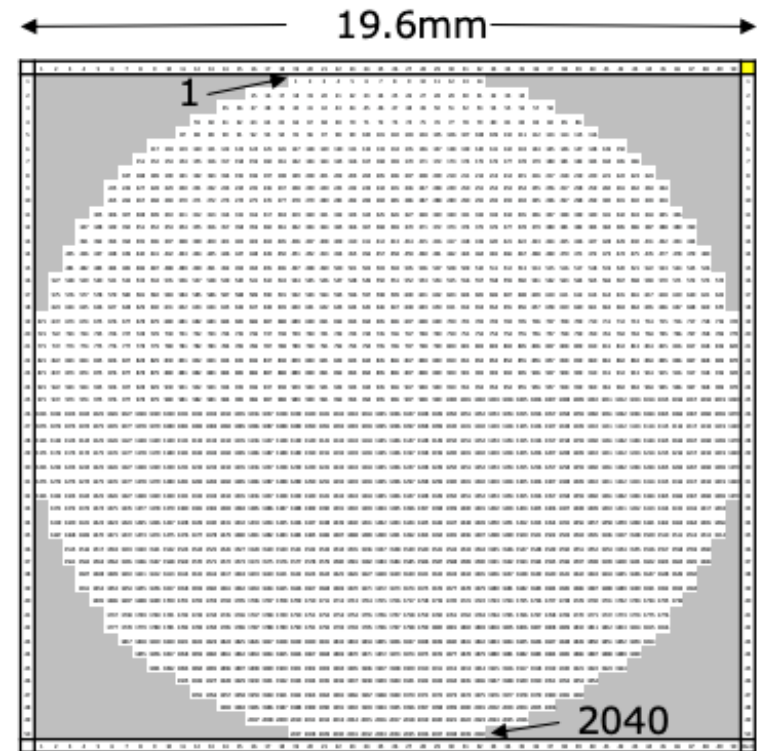
MEMS deformable mirrors rocket launch survivability

TEST PLANS

Devices Under Test (DUT)

Boston Micromachines MEMS Deformable Mirror

DM Actuator count	2040 actuators
Active Aperture Diameter	19.6 mm
# Actuators across active diameter	50
Actuator Pitch	400 μm
Actuation architecture	electrostatic
Actuator Resolution	< 20 μm
Operating Voltage	0-100 V
Mirror Surface Figure	< 5 nm RMS (400 μm < λ < 5 μm)
Fill Factor	> 99.9%
Mirror material	Silicon, Aluminum coating

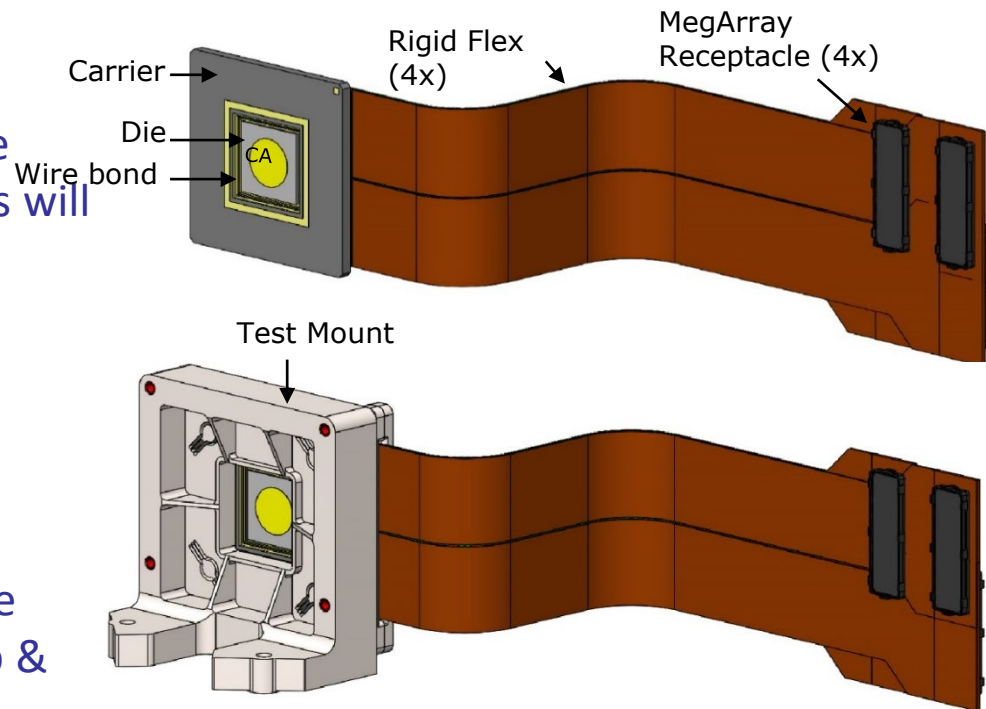


- ❖ **Unit 1:** 100% working actuators, Al coated.
- ❖ **Unit 2:** 3-5 non-working actuators, un-coated.

Scope of Testing

- **Areas to validate**

- Actuator anomalies after random vibrate.
- Carrier, die, die bonds, PGA joints, wire bonds, and carrier to test mount bonds **will** be included in random vibrate.
- MegArray receptacles **NOT** included in random vibrate.



- **Test mount**

- Use CGI-comparable mount to simulate thermal and launch load w/o x, y, z, tip & tilt adjustment.

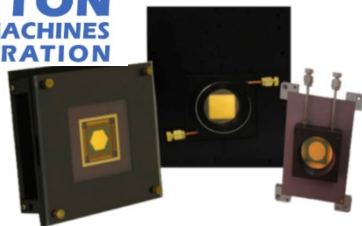
Objectives: Understand effect of launch vibrations loads on next generation MEMS DMs (50x50) and their failure mode.

a. Understand effect of launch vibrations loads on perfect actuators and faulty actuators.

b. Understand the failure mode of the pre-test faulty actuators.

Testing Block Diagram

BOSTON
MICROMACHINES
CORPORATION

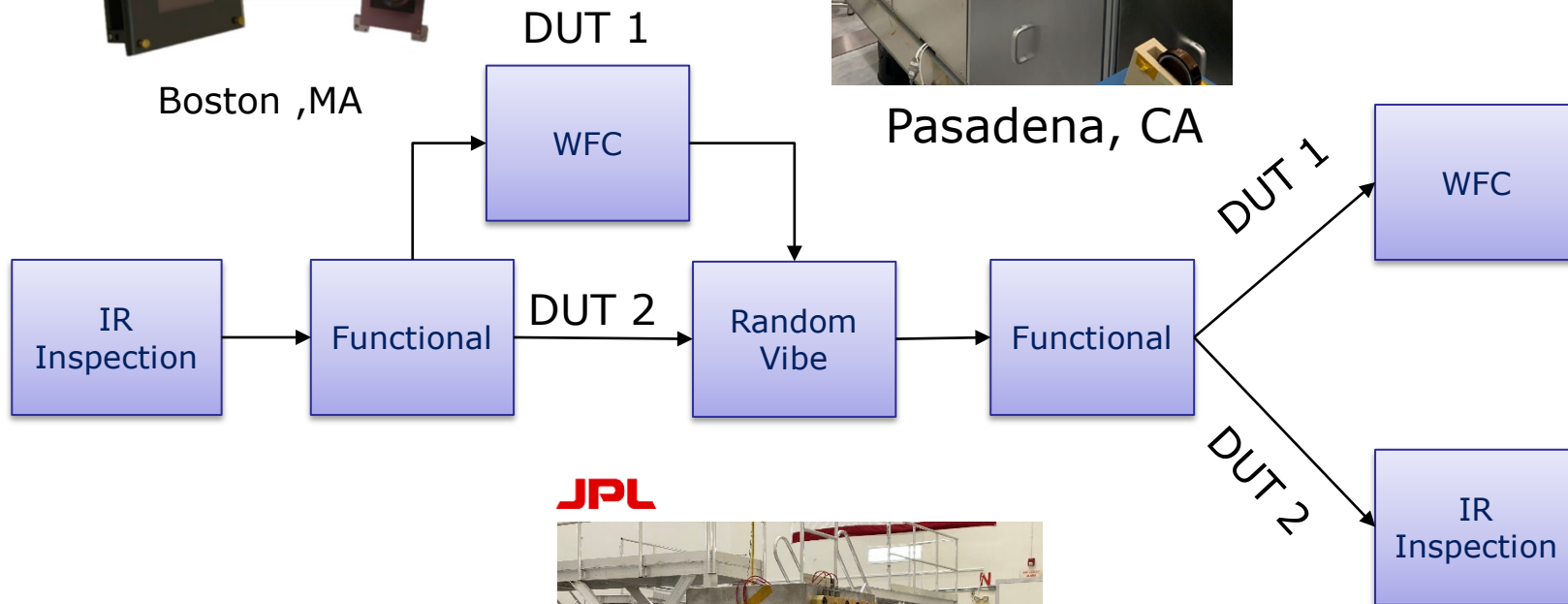


Boston, MA

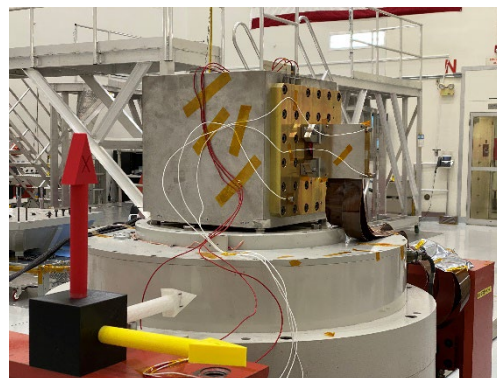
JPL



Pasadena, CA



JPL

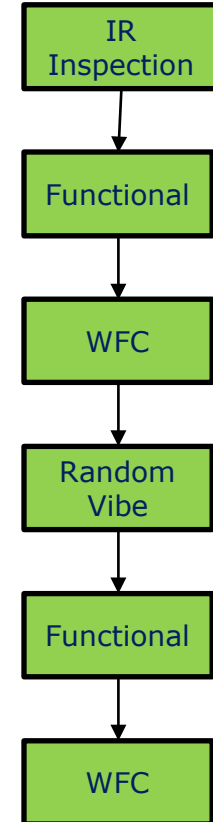


Pasadena, CA

Test Plan DUT 1

- **Unit 1 is a 100% functional unit with an Al coated face sheet.**
- **Confirm or reject the hypothesis that a 100% yield 2K MEMS DM will pass vibration test.**
 - Characterize response with ZYGO.
 - Dig a dark hole on shorter wavelength.
 - Shake DM and recharacterize.
- **These DMs were fabricated from BMCs wafers and using ceramic substrate interconnect developed at JPL.**
- **Test success Criteria:**
 - Structure damage – visual inspection.
 - Connection/actuator damage – actuator liveness test, stroke, and gain.
 - Bulk die damage – unpowered or powered surface figure change measurements.

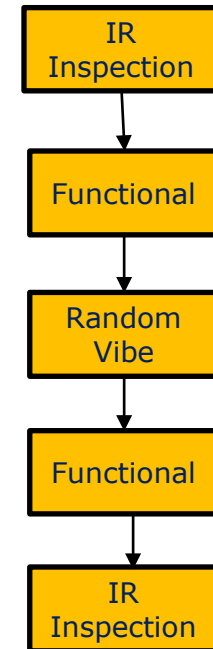
Unit 1



Test Plan DUT 2

- **Unit 2 has some dead actuators and has an uncoated face sheet.**
 - Allows for post-vibe IR inspection to help understand the failure mode.
- **Confirm or reject the hypothesis that anomalous actuators propagate to neighbors after shaking (as well as characterize the anomaly).**
 - Characterize the DM with the IR microscope before and after shaking
 - Characterize response with ZYGO.
 - Shake DM and recharacterize.
- **These DMs were fabricated from BMCs wafers and using ceramic substrate interconnect developed at JPL.**
- **Test success Criteria:**
 - Structure damage – visual inspection.
 - Connection/actuator damage – actuator liveness test, stroke, and gain.
 - Bulk die damage – unpowered or powered surface figure change measurements

Unit 2



Test: Infrared Inspection

- **Performed on both DUT 1 and DUT 2 before vibration load tests.**
 - Repeated for DUT 2 after vibration load test.
- **Facility: IR microscope at BMC's cleanroom**
- **Tests:**
 - Candidate die was evaluated for yield and surface finish.
 - Two die were selected for processing
 - DUT 1 has demonstrated 100% yield after probe.
 - DUT 2 has demonstrated less 100% but more that 97% yield after probe.
 - DUT 1 and 2 were evaluated using an IR microscope.
 - DUT 1 was coated with Aluminum and DUT 2 was not coated.
 - Both die were packaged in JPL ceramic carrier.
 - The final devices were shipped to JPL using hand-carry approach.

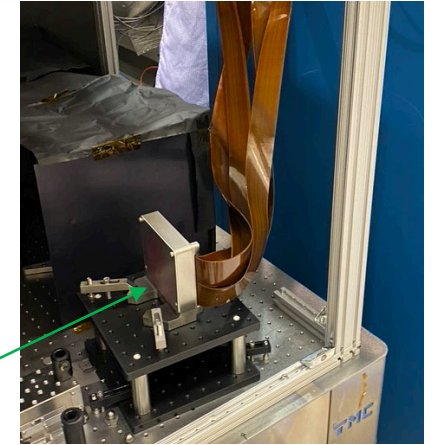


Test: Functional



Dry air tent
(DM inside)

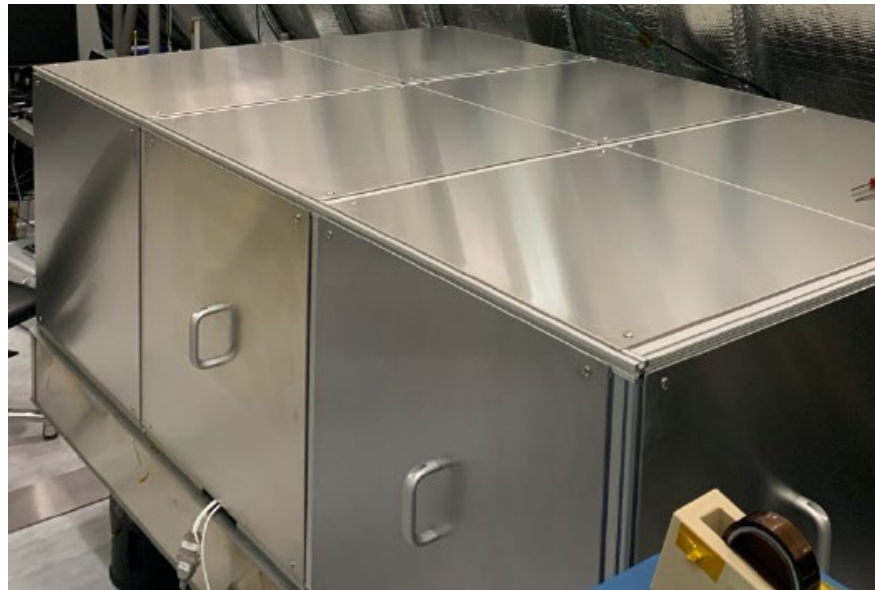
DM



- **Performed on both DUTs before and after launch vibration load test.**
- **Facility:** Zygo in 318 HB with dry air tent surround DM
- **Tests:**
 - Uniform voltage.
 - Poke each rows and columns.
 - Poke grids of actuators (4x4).
 - Poke all actuators.
 - Stability.
 - Repeatability.
 - Temporal response time.

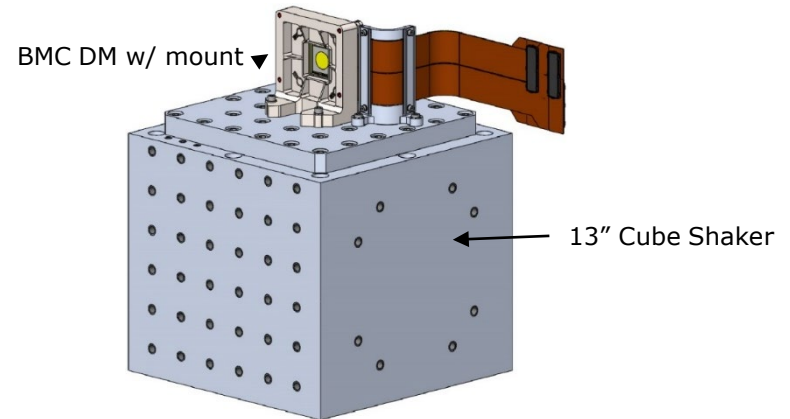
Test: Performance

- Performed before and after launch vibration load test on DUT 1.
- Facility: 318 HB
- Tests:
 - Use DM to control wavefront on an in-air coronagraph testbed dedicated to exoplanet imaging.
 - Dig a dark hole.
 - Repeat test after vibration load to determine changes to ability to control wavefront.

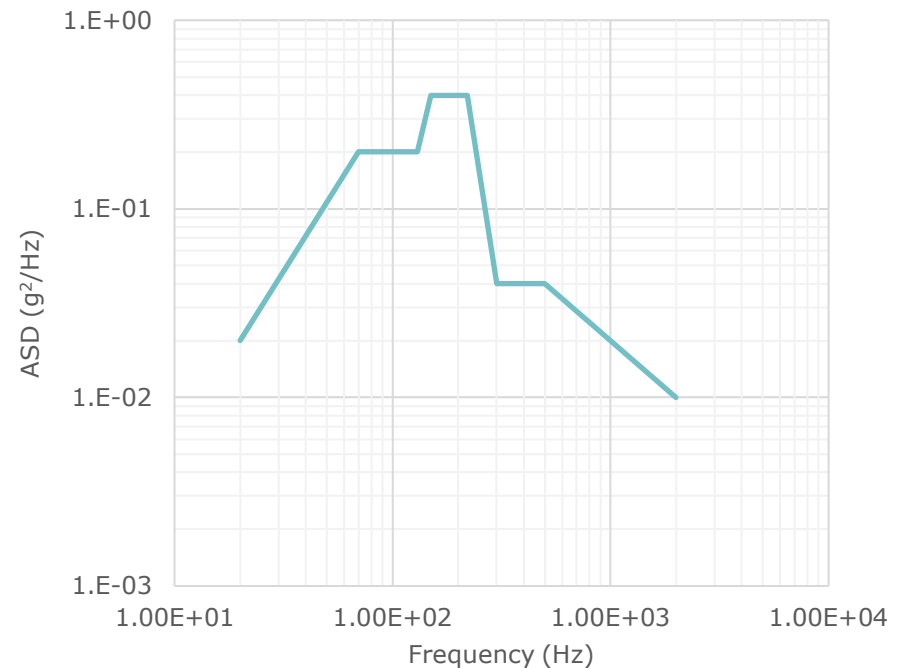


Test: Random Vibration

- **Facility: NTS 13" cube shaker**
 - Class 100k clean room with humidity control.
- **PSD Spec:**
 - Follows Roman-CGI instrument Environmental Requirements Document.
 - Not specific to a particular launch vehicle. Intended to be conservative to and encompass all potential launch vehicles.
 - PSD's have been refined as the Roman-CGI analysis has progressed.
 - Used version shown currently in CCB.



DM 2 Environment		
Frequency (Hz)	FA (g ² /Hz)	PF/Qual (g ² /Hz)
20	0.01	0.02
70	0.1	0.2
130	0.1	0.2
150	0.2	0.4
220	0.2	0.4
300	0.04	0.04
500	0.04	0.04
2000	0.01	0.01
Overall	8.29	9.91
Duration (per axis)	1 min	2 min



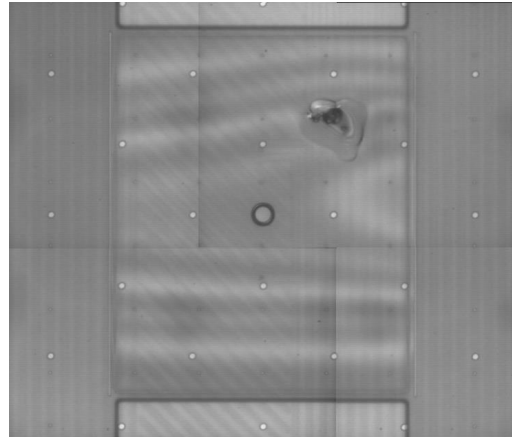
MEMS deformable mirrors rocket launch survivability

SURVIVABILITY RESULTS

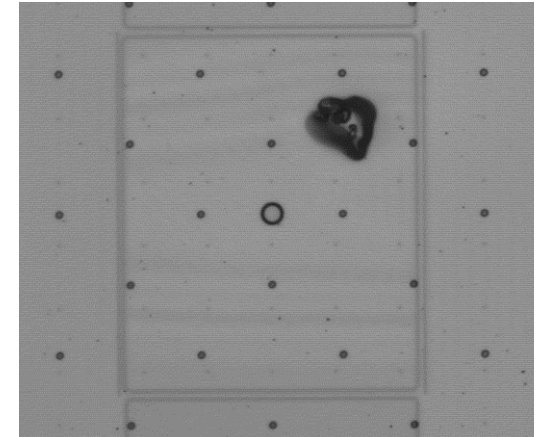
Infrared Inspection Test Results

- DUT 2 – Actuator 1999:
(Damaged actuator)

Pre-RV

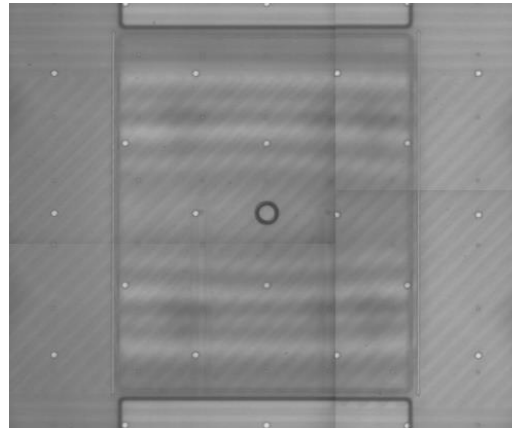


Post-RV

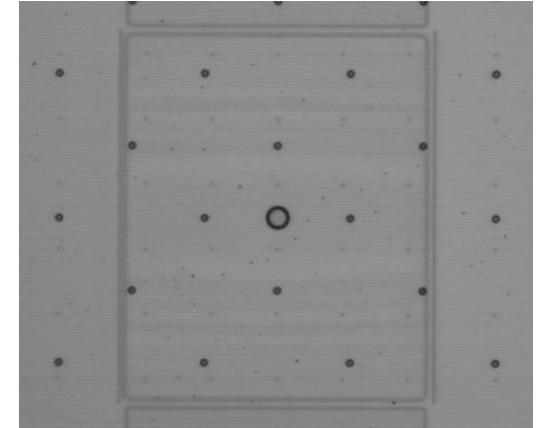


- DUT 2 – Actuator 1284
(Neighbor of a
damaged actuator)

Pre-RV



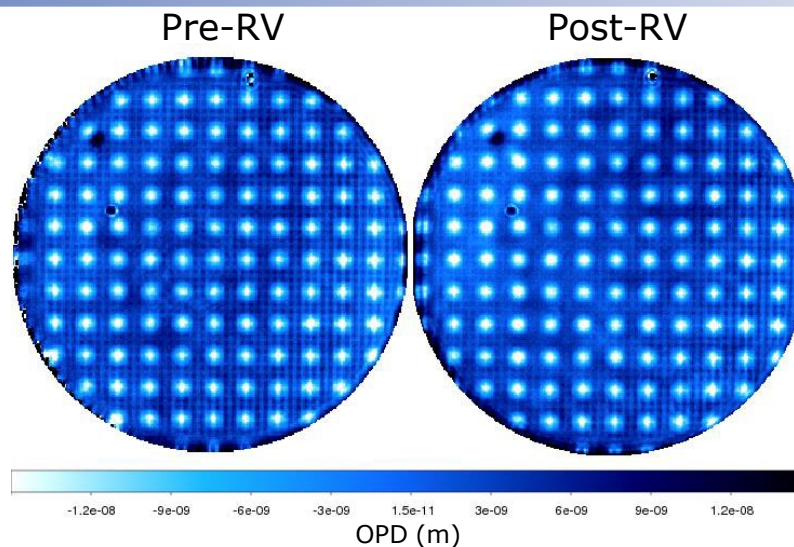
Post-RV



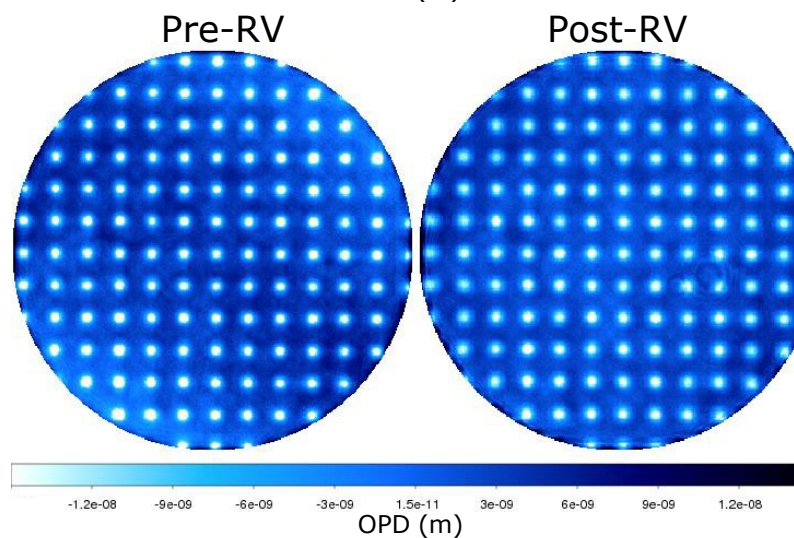
Results: No changes to the anomalous actuators and the actuators that neighbor the Non-Responding Actuators were noted in the IR inspection post vibration test.

Functional Test Results

- Example DUT 2 - Grid 4x4:



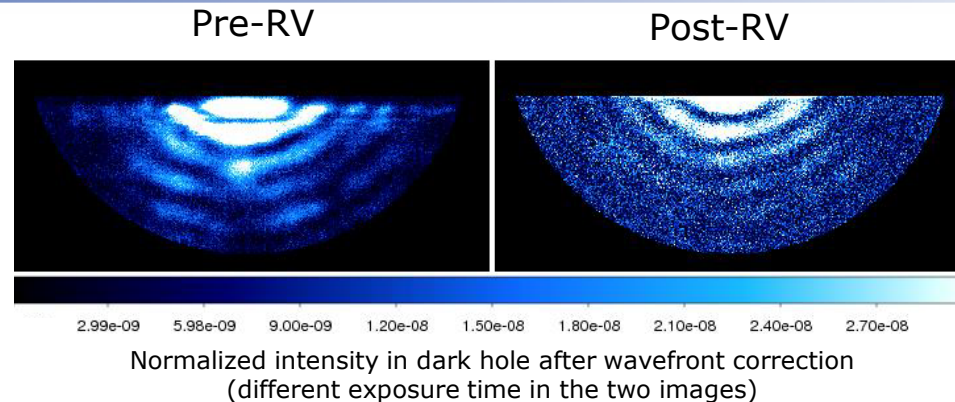
- Example DUT 1 - Grid 4x4:



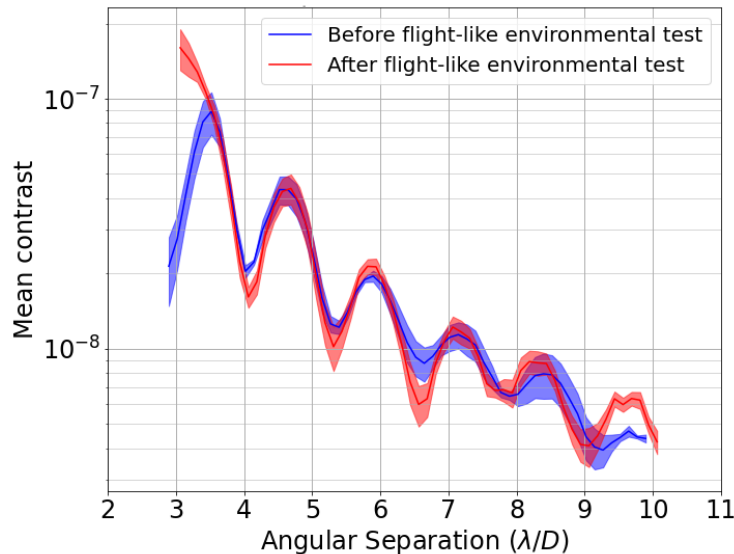
Results: No noticeable differences pre and post vibe on both DUTs during the functional tests.

Performance Test Results

- WFC with DUT 1:



Radial profile in the half dark hole before and after random vibrate



- Pre and post vibrate performance are equivalent.
- Contrast in the DH limited by an incoherent leakage due to the vortex coronagraph that is not related to the DM state.
- Contrast levels down to 10^{-8} in-air already demonstrate readiness of the MEMS DM technology for high-contrast imaging.

Results: Equivalent wavefront sensing and control performance pre and post vibrate on DUT 1.

MEMS deformable mirrors rocket launch survivability

CONCLUSION

Conclusion

- DUT 1 and 2 were tested before and after random vibration simulating rocket launch. Infrared inspection, functional and performance tests were performed.
- Infrared inspection and functional test on DUT 2 reject the hypothesis that anomalous actuators propagate to neighbors after shaking.
- Functional and performance tests on DUT 1 confirmed that a 100% yield 2K MEMS Deformable Mirror will fully survive to a launch environment.

BMC's 2K continuous face sheet MEMS deformable mirrors have passed 3-axes random vibe environmental testing at bounding launch loads encompassing those of future launch vehicles.